Assessment of the Melting Behavior of Batches Containing Boron Oxide Carrier Raw Materials

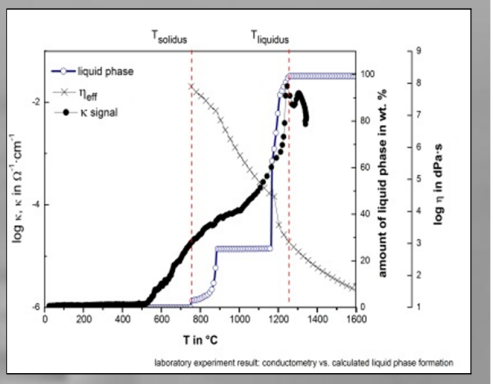

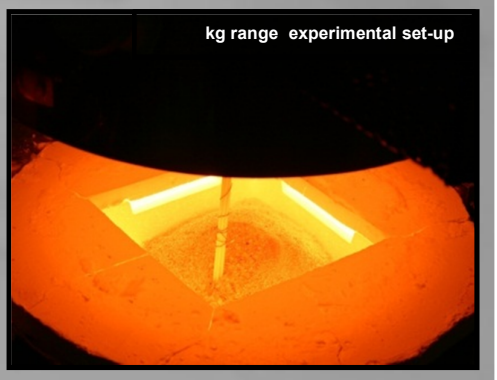

Widiya Jatmiko

Faculty of
Georesources and Material Engineering

RWTH Aachen University

Assessment of the melting behavior of batches containing boron oxide carrier raw materials

Von der Fakultät für Georessourcen und Materialtechnik der
Rheinisch-Westfälischen Technischen Hochschule Aachen

zur Erlangung des akademischen Grades eines

Doktors der Ingenieurwissenschaften

genehmigte Dissertation

vorgelegt von **M.Sc.**

Widiya Jatmiko

aus Purbalingga, Indonesia

Berichter : Univ.-Prof. Dr. Reinhard Conradt
Univ.-Prof. Dr.-Ing. habil. Joachim Deubener

Tag der mündlichen Prüfung: 15. Mai 2014

Acknowledgement

On this particular occasion, I should like to thank everyone who have extended their whole-hearted support and encouragement to me in framing technical as well as non-technical aspects of my doctoral study, especially my dissertation at *Institut für Gesteinshüttenkunde*, GHI, RWTH Aachen.

I am grateful most specifically to Prof. Dr. rer. nat. Reinhard Conradt for giving me the opportunity to work with him in the capacity of a doctoral student at GHI. I cannot describe in words how grateful I and my family in Aachen remain to you for your invaluable contribution to my professional career in research and development areas. Last but not least, this dissertation would not have been finished without your advice, guidance, and presence.

My acknowledgments go to my co-workers at GHI, in particular, Dr Andreas Prange, Tanja Mund, (DTA-TG, HSM, TOMMI), Margit Kehren and Lena Kalf (XRF, ICP, volumetry), Petra Schott (XRD), Peter König (laser granulometer and Al_2O_3 crucibles), Lee Young Suk, Malte Grimm and Wolfgang Wilsmann (for discussion time); all members of the workshop department at GHI; all my colleagues, for our togetherness and friendship: Swantje Thiele, Li Zhang, Peter Djambazov, Lisa Becker, Amelie Neumann, Anna Schusser, Gesche Riesner, Erik Wanko, and Beatrice Cela; my fellow enthusiastic HiWis: Jürgen Lenger, Vera Peters, and Fritz Maten. Thanks to Marian Michalski for English correction, and of course, for precious discussions about the industrial practice.

Special thanks go to my family members, Ilma, Naura, and Kana for your continuous love and support. You have strongly motivated me to finish what I had started in Germany. I should also like to express my gratitude and dedicate this dissertation to my parents, my brother, and my family in Balikpapan, and all my family members in Tinggarwangi and Jakarta, Indonesia.

Many thanks to the *Arbeitsgemeinschaft industrieller Forschungsvereinigungen* (AiF), for the financial support within the frame of '*Einsatz alternative boroxidhaltiger Rohstoffe in der Glasindustrie*' (AiF No. 16185 N) in 2011.

Dedicated to my family in Kelmis, Belgium, and my parents in Indonesia:
Ilma, Naura, Kana, Eli Asmarawati, and Sudjatmiko

Abstract

The kinetic aspects of batch melting related to grain size, primary melt formation, gas liberation, and quartz dissolution can only be characterized by performing laboratory experiments, whereas the thermodynamic aspects can be quantified theoretically. One approach to close the gap between laboratory and industrial practice is scaling up experiments from the milligram to the kilogram range. In the micro scale (less than 150 mg sample), physical and chemical reactions of one component, as well as binary and ternary systems, can be observed through the differential thermal analysis (DTA), coupled with the thermo-gravimetry instrument (TG). Experiments at the mesoscale are: thermal-optical observations (30 g batch), conductometry (200 g batch), modified batch-free time (50 g batch and 250 g cullet), and kilogram 10 kg tests in which 4 kg batch and 7 kg cullet are involved. The present study aims to investigate whether these methods could be applied to free alkali and B_2O_3 containing glass batches. The investigated system were the eutectic CaO-Al_2O_3-SiO_2 (CAS) and CaO-MgO-Al_2O_3-SiO_2 (CMAS) based E-glass combined with various B_2O_3 content. The onset of melting or primary melt formation in free alkali glass batches is generated by its eutectic melting, while in soda-lime-silica batch, the onset of melting corresponds to physical melting of soda ash. The last part of the present paper is feasibility study of alternative B_2O_3 carriers applied in boron containing glass batches. Conventional borax pentahydrate is one of the substance in the list of SVHC (Substance of Very High Concern) under EU REACH (Registration, Evaluation, Authorization of Chemical substances) regulation. For borosilicate batches, no significant impact is observed between the conventional and alternative B_2O_3 carrier. Ulexite as alternative B_2O_3 carrier shows kinetic advantages in E-glass and insulation wool glass in terms of early onset of melting and short foaming decay, respectively. However, these advantages could not be seen during industrial trial in insulation wool glass melter tank, due to insufficient ulexite data. Both borax pentahydrate and ulexite batches demonstrate similar behavior in respects to energy consumptions. Furthermore, since ulexite is beneficiated in finely ground powder, it contributes to higher emission level after filtration in an electrostatic precipitator equipment.

Kurzfassung

Die Betrachtung der Reaktionskinetik im Gemenge wird durch geeignete Charakterisierungsmethoden vom Mikrobereich bis hin zum 10-kg-Maßstab durchgeführt. Physikalische und chemische Reaktionen der einzelnen Rohstoffen sowie binärer und ternärer Mischungen der Rohstoffe werden mit der Hilfe der konventionellen DTA-TG charakterisiert. Um die Laborergebnisse auf eine reale Glaswanne übertragen zu können, ist es nötig, die Experimente in größerem Maßstab durchzuführen. Die im Institut verfügbaren Methoden sind thermisch-optische Untersuchung mittels Beobachtungsofen (30 g Proben), modifizierte Batch-Free-Time (50 g Proben), Conductometrie (200 g Proben) und Schmelzversuche im 10-kg-Maßstab (4 kg Gemenge; 7 kg geschmolzene Glasscherben bei 1200 °C). In der vorliegenden Arbeit werden alkalfreie- und borhaltige Gemengesysteme untersucht. Gemengen im eutektischen CaO-Al_2O_3-SiO_2 (CAS) und verschiedenen CaO-MgO-Al_2O_3-SiO_2 E-glassystemen mit variierendem Boroxidgehalt werden charakterisiert. Es wird gezeigt, dass sich die Methoden auch für diese Gemenge eignen. Das unterschied ist die Bildung von Erstschmelze nicht einem rasch aufschmelzenden Rohstoff wie Soda; ausschlaggebend ist vielmehr die eutektische Temperatur des Oxydsystems. In einer anschließenden Studie wird die Einsetzbarkeit von alternativen Boroxidträgern in Gemengen verschiedener borhaltiger Gläser diskutiert, da sich konventionelles Boraxpentahydrat auf der Liste der SVHC (*Substance of Very High Concern*) innerhalb von REACH (*Registration, Evaluation, Authorization of Chemicals*) befindet. Aufgrund unzureichender Versuchdaten eines durchgeführten industriellen Schmelzversuchs mit dem Borträger Ulexit konnte kein wesentlicher Unterschied im Schmelzverhalten und im Wärmebedarf im Vergleich zum konventionellen Gemenge festgestellt werden, obwohl man kinetische Vorteile des Gemenges mit Ulexit in den Laborexperimenten beobachten kann. Allerdings wurden bei der Analyse des Elektrofilterstaubes an der Wanne erhöhte Primäremissionen festgestellt, da das Ulexit als feingemahlener Rohstoff in das Gemenge eingebracht wird.

Table of contents

List of figures

List of tables

Lists of symbols and abbreviations

Greek symbols

η	=	viscosity [dPa·s]
η_{re}	=	efficiency of heat recovery by the heat exchanger
η_{ex}	=	ratio of exploited and input heat
η_{fluid}	=	viscosity of a pure one phase fluid [dPa·s]
η_{eff}	=	effective viscosity of two fluid phases, calculated from the solid-liquid ratio within the solid bulk [dPa·s]
Φ_{solid}	=	solid fraction in a two-phase fluid
κ	=	conductivity [$\Omega^{-1}\cdot$ cm^{-1}]

Latin symbols

$\Delta H°_{chem}$	=	chemical heat demand [kWh/t]
$\Delta H°_{batch}$	=	standard heat of formation of a batch [kWh/t]
$\Delta H°_{glass}$	=	standard heat of formation of glass [kWh/t]
$\Delta H°_{gas}$	=	standard heat of formation of gas products [kWh/t]
ΔH_T	=	heat stored in the glass melt at temperature T [kWh/t]
a	=	thermal diffusivity [cm^2/s]
a	=	intercept of a graph between power input vs. pull rate [kW]
b	=	slope of a graph between power input vs. pull rate [kWh/t]
c_P	=	heat capacity [J/(mol·K)]
e	=	elementary charge [1.602 · 10^{-19} C]
H_{in}	=	input energy [kWh/t]
H_{ex}	=	exploited heat [kWh/t]
H_{wu}	=	upper wall loses energy [kWh/t]
H_{wo}	=	lower wall loses energy [kWh/t]

H_{wx} = heat exchanger wall loses energy [kWh/t]

H_{sf} = set free energy [kWh/t]

H_{stack} = energy at passage of stack [kWh/t]

H_{re} = recovered energy [kWh/t]

H_{off} = off-gas energy [kWh/t]

H_{ht} = transferred heat [kWh/t]

H^{vit} = heat of vitrification

H^{fus} = energy required for melting all batch components

H_{NCV} = net calorific heat value [kWh/m^3]

k_B = Boltzman constant [1.238 · 10^{-23} J/K]

M = molar mass [g/mol]

p = production rate [t/h]

P = power [kW]

P_{in} = input power [kW]

P_{ex} = exploited power [kW]

P_{loss} = power loss [kW]

q = heat flux [kW/m^2]

r = pull rate [t/(m^2·h)]

R = electrical resistance [Ω]

S^{vit} = entropy of vitrification

S^{fus} = entropy of the melting of batch components

T_{ad} = adiabatic flame temperature [K]

T_{off} = off-gas temperature [K]

T_o = ambient temperature [K]

T_{ex} = pull temperature [K]

T_{wo} = upper wall temperature [K]

T_{wu} = lower wall temperature [K]

T_g = glass transition temperature [K]

U_0 = initial voltage [V]

U_x = output voltage [V]

v = charge number

V'_H = volumetric flow of gas [m^3/h] at normal condition; 0 °C, 1 atm

y_C = fraction of cullet added to the batch; $0 < y_C < 1$

Abbreviations

In this thesis, the so-called element notation of oxide formulae is used, with $A=Al_2O_3$, $B=B_2O_3$, $C=CaO$, $H=H_2O$, $M=MgO$, $S=SiO_2$; thus, for example, CAS refers to $CaO \cdot Al_2O_3 \cdot SiO_2$. CAS_2 denotes the compound $CaO \cdot Al_2O_3 \cdot 2SiO_2$

AC = Alternating Current

AiF = *Arbeitsgemeinschaft industrieller Forschungsvereinigungen*, (German Federation of Industrial Research Associations)

BFT = batch-free time

CIPW = **C**ross, **I**ddings, **P**irrson, and **W**ashington—a calculation method to predict possible phases formed from particular oxide systems

c.r.s = crystalline reference system

DTA = different thermal analysis

EGA = evolved gas analyser

HVG = Hüttentechnische Vereinigung der deutschen Glasindustrie (The Research Association of German Glass Industry)

HSM = hot stage microscopy

HT-XRD = high-temperature X-Ray diffraction

TG = thermogravimetry

TOMMI = thermo-optical measuring instrument

1. Introduction

1.1 Motivation

Batch melting is the first step of high temperature process in glass production. It is characterized by endothermic reactions in which high energy is required. Tailoring batch melting reactions is one of the many attempts to decrease the energy consumption and emission produced by glass industries. It poses a challenge for many glass technologists on how to obtain proper and reliable batch melting characterizations in laboratory, whose results could then be transferred to the industrial melting tank. Modification of raw materials or batch formulation is of high risk, which could have a serious impact on the stability of the furnace and its lifetime.

In general, the batch melting can be examined from both thermodynamic and kinetic aspects. The former is related to the intrinsic enthalpy formation of individual raw materials, while the latter is associated with grain-to-grain contact, particle size, nature and viscosity of primary melt, gas release, and dissolution of quartz in molten glass. Unfortunely, these batch properties cannot be characterized by conventional methods, such as different thermal analysis integrated with thermogravimetry (DTA-TG) and hot-stage microscopy (HSM). Experiment results from these methods give rather a fair insight of the reactions that occur under particular heating rates and are difficult to help in evaluating batch melting phenomena in the industrial melter in a straightforward way. The main reason is significantly different boundaries and heat transfer conditions between laboratory experiments and the industrial glass tank.

Since the results of conventional methods cannot be used to evaluate the batch melting occurrence in industrial scale, new methods of batch characterization is necessary. Conradt and his co-workers [CON 1994, 1997] [DUB 2004] have developed methods to deliver detailed information on the occurrences within the batch during melting in the laboratory scale. The methods are the measurement of batch conductivity, batch-free time (BFT) and 10 kg range test in the soda-lime silica batches. However, these methods have not been ascertained yet for either

poor alkali or B_2O_3-containing glass batches, which obviously have different properties from that of the soda-lime-silica glass. Moreover, employing the results of the laboratory experiment to an industrial campaign is also a challenge; this is not only to get a better understanding of the batch melting behaviour in the industrial melter, but also to gauge the relationship between batch and energy consumption. Evaluation of the fuel flow rate used for combustion process, melter temperatures (stack, crown, bottom, throat, riser), and production rate (pull) provides us with a comprehensive understanding of the batch melting behaviour corresponding to the furnace performance.

1.2 Objective

It is the objective of the present study to characterize the batch melting of free or low- alkali content E-glass batches. The batch melting experiments, which are limited to the DTA-TG, represent conventional experimental methods; while the newly developed methods characterizing the batch by a much bigger sample size are observation furnace in a sample size of 30 g, conductometry in a sample size of 200 g, modified batch-free time in a sample size of 250 g, and 10 range kg experiment. The results of the experiments, using both conventional and newly developed methods, are then compared, to get a better understanding of the batch melting occurrences under a particular heating rate.

The knowledge gained from the previously mentioned methods are then applied to investigate the batch melting behaviour of the B_2O_3-containing E-glass batches with varied B_2O_3 content and the feasibility study of alternative B_2O_3 carriers in the E-glass as well as in borosilicate, lamp, and insulation wool batches. Selection of the alternative B_2O_3 carrier for industrial trials is not only assessed by the laboratory experiment results, but also by its availability in large amounts. The industrial trial results, using an alternative batch, are evaluated with the conventional batch with regard to the energy demand and emission level.

1.3 Scope

The chapter with results and discussions will be divided into three main sub-chapters. The first sub-chapter discusses the batch melting behaviour of the E-glass batches derived from the ternary as well as quaternary systems of CaO-Al_2O_3-SiO_2 (CAS) and CaO-MgO-Al_2O_3-SiO_2 (CMAS). The second sub-chapter

describes the investigation of the batch melting behaviour of the E-glass batch with varied B_2O_3 content. The results of the two-year project of alternative boron oxide carriers for glass industries will be reported at the end of Chapter 4 (results and discussions), and the results of industrial trials will be addressed separately in Chapter 5. The latter is a project sponsored by the German government through the German Federation of Industrial Research Associaion, also known as *Arbeitsgemeinschaft industrieller Forschungsvereinigungen* (AiF). This is a collaboration between Institute of Mineral Engineering, RWTH Aachen (GHI), German Glass Society (DGG-HVG), and industrial partners. A part of the project scope is devoted to the study of borate minerals (mineralogy, petrology, and availability), and will be described at the end of Chapter 2 (theory). Due to confidential issues, both glass and batch compositions of the last study case cannot be shown in the chapter of experiments (Chapter 3). They will be, however, assumed to be similar to the acknowledged compositions derived from different sources.

1.4 Literature survey

Many studies have been published in the field of batch melting process. Four different scales are required to get a comprehensive view of the batch melting process:

- atomic scale of thermochemical reactions and local equilibrium
- microscopic scale of grain-to-grain-contact
- mesoscopic scale of local transport process, including heat transfer, viscous fluid, and gas reactions within a batch
- macroscopic scale of mass, heat, and power balance of the total glass melting process. This also considers batch heap distribution, primary emission, and carryover.

Application of either the thermodynamic data base [KUB 1993] or computer-based calculation [GTT 2004] can be utilized to understand the atomic scale of thermochemical reactions and local equilibrium of different types of glass and batch. The soda-lime glass system is the main subject of earlier publications from Tamman [TAM 1930], Kröger [KRÖ 1948], [KRÖ 1952], [KRÖ 1953a], [KRÖ

1955], [KRÖ 1957], Kautz [KAU 1969], Frischat [FRI 1986], and Hrma [HRM 1982] with regard to the atomic scale of batch melting.

The method that uses DTA-TG was applied for comprehensive studies on the transition from atomic to microscale of batch melting. Thermochemical and kinetics reactions are characterized as either endothermal or exothermal reaction during the heating process. Grain size should be taken into consideration since it normally requires small amounts of sample (10–100 mg). Several works of Abou-El-Azm [ABO 1953], Wilburn et al. [WIL 1961], [WIL 1963], [WIL 1965], Speyer et al. [SPY 1993a], [SPY 1993b], and Hrma [HRM 1985] comprise the DTA-TG studies on various batches. Other authors investigated batch melting by using various methods, such as X-ray diffraction (XRD), to investigate the reaction product [MUK 1980], [IZA 2001a], [IZA 2001b], [DOL 2004a], [DOL 2004b] hot-stage microscopy (HSM), to observe reactions that occur [WIL 1965] and the evolved gas analysis (EGA), to determine the rate of the evolved gas produced from the batch during heating [KRÄ 1980], [LAI 1998], [LAI 2000], [KAW 1999], [KIM 2002]. Except the work of Dolan et al. [DOL 2004c], most of the publications are focused on the soda-lime glass batch.

Other publications on the subject of the microscale of grain-to-grain contact can be found in the works of Hrma [HRM 1999], Babushkin et al. [BAB 1985], Flick et al. [FLI 1995], and Sheckler et al. [SHE 1990]. The microscopic scale of grain-to-grain of batch melting is difficult to quantify; thus the above publications only showed the nature of the phenomena in empirical ways. There are approaches, however, to evaluate batch melting in a reliable way. Batch-Free-Time (BFT) is the time required for a batch to dissolve up to 98% in molten glass at isothermal conditions; this method was introduced by Bieler et al. [BIE 1969], [BIE 1984] to investigate the influence of NaOH in the soda-lime glass system. Pimkhaokham et al. [PIM 1993], [PIM 1995] and Conradt et al. [CON 1994], [CON 1997] have published papers on a newly developed method to determine and to observe this microscale of batch melting thoroughly. Kim et Al. [KIM 1990], Hrma et al. [HRM 2011] have published batch melting characterizations, based on the expansion of a batch. Batch samples can be in the range of 5–25 g of size with this method. A batch is heated with a particular heating rate, and then, observed through the quartz window. The gas evolved during the decomposition of the gas product mainly CO_2

is analysed by the integrated EGA, and the batch's shrinkage or expansion is recorded through the image software analysis.

Studies on the mesoscale of batch melting, in which temperature fields in batch heap are distributed, can be found in the publications by Fuhrmann [FUH 1973], Daniels [DAN 1973], Costa [COS 1977], Beerkens et al. [BEE 1992-1], [BEE 1992-2], as well as by Conradt [CON 1994] and Dubois [DUB 2004]. The last two publications showed not only the temperature field, but also the development of the first liquid phase within the batch as a function of position and melting time. Observation of this mesoscale leads to the development of either mathematical or computer modelling of batch heap in the furnace tank, as reported by Mase [MAS 1980], Hilbig [HIL 1986], and Ungan-Viskanta [UNG 1986]. One way to overcome the limitations and boundary conditions of the furnace tank model for batch heap is by performing mass, energy, and power balance, based on the fundamental principles presented by Kröger [KRÖ 1953, 1955]. Conradt [CON 1990], [CON 2008, 2012] calculated the mass, heat, and power balance by utilizing the thermodynamic, fuel gas, daily routine temperature, and glass capacity data. Based on the work of Madivate et al. [MAD 1996] and data from Conradt [CON 1990], it is found that the deviation of thermochemistry calculations from the calorimetrical measurement of a industrial glass batch is around 3–5 %.

2. Basic theory

2.1 Heat, power, and mass balance

Glass melting tank can be considered as a heat exchanger, where the heat transfer from the hot stream coming from combustion space passes through the tank basin. Off-gas heat is recovered partly by the external heat exchanger equipment (a regenerator or recuperator), and recycled into a hot stream. A typical heat/power balance of the glass melting tank is illustrated by Figure 1, which is associated with the amount of heat that flows through the basin from combustion space and heat losses through the boundaries of the system. All quantities are referred to a standard temperature, T = 298.15 K, and pressure level 1 bar to simplify the calculation.

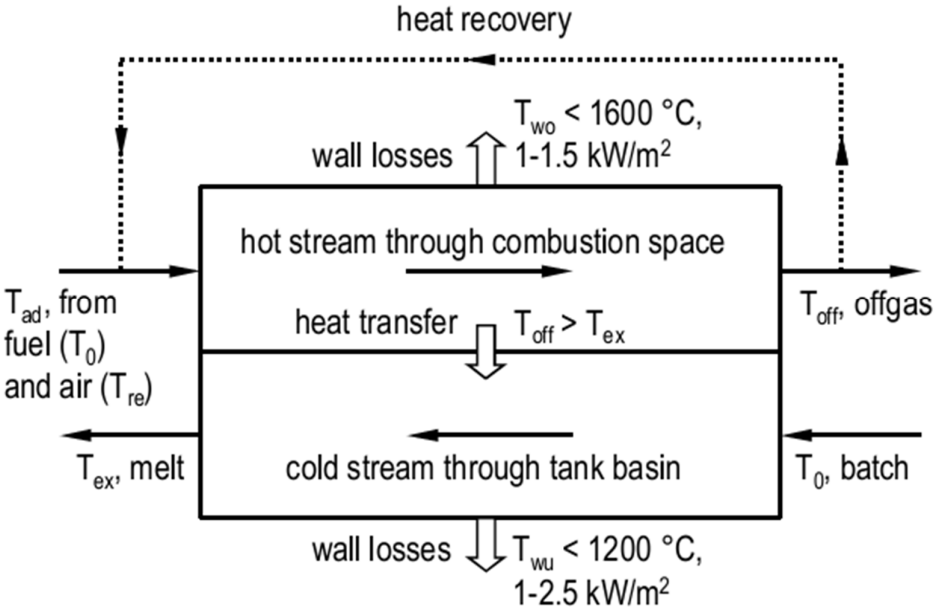

Fig. 1. The glass furnace viewed as a heat exchanger between adiabatic temperature, T_{ad}, and off-gas, $T_{off,}$ on the hot stream side, and ambient temperature, $T_{0,}$ and pull temperature, $T_{ex,}$ on the cold stream side; the T_{wo} and T_{wu} are upper and lower wall temperatures, respectively; the dotted line denotes the temperature of the heated air from a regenerator or recuperator [CON 2012b]

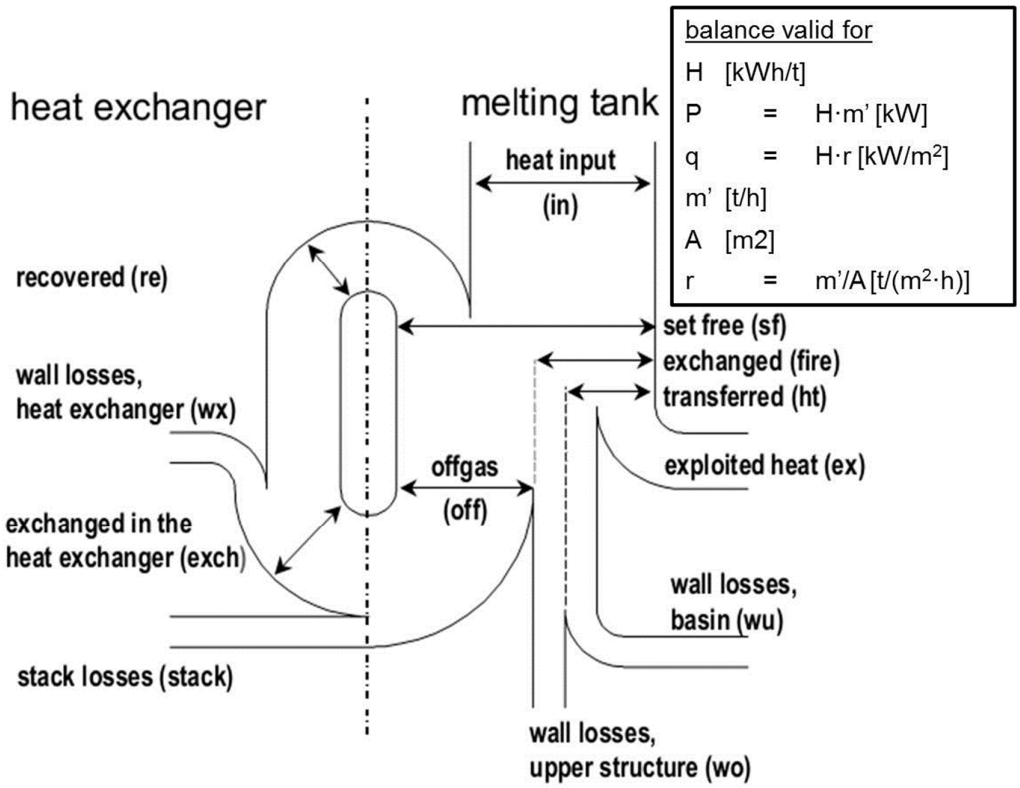

Fig. 2. Heat balance of a glass melting tank, with a heat recovery system [CON 2007]

The individual quantities of the heat balance, as illustrated by Figure 2, can be expressed either through the heat quantities with respect to 1 t of the produced glass [kWh/t], or to powers, P [kW/t], or even to heat fluxes q [kW/(t·m^2)]. Those quantities are correlated to the production rate (m') or pull [t/h], and pull rate r [t/(m^2·h)], respectively, as they are marked within the box in Figure 2. The following equations can be derived to determine individual balances [CON 2007]:

The complete installation

$$H_{in} = H_{ex} + H_{wu} + H_{wo} + H_{stack} + H_{wx} \quad (1)$$

The furnace

$$H_{sf} = H_{in} + H_{re} = H_{ex} + H_{wu} + H_{wo} + H_{off} \quad (2)$$

$$H_{in} = H_{ex} + H_{wu} + H_{wo} + H_{off} \cdot (1 - \eta_{re}) \quad (3)$$

in which, $\eta_{re} = H_{re}/H_{off}$

The heat exchanger

$$H_{off} = H_{re} + H_{stack} + H_{wx} \quad (4);$$

The combustion space:

$$H_{sf} = H_{in} + H_{re} = H_{ht} + H_{wo} + H_{off} \quad (5);$$

$$H_{in} = H_{ht} + H_{wo} + H_{off} \cdot (1 - \eta_{re}) \quad (6);$$

The tank:

$$H_{ht} = H_{ex} + H_{wu} \quad (7).$$

All the individual quantities can be calculated by an assessment of the amount of fuel and air (or oxygen) used, glass melt produced, the temperatures of the off-gas at flue gas exit (T_{off}), stack (T_{stack}), pre-heated air (T_{re}), as well as of the melt pulled from the furnace (T_{ex}). The symbol $\eta_{re} = H_{re}/H_{off}$ denotes the efficiency of the heat exchanger. The amount of heat corresponding to the combustion space can be derived by combustion calculations. Heat required for the batch to produce 1 t of glass melt is expressed by H_{ex} in the balance system, and it is strongly related to the pull temperature T_{ex} at the throat of the glass tank. This quantity can be expressed by the following equation:

$$H_{ex} = (1-y_C) \cdot \Delta H^\circ_{chem} + \Delta H_{T=Tex} \quad (8)$$

The standard enthalpy difference between the batch converted to glass and batch gases, at T=298 K, is denoted as ΔH°_{chem}.

batch (298 K) → glass (298 K) + batch gases (298 K) (9)

$$\Delta H^\circ_{chem} = H^\circ_{glass} + H^\circ_{gas} - H^\circ_{batch} \quad (10)$$

While y_C and $\Delta H_{T=Tex}$ indicates the percentage of internal cullet addition to the batch, and the enthaply difference between the glass at 298 K and the glass melt at pull temperature, $T=T_{ex}$, respectively. Note that, the temperature at 298 K is a fictive temperature to simplify the thermochemical calculation of the batch-to-melt conversion, which is known as chemical heat demand, ΔH°_{chem}, i.e. the standard enthalpy formation; the total reaction is denoted by the Equation 10. Symbolization

of the heat formation of solid glass, individual raw materials, and gaseous products from decomposition process in the batch at 298 K and 1 bar pressure is designated as $\Delta H°_{glass}$, $\Delta H°_{batch,}$ and $\Delta H°_{gas,}$ respectively.

The quantities of the heat balance in Figure 2 can be accurately evaluated from the daily routine production data. H_{in}, H_{off}, $H_{stack,}$ and H_{re} are contributed by the combustion calculation. The exploited heat H_{ex} depends on the available data of the heats of formation of: (1) individual batch materials at room temperature; (2) multicomponent glass at room temperature; and (3) multicomponent melts at arbitrary temperature T. The heat loses from the furnace walls through the boundaries can only be estimated roughly, due to the fact that the industrial glass tank has a very complex design, small openings and the corrosion of refractories which gives impact to heat loss as function of furnace age. Accurate calculation of H_{ex} leads to the completion of overall heat balance evaluation which includes the amount of heat loss through the boundary.

2.2 Thermodynamic aspects of batch melting

2.2.1 Multi-component glasses and glass melts

The thermodynamic approach to describe the batch-to-melt process and the quantities $\Delta H°_{chem}$, ΔH_{ex}, $H°_{batch}$, $H°_{glass}$, and $H°_{gas}$ has been partially discussed in the previous sub-chapter. Some problems may occur in determining the ΔH_{glass} of a multicomponent system since it cannot be derived by a set of experimental data through statistical methods. There are several approaches or models to describe the thermodynamic properties of a multicomponent system, e.g. the (modified) quasi-chemical model [PEL 1986], the cell model [GAY 1984], and the model of ideal mixing of complex component [BON 1990, SHA 1994]. However, a major problem can occur even though the computer-based calculation of codes and databases is utilized [ERI 1990, GTT 2004]. The most recent approach explores the concept of crystalline reference system developed by Conradt [CON 2009].

The rigid glass and the glass melt are identified by their crystalline reference system (c.r.s) which describes the energetic and entropic difference to a normative state of mineral phases k. Both the c.r.s and the glass state would form and co-exist at the glass transition temperature T_g under equilibrium conditions. The rigid

glass and its crystalline system can be distinguished by the enthalpy and entropy of vitrification, H^{vit} and S^{vit}, respectively, in the temperature interval from absolute zero to T_g. Analog to this approach, the melt at the liquidus temperature T_{liq} is characterized by the enthalpy and entropy of fusion, H^{fus} and S^{fus}, respectively.

The glass and the melt are associated with a mixture of glass and melted compounds k. In the c.r.s system, the heats and entropies of mixing are negligible if referred to the oxide component j. The key step is the identification of the suitable set of compounds k, which can be determined by exploiting two basic principles known in the mineral world. They are the principle of majoritty partition in which multi-component systems, such as magmatic and igneous rock melts, can be represented by a predominant quaternary comprising more than 85–95 % of the oxides on a molar basis. The second principle is the principle of parsimony in which quaternary predominant oxides are identified and reconstructed by the evaluation of the existing phase diagrams, while the minor oxides are alotted to a set of a normative phases as suggested by the CIPW norm calculation.

According to Gibbs' phase rule, the number of the oxides j in a glass composition is identical to the number of the compounds k in the corresponding c.r.s.; the molar amounts n or masses m of j and k (given in kmol or kg, respectively, per 1000 kg of glass) are thus related by a linear equation system,

$$n_j = (v_{jk}) \cdot n_k \tag{11}$$

$$n_k = (B_{kj}) \cdot n_j \tag{12}$$

in which $(B_{kj}) = (v_{jk})^{-1}$

$$m_j = (\mu_{jk}) \cdot m_k \tag{13}$$

$$m_k = (A_{kj}) \cdot m_j \tag{14}$$

in which $(A_{kj}) = (\mu_{jk})^{-1}$.

Here, v_{jk} is the matrix element indicating how many mol of the oxides j are found in the compound k; μ_{jk} is the weight of the oxides j contained in 1 kg of the compound k. A_{kj} and B_{kj} are the elements of the inverted matrices (v_{jk}) and (μ_{jk}), respectively.

The thermodynamic quantities of a glass or its melt are obtained by the following set of equations:

$$H^{\circ}_{glass} = \sum_k n_k \cdot (H^{\circ}_k + H^{vit}_k) \quad (15),$$

$$H^{\circ}_{1673,melt} = \sum_k n_k \cdot H^{\circ}_{1673,melt,k} \quad (16),$$

$$S^{\circ}_{glass} = \sum_k n_k \cdot (S^{\circ}_k + S^{vit}_k) \quad (17),$$

$$S^{\circ}_{1673,melt} = \sum_k n_k \cdot S^{\circ}_{1673,melt,k} \quad (18),$$

$$c_{P,melt} = \sum_k n_k \cdot c_{P,melt} \quad (19),$$

$$H_{T,melt} = H^{\circ}_{1673,melt} + c_{P,melt} \cdot (T - 1673) \quad (20),$$

$$S_{T,melt} = S^{\circ}_{1673,melt} + c_{P,melt} \cdot ln(T - 1673) \quad (21),$$

Standard enthalpy or heat formation of the rigid glass at 25 °C and enthalpy of the melt at 1400 °C,1 bar pressure are denoted as $H°_{glass}$ and $H°_{1673,liq}$. The latter gives a generalization of $H_{T,liq}$, i.e., enthalpy of the melt at the arbitrary temperature T. Entropies S have the analogous meaning; $c_{P,liq}$ is the heat capacity of the melt above T_{liq}. The quantities of the individual compounds k used in the above equations are compiled in Table 1. This table can be used to calculate different kinds of glass systems, ranging from the conventional soda-lime silica to boron oxide-containing glasses [CON 2004].

Table 1 Thermodynamic data of the compounds k related to the c.r.s of industrial glasses; enthalpies H in kJ/mol, entropies S and heat capacity c_P in J/(mol·K); the superscripts ° denotes standard state at 298.15 K, 1 bar, subscripts vit = vitrification;: liq = liquid state: 1673 = 1673,15 K [CON 2009]

phase k	**-H°**	**S°**	**H^{vit}**	**S^{vit}**	**$-H_{1673,\ liq}$**	**$c_{P,\ liq}$**
$P_2O_5 \cdot 3CaO$	4117.1	236.0	51.5	3417.1	898.7	324.3
Fe_2O_3	823.4	87.4	17.2	550.2	370.3	142.3
$FeO \cdot Fe_2O_3$	1108.8	151.0	31.4	677.8	579.9	213.4
$FeO \cdot SiO_2$	1196.2	92.8	13.8	962.3	342.7	139.7
$2FeO \cdot SiO_2$	1471.1	145.2	20.5	1118.8	512.1	240.6
$MnO \cdot SiO_2$	1320.9	102.5	15.1	1085.3	345.2	151.5
$2ZnO \cdot SiO_2$	1643.1	131.4	31.4	1261.1	494.5	174.5
$ZrO_2 \cdot SiO_2$	2034.7	84.5	32.6	1686.2	381.2	149.4
$CaO \cdot TiO_2$	1660.6	93.7	25.5	1365.7	360.2	124.7
$BaO \cdot Al_2O_3 \cdot SiO_2$	4222.1	236.8	95.4	3454.3	1198.3	473.2
$BaO \cdot 2SiO_2$	2553.1	154.0	26.8	2171.1	533.5	241.4
$BaO \cdot SiO_2$	1618.0	104.6	41.0	1349.8	361.1	146.4
$Li_2O \cdot SiO_2$	1648.5	79.9	6.3	1416.7	339.7	167.4
$K_2O \cdot Al_2O_3 \cdot 6SiO_2$	7914.0	439.3	29.3	6924.9	1559.4	765.7
$K_2O \cdot Al_2O_3 \cdot 2SiO_2$	4217.1	266.1	22.1	3903.7	666.5	517.6
$K_2O \cdot 4SiO_2$	4315.8	265.7	21.3	3697.8	983.7	410.0
$K_2O \cdot 2SiO_2$	2508.7	190.6	23.9	2153.1	595.4	275.3
$Na_2O \cdot Al_2O_3 \cdot 6SiO_2$	7841.2	420.1	28.4	6870.1	1512.5	648.1
$Na_2O \cdot Al_2O_3 \cdot 2SiO_2$	4163.5	248.5	27.9	3614.1	856.9	423.8
B_2O_3	1273.5	54.0	11.3	1088.7	271.1	129.7
$Na_2O \cdot B_2O_3 \cdot 4SiO_2$	5710.9	270.0	21.1	4988.0	1090.2	637.6
$Na_2O \cdot 4B_2O_3$	5902.8	276.1	40.1	4986.7	1275.5	704.2
$Na_2O \cdot 2B_2O_3$	3284.9	189.5	26.6	2735.9	780.3	444.8
$Na_2O \cdot B_2O_3$	1958.1	147.1	19.5	1585.7	538.7	292.9
$2MgO \cdot 2Al_2O_3 \cdot 5SiO_2$	9113.2	407.1	41.4	7994.8	1606.2	1031.8
$MgO \cdot SiO_2$	1548.5	67.8	13.6	1318.0	296.2	146.4
$2MgO \cdot SiO_2$	2176.9	95.4	11.0	1876.1	402.9	205.0
$CaO \cdot MgO \cdot 2SiO_2$	3202.4	143.1	25.7	2733.4	621.7	355.6
$2CaO \cdot MgO \cdot 2SiO_2$	3876.9	209.2	32.0	3319.2	775.3	426.8
$CaO \cdot Al_2O_3 \cdot 2SiO_2$	4223.7	202.5	37.7	3628.8	791.2	380.7
$2CaO \cdot Al_2O_3 \cdot SiO_2$	3989.4	198.3	49.4	3374.0	787.8	299.2
$CaO \cdot SiO_2$	1635.1	83.1	18.8	1382.0	329.7	146.4
$2CaO \cdot SiO_2$	2328.4	120.5	38.5	1868.2	509.2	174.5
$Na_2O \cdot 2SiO_2$	2473.6	164.4	13.2	2102.5	588.7	261.1
$Na_2O \cdot SiO_2$	1563.1	113.8	9.8	1288.3	415.1	179.1
$Na_2O \cdot 3CaO \cdot 6SiO_2$	8363.8	461.9	20.5	737206.0	1555.6	786.6
$Na_2O \cdot 2CaO \cdot 3SiO_2$	4883.6	277.8	13.4	4240.9	990.4	470.3
$2Na_2O \cdot CaO \cdot 3SiO_2$	4763.0	309.6	22.6	4029.6	1107.9	501.2
SiO_2	908.3	43.5	4.0	809.6	157.3	86.2

Table 2 Comparison of the chemical heat demand $\Delta H°_{chem}$ of two different E-glass batches calculated for 1000 kg glass; M = molar mass, H° = standard enthalpy [CON 2009]

	M	H°	batch 1		batch 2	
	g/mol	KWh/kg	kg	kWh	kg	kWh
sand	60.084	-4.2211	-562.0	2366.7	-562.0	2366.7
Al_2O_3	101.961	-4.5652	-144.0	657.4	-144.0	657.4
$3H_2O \cdot B_2O_3$	123.664	-4.9152	-97.3	78.2	-97.3	478.2
$Na_2O \cdot 2B_2O_3 \cdot 5H_2O$	291.292	-4.5676	-28.9	132.0	-28.9	132.0
dolomite	184.410	-3.4859	-192.8	672.1	-	0.0
burnt dolomite	96.390	-3.5634	-	0.0	-100.8	359.2
limestone	100.089	-3.3495	-211.5	708.4	-	0.0
burnt lime	56.079	-3.1449	-	0.0	-118.5	372.7
I. sum of batch			-1236.5	5014.8	-1051.5	4366.2
CO_2	44.010	-2.4837	185.0	-459.6	0.0	0.0
H_2O	18.015	-6.7284	51.5	-191.9	51.5	-192.0
II. sum of gases			236.5	-651.4	51.5	-192.0
III: glass		-4.107	1000.0	-4106.5	1000.0	-4106.5
$\Delta H°_{chem}$ = I + II + III				256.9		67.7

2.2.2 Individual raw materials and batch gases

For simple batches containing chemically pure raw materials, the equation may be evaluated in a straightforward way by using tabulated data for pure substances. This is, however, an over-simplification. The formation data of some natural raw materials deviate considerably from those of their chemically pure counterparts. Fundamentally, each of such raw materials represents an individual multicomponent mineral system of its own and has to be treated this way. Table 2 shows an example of calculating the chemical heat demand ΔH°chem of two different E-glass batches. Further details of the thermodynamic properties of batch-to-melt can be read in the book authored by Conradt: The SGTE Casebook-Thermodynamics at work [CON 2008] and continuous glass fibres Chapter 9, Section II: 'Thermodynamics of glass melting process' [CON 2009].

2.3 Thermochemistry and local reaction kinetics of batch melting

2.3.1 Thermochemistry of batch reactions

The following thermochemical reactions can be observed within the batch during the melting process [CON 1999]:

- physical melting from low temperature raw materials or eutectic reactions among the batch raw materials
- evolution of gaseous products from the decomposition of raw materials, mainly from dolomite and limestone

  $CaCO_3 \rightarrow CaO + CO_2$

- the two-step decomposition process of dolomite:

  $CaMg(CO_3)_2 \rightarrow (MgO, CaCO_3) + CO_2$,

  $(MgO, CaCO_3) \rightarrow MgO + CaO + CO_2$,

- formation of double carbonate, leads to lower melting at 785 °C

  $Na_2CO_3 + CaCO_3 \rightarrow Na_2Ca(CO_3)_2$,

- formation of the first liquid formation of eutectic reactions between silicate and soda ash via the following reaction:

  $Na_2CO_3 + n \cdot SiO_2 \rightarrow Na_2O \cdot nSiO_2 + CO_2$,

  n = ½, 1, 2 at temperature 837 °C

- formation of higher silicate melts in the limestone-containing batch in the dolomite-containing batch:

  837 °C ($NS\text{-}NS_2$) → 821 °C ($NS\text{-}NS_2\text{-}N_2CS_3$),

  837 °C ($NS\text{-}NS_2$) →731 °C ($NS\text{-}NS_2\text{-}N_2M_3S_5$),

- coal-sulphate reactions,

  $Na_2SO_4 + 4CO \rightarrow Na_2S + 4CO_2$

Water is usually added to the batch to make material handling easier and avoid dust problems due to fine particles. Water is also used to help to ease the mixing process. However, addition of water in the batch increases the energy heat demand $\Delta H°_{chem}$ and the impregnation of the soda ash-containing batch. Water in the batch influences the formation of cement phase ($CaO\text{-}SiO_2\text{-}H_2O$) and the coal-sulphate reaction at high temperature. The cullet-containing batch reactions do not have an impact on the amount of $\Delta H°_{chem}$ and react first with soda ash, limestone, and dolomite.

2.3.2 Liquid phase formation and batch-to-melt turnover

Thermodynamically, the oxide components such as SiO_2, CaO, and Na_2O in a simple glass system form eutectic melting at temperatures lower than 300 °C (see Table 3).

Table 3 Equilibrium temperatures of various eutectic phase compounds in system $NaO\text{-}CaO\text{-}SiO_2$

eutectic systems	**T_{eq} in °C**
$2Na_2O{\cdot}SiO_2$	703
$Na_2O{\cdot}SiO_2$	287
$Na_2O{\cdot}2SiO_2$	256
$2Na_2O{\cdot}CaO{\cdot}3SiO_2$	281
$Na_2O{\cdot}2CaO{\cdot}3SiO_2$	175
$Na_2O{\cdot}3CaO{\cdot}6SiO_2$	153

However, the batch-to-melt reactions occur at higher temperatures than the thermodynamically predicted temperatures. This can be explained by considering the kinetic aspects of batch melting. At lower temperatures, the batch-to-melt turnover is indicated by the atomic mobility, and restricted by heterogeneous grain sizes, grain-to-grain-contact, humidity, and temperature in the batch. A simple

description of the correlation between the reaction turnover and the atomic mobility can be seen in Equation 22.

$$reaction\ turnover = \frac{cross\ section \times mobiliy}{distance} \qquad (22),$$

Atomic movement within the grains also depends on both defect formation and thermal process at lower and higher temperatures. The batch-to-melt process yields high turnover rates as soon as the liquid phase formation is formed, and acts as a bridge which connects unreacted raw materials.

An illustration of the connection between two solid particles through the liquid phase formation can be seen in Figure 3. The easier the melt is spread through the entire batch, the higher is the atomic mobility in the system, and thus higher turnover rates of the batch-to-melt reactions. The melting properties, along with the liquid phase formation, such as viscosity and surface tension of the batch, play an important role for successful batch-to-melt conversions.

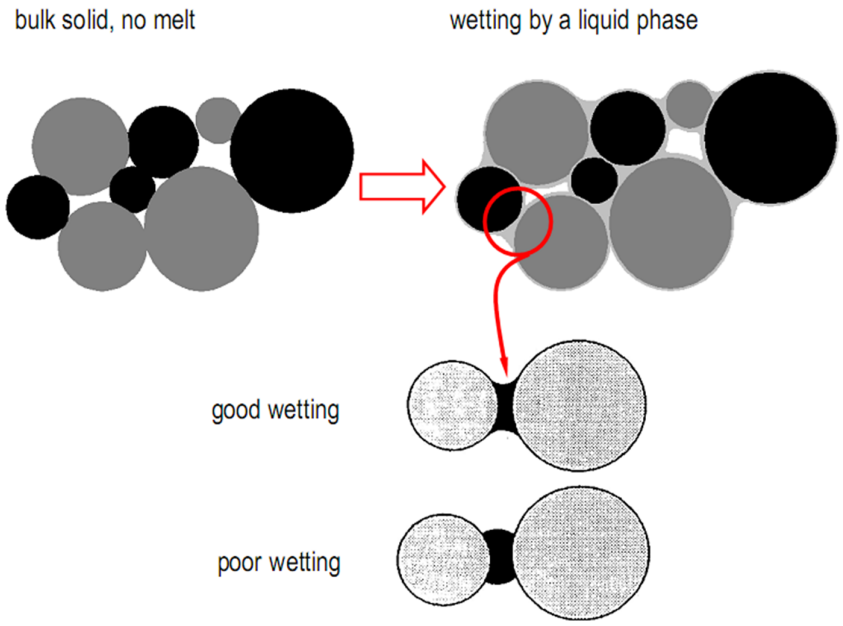

Fig 3. Illustration of the reaction steps of batch grains before and after the liquid phase formation; the pictures below show two different wetting scenarios as the liquid phase makes a bridge between two grains; [CON 1999]

2.4 Experimental assessment of batch melting behaviour

To view batch melting, one should consider both the thermodynamic and kinetic aspects. The thermodynamic aspects are associated with the theoretical heat

demand required for a batch-to-melt conversion, and can be calculated by utilizing the thermodynamic data and daily production data, such as temperatures and production rate. On the other hand, the kinetic aspects are correlated to the following occurrences within the batch:

- onset of melting/primary during the liquid phase formation
- batch gas release
- time required to reach the stage of clear melt
- dissolution rate of residual crystalline matters

These phenomena can only be quantified by performing laboratory experiments. Problems may arise in selecting suitable laboratory experiments because the results should be transferrable to the industrial scale. In other words, closing the gap between laboratory experiments and the industrial glass tank has still remained a novel and challenging task. Some approaches used for this are:

- scaling up laboratory experiments from the milligram to kilogram scale
- calculating the intrinsic heat demand of the batch-to-melt conversion
- analysing furnace performance by plotting power inputs against either the relative pull rate or power drawn from the furnace

Scaling up laboratory experiments from milligram to kilogram can be carried out, based on either the amount or size of the sample. These are:

- Microscale (milligram range of the sample). Fundamental thermochemical reactions of the batch constituents, up to ternary combinations, are evaluated. For example:
  - ♦ different thermal analysis-thermogravimetry (DTA-TG),
  - ♦ high temperature X-ray diffractometer (HT-XRD),
  - ♦ hot-stage microscopy (HSM),
- Mesoscale. The local progress of batch reactions in the range of 10 g to 400 g is characterized. The advantage of this method is that the

sample can be a complete batch with industrial grain size raw material. These methods are:

- ♦ thermo-optical observation (thermo optical measurement device and observation furnace)
- ♦ conductometry (electrical and thermal diffusivity),
- ♦ modified batch-free time (BFT),

- Kilogram scale. Up to 4 kg of batch is charged into 7 kg melting cullet at 1200 °C. A detailed description of the respective method will be discussed in the next chapter on materials and methods.

2.5 Mineralogy and petrology of borate minerals

As mentioned in Chapter 1, the application of the alternative boron oxide carriers, in terms of batch melting behaviour, were studied and investigated. The following sub-chapter is one of the results of the respective study, specifically, research on the mineralogy and petrology of borate minerals. From the literature research, one gets an ample knowledge of origins, particle size distribution, phase, and the oxide composition of borate minerals.

High demand of the high-quality optical glass at the end of the 19th century changed the role of borate from enamel glaze and ceramics to glass applications. The new discovery of large deposits of borate in North and South America at the end of the 19th century lowered the price, and borate was widely used, particularly in the production of soap and detergent. At the beginning of this century, two large borate deposits were found in Death Valley and Turkey; they played an important role in increasing the borate consumption around the world and made the US and Turkey as the largest borate producers in the world [SIM 2000]. Boron, in comparison to that of other minerals, is a minor component, even though mineralogists have identified more than 200 minerals containing boron oxide. Figures 4 and 5 show the boron deposits in the world and boron oxide production between 2002 and 2006.

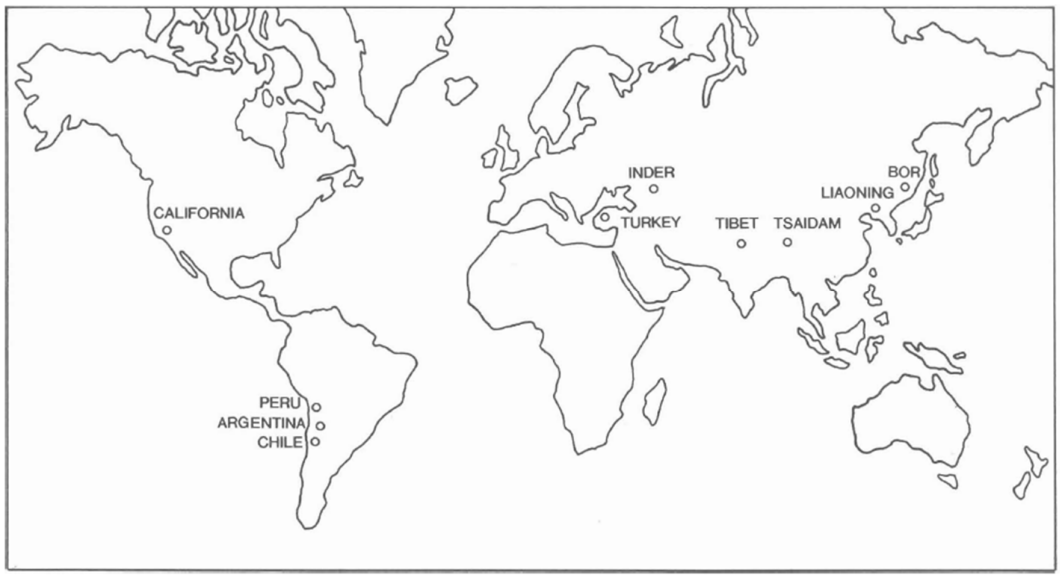

Fig. 4 Mining sites of boron oxide production around the world [KIS 1975]

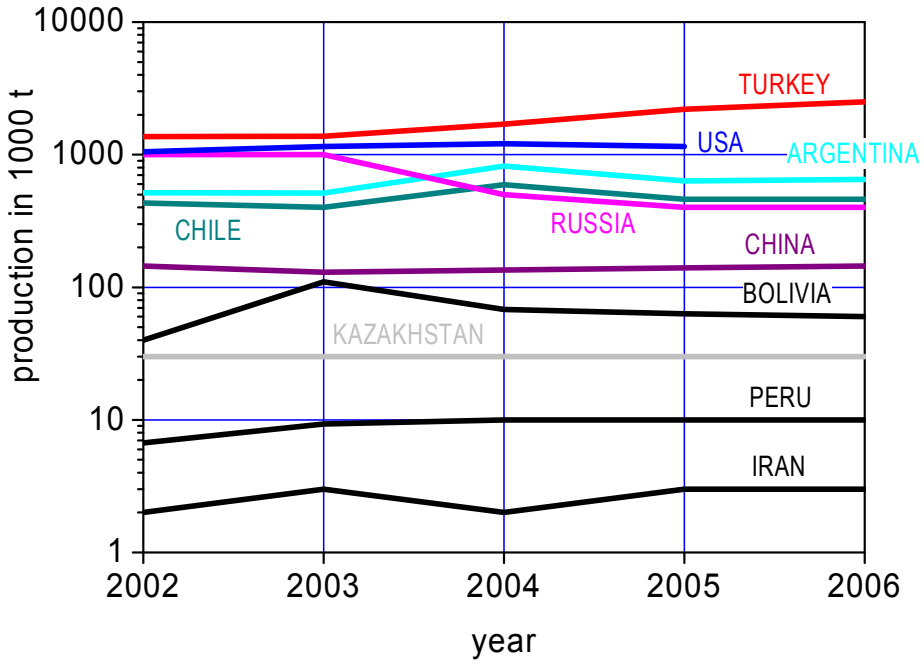

Fig. 5 Commercial production of borate minerals between 2002 and 2006 [CON 2012a]

The main deposits of borate minerals can be found along extensive deep-seated fault systems at which the Cenozoic tectonic volcanic belts pass through the regions of arid climate. The Pacific Ocean boron belts have produced deposits in

North and South America while the Mediterranean boron belts have produced large borate deposits in Turkey. The two major borate producing regions in Southern California and Turkey supply about 80% of the world's demand of borate.

In North America, sodium borates are extracted from large deposits of Boron and also as a by-product of the Searles Lake brines operations near Death Valley. In Turkey, there are three main borate production sources: Kirka which produces borax, Emet basin which produces colemanite, and Bigadic basin which produces colemanite and ulexite. Deposits of sodium-calcium-magnesium borate minerals such as ulexite, colemanite, and hydroboracite can be found in South American nations like Argentina, Chile, Bolivia, and Peru. In Asia, deposits ulexite and ascharite are found in China and Korea, respectively. A rare and an unusual borate mineral, datolite, is mined in the eastern part of Russia at Dalnegorsk; it is used mainly for the production of boric acid.

Formation of various types of borate minerals in nature largely depends on the source of their occurrence. Based on the type of occurrences, borate minerals can be classified into:

- Intrusive magmatic activities. This includes skarn-type minerals which is mainly associated with silicate and iron oxide-containing minerals (example: datollite, tourmalline, and ludwigite)
- Marine evaporite. Sediment for magnesium-containing borate minerals are the typical minerals that formed from this process
- Continental/volcanic source. It supplies 90 % of all borate minerals such as sodium borate, ulexite, colemanite, and tincal.

Natural borates are widely distributed in low concentration. They are typically found in soil and rock in concentrations of up to 450 ppm of total boron [KIS 1975], distributed in more than 150 minerals primarily as salts of sodium, calcium, and magnesium. The average of boron in surface water is 0.1 ppm and about 4.6 ppm in sea water. In general, various types of borate minerals undergo physical and chemical reactions, also known as diagenesis. Diagenesis is classified into two processes—thermal and reactive diagenesis. The first one is the alteration of a mineral mainly due to a change of temperature and pressure. The reactive

diaganesis can be defined as the change of mineral composition in the isothermal way. The burial process of borate minerals is an example of the concurrent diagenesis process. Pressure and temperature changes at different levels from surface lead to thermal diagenesis, in which the amount of water molecules change significantly. The change of type and content of cations occurs at the same temperature level, and it leads to reactive diagenesis in the burial process. This simultaneous process during burial could be the reason of the existence of alkali, alkaline earth cations as well as hydrated water molecules in natural borates.

The shift of the cations related to the species of borate minerals can be observed in the cation-water-phase diagram as seen in Figures 6 ($Na_2O \cdot B_2O_3 \cdot 4H_2O$–$2CaO \cdot 3B_2O_3 \cdot 5H_2O$–$H_2O$), Figure 7($2CaO \cdot 3B_2O_3 \cdot 5H_2O$-$2MgO \cdot 3B_2O_3 \cdot 7H_2O$–$H_2O$), and 8 for the systems $4CaO \cdot 5B_2O_3 \cdot 7H_2O$–$B_2O_3 \cdot H_2O$–$H_2O$. Hundreds of borates are identified; however, only a few of them can be applied in glass industries. Table 4 shows several natural borates and their main oxide compositions relevant to the glass applications.

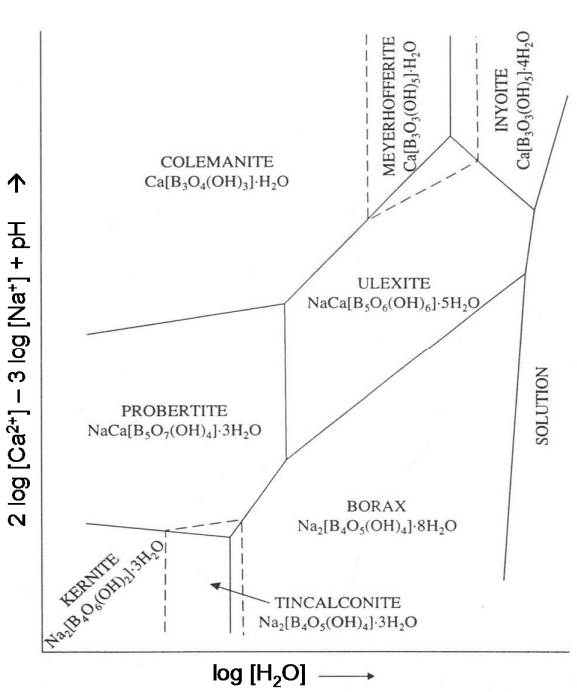

Fig. 6 Equilibrium phase diagram of $Na_2O \cdot B_2O_3 \cdot 4H_2O$ – $2CaO \cdot 3B_2O_3 \cdot 5H_2O$ – H_2O at isotherm and isobar conditions. Solid lines denote the limit of co-existence area in saturated solution; the dashed line denotes a metastable area [CHR 1976]

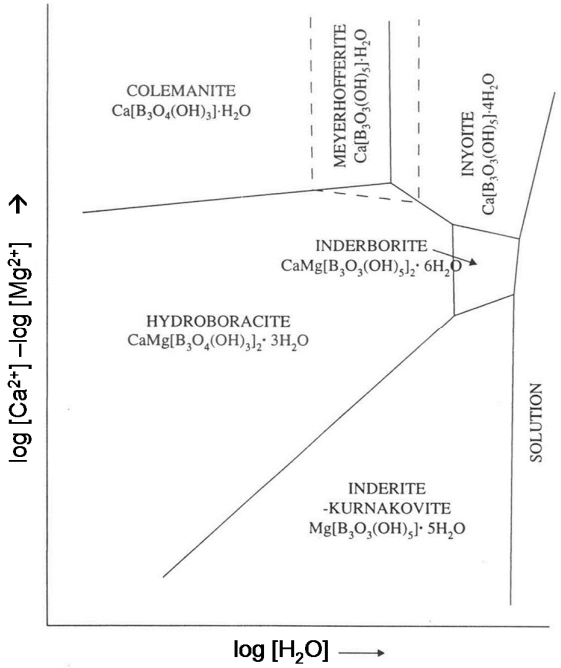

Fig. 7 Equilibrium phase diagram of $2CaO\cdot 3B_2O_3\cdot 5H_2O$ – $2MgO\cdot 3B_2O_3\cdot 7H_2O$ – H_2O [CHR 1976]

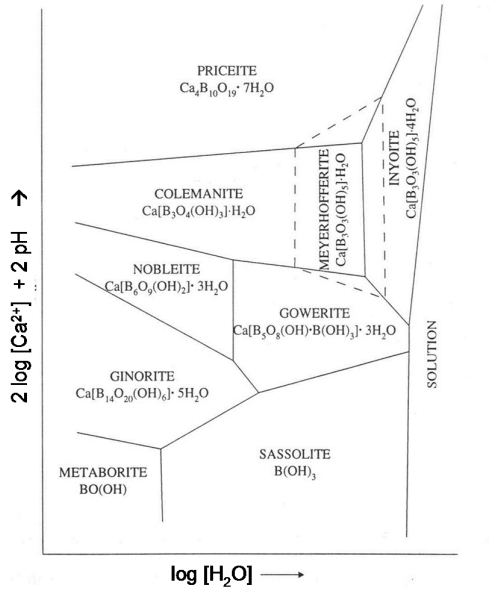

Fig. 8 Equilibrium phase diagram of $4CaO\cdot 5B_2O_3\cdot 7H_2O$ –$B_2O_3\cdot H_2O$ – H_2O [CHR 1976]

Table 4 List of natural borate minerals relevant to glass industries [CHR 1976]

name	oxide formula	B_2O_3	Na_2O	CaO	MgO	H_2O	SiO_2
sassolite	H_3BO_3	56.30				43.70	
borax	$Na_2O·2B_2O_3·10H_2O$	36.51	16.25			47.24	
kernite	$Na_2O·2B_2O_3·4H_2O$	47.97	21.35			27.93	
tincalconite	$Na_2O·2B_2O_3·5H_2O$	48.81	21.73			29.47	
ulexite	$Na_2O·2CaO·5B_2O_3·8H_2O$	42.95	7.65	13.84		35.57	
probertite	$Na_2O·2CaO·5B_2O_3·15H_2O$	49.56	8.82	15.97		26.65	
colemanite	$2CaO·3B_2O_3·5H_2O$	50.81		27.28		21.91	
inyoite	$2CaO·3B_2O_3·13H_2O$	34.62		20.20		42.18	
priceite	$4CaO·5B_2O_3·7H_2O$	49.83		32.11		18.05	
meyerhofferite	$2CaO·3B_2O_3·7H2O$	46.71		25.08		28.20	
inderite	$2MgO·3B_2O_3·11H_2O$	37.32			14.40	48.28	
szaibelyite	$2MgO·B_2O_3·H_2O$						
hydroboracite	$CaO·MgO·3B_2O_3·6H_2O$						
howlite	$4CaO·2SiO_2·5B_2O_3·5H_2O$	44.48		28.66		11.51	15.35
datolite	$2CaO·2SiO_2·B_2O_3·H_2O$	21.76		35.05		5.63	37.56
danburite	$CaO·2SiO_2·B_2O_3$	28.32		22.81			48.88

3. Materials and methods

3.1 Composition of glass batch and raw materials

Compositions of the E-glass model in the present work were derived from the eutectic composition of the system CaO-Al_2O_3-SiO_2 (CAS) and CaO-MgO-Al_2O_3-SiO_2 (CMAS). Two types of CMAS glass batches will be investigated; the first one is the B_2O_3-containing CMAS glass systems with adjusted MgO, while the second type of batch is the CMAS-based E-glass as described in the literature [WALL 2009] with variations of B_2O_3 content. The compositions are given in Table 5 below.

The amount of B_2O_3 added to the E-glass composition was adjusted accordingly by the amount of SiO_2 (see Table 6). The designations of the sample are 0B, 3B, 5B, and 7B, which correspond to B_2O_3 content of 0 wt. %, 3 wt. %, 5 wt. %, and 7 wt. % B_2O_3, respectively.

Table 5 CAS and CMAS-based E-glass target composition in wt. %

	glass systems				
oxide	**CAS**	**CMAS 1**	**CMAS 2**	**CMAS 3**	**CMAS 4**
SiO_2	62.00	61.00	61.00	57.50	56.50
Al_2O_3	14.50	16.50	13.50	13.50	13.50
B_2O_3	0.00	0.00	0.00	1.50	5.00
MgO	0.00	8.50	3.00	2.50	2.00
CaO	23.50	14.00	22.50	25.00	23.00
Sum	**100**	**100**	**100**	**100**	**100**

Table 6 Glass composition of E-glass derived from the CMAS system with varied B_2O_3 content

Oxides	**0B**	**3B**	**5B**	**7B**
SiO_2	60.0	57.0	55.0	53.0
Al_2O_3	13.5	13.5	13.5	13.5
B_2O_3	0.0	3.0	5.0	7.0
MgO	3.0	3.0	3.0	3.0
CaO	22.0	22.0	22.0	22.0

The industrial grade of silica flour, kaolin, colemanite, dolomite, and limestone were applied as oxide carriers for the following oxides: SiO_2, Al_2O_3, B_2O_3, MgO, and CaO, respectively. Very low amounts of sodium sulfate (Na_2SO_4) and coal (C) were also added to the batch as a redox and fining agent.

The oxide composition of laboratory glassware borosilicate, lamp, insulation wool, and E-glass in Table 7 are the approximated values due to confidential issues of the industrial partners. Similar to the previous studies, industrial grade raw materials were also used. Borax pentahydrate $Na_2O{\cdot}2B_2O_3{\cdot}5H_2O$ (NB_2H_5) was used as conventional boron oxide carrier, while colemanite, $CaO{\cdot}3B_2O_3{\cdot}5H_2O$ (CB_3H_5), ulexite, $Na_2O{\cdot}2CaO{\cdot}\ 5B_2O_3{\cdot}8H_2O$ ($NC_2B_5H_8$), hydroboracite, $CaO{\cdot}MgO{\cdot}3B_2O_3{\cdot}6H_2O$ (CMB_3H_6), tincal, $Na_2O{\cdot}2B_2O_3{\cdot}5H_2O$ (NB_2H_5), and kernite, $Na_2O{\cdot}2B_2O_3{\cdot}4H_2O$ (NB_2H_4), were applied as the alternative boron oxide carriers. In the laboratory glassware and lamp glass, the amounts of MgO and CaO are strictly limited. On the other hand, the total amount of alkaline oxide in E-glass fibre is limited to 1.0 wt. %. The composition of insulation wool glass is not restricted to the amount of alkaline and alkaline-earth oxides; however, care should be taken in adjusting the amount of dolomite, the only MgO and CaO carriers, since it significantly affects the viscosity range of fibrization temperature, i.e. the temperature at which log η = 3.0 dPa·s.

Table 7 Glass composition of the B_2O_3-containing glasses

	glass types			
	laboratory ware	**lamp**	**insulation**	**E-fibre**
SiO_2	77.00	68.00	64.00	54.00
TiO_2	0.05	0.02	0.25	0.40
Al_2O_3	4.00	2.00	2.50	13.50
B_2O_3	12.00	3.00	5.00	6.00
Fe_2O_3	0.02	0.07	0.10	0.30
ZrO_2	0.85	0.00	0.00	0.00
MgO + CaO	0.04	0.01	10.50	24.50
SO_3	0.01	0.00	0.10	0.05
ZnO	0.00	0.00	0.00	0.00
SrO	0.00	0.00	0.00	0.25
BaO	0.03	6.50	0.05	0.00
$Na_2O + K_2O$	6.00	19.50	17.50	1.00
CeO_2	0.00	0.90	0.00	0.00

3.2 Experimental methods

3.2.1 DTA-TG

DTA-TG is used for evaluation of the reactions that might take place in one, binary, ternary, and multicomponent systems under a particular heating rate, which, in this case, is 10 K/min. Figure 9 shows a typical curve produced from the DTA-TG measurement in a glass batch. The general principle of DTA measurement is simultaneous heating/cooling of test sample and an inert reference. Any changes in the sample, resulting in the absorption or evolution of the heat, can be detected as temperature differences between the sample and the inert reference. Thus, each physical reaction creates a peak related to either the endothermal or exothermal reactions. In many cases, the DTA peak for the endothermal reaction is towards a negative value of the DTA signal, and positive value for the exothermal reaction. Typical endothermal reactions that can be detected by the DTA-TG measurement are the dehydration process (removal of physical or crystallized water), dehydroxylate (removal of –OH from the main structure), phase transformation, gas evolution, and melting. Both dehydration and

gas evolution are usually followed by a reduction of the sample mass, which can be evaluated through the TG curve. Therefore, the endothermal peak, followed by the mass loss, is associated with the physical reactions that involve mass reduction. In general, exothermal reaction refers to the process of crystallization within the batch, and is not followed by the mass loss.

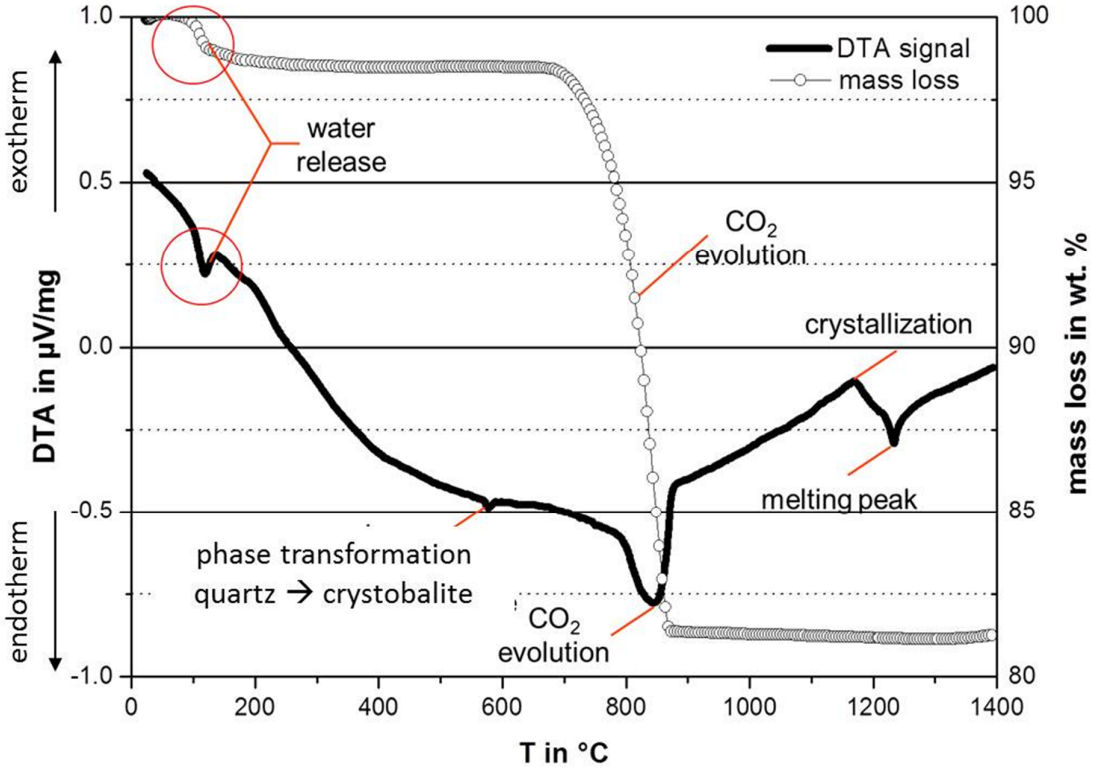

Fig. 9 The result of a typical DTA-TG analysis of a single, binary, and ternary batch. Water release and gas evolution are typical endothermal reactions followed by the mass reduction. Melting reaction is normally indicated by the endothermal reaction without mass loss.

3.2.2 Conductometry

Moving to larger experiment scales, in which the multicomponent system and particle size distribution as well as grain size of the real glass batch can be easily compensated, the conductometry method was conducted in a 200 g sample. Figure 10 shows a schematic diagram of the self-developed conductometry method. Voltage drop Ux that is associated with electrical resistivity, and ion

conductivity of the batch, are measured through multimeter KEITHLEY™ model 2800.

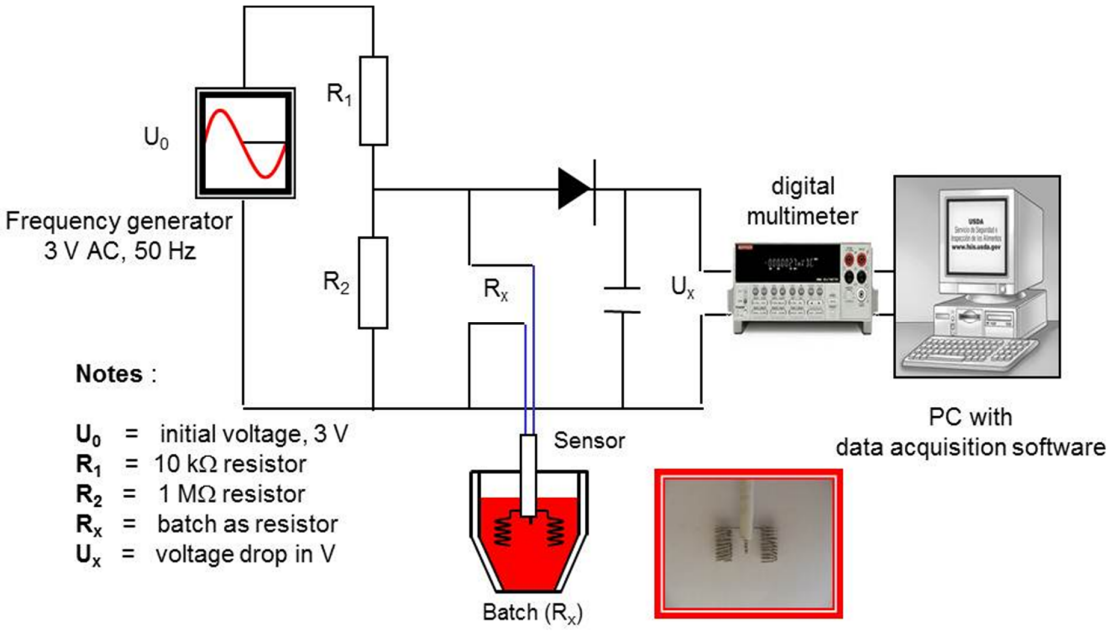

Fig. 10 Schematic diagram of an experimental set-up of conductometry measurement of the batch [CON 1994]

The following equation explains the physical relationship between resistivity and conductivity:

$$\kappa = \frac{C_{cell}}{R_x} \tag{23}$$

with C_{cell} as a cell constant; C ≈ 1 cm^{-1}. R_x can be calculated by the principle of combination series and parallel electrical circuit from Figure 10 .

$$\frac{1}{R_y} = \frac{1}{R_x} + \frac{1}{R_2} \tag{24}$$

$$R_y = \frac{R_2 \cdot R_x}{R_2 + R_x} \tag{25}$$

R_y is a substitute electrical resistor of the parallel circuit between R_x and R_2. The recorded U_x are converted to batch resistivity R_x by applying the Kirchoffs equation (see Equation 26 and 27) in which the current flow from U_0 through R_1 and R_y is similar to that of from U_x through R_y.

$$\frac{U_x}{R_y} = \frac{U_0}{R_2 + R_y} \tag{26}$$

$$R_x = \frac{U_x \cdot R_1 . R_x}{R_2 \cdot (U_0 - U_x) - U_x \cdot R_1} \tag{27}$$

A special solenoid-type sensors (snippet picture in Figure 10) is applied to measure the electric resistance under the Alternating Current (AC) circuit. The resistors R_1 and R_2 are 1 MΩ and 10 kΩ, respectively, and used for smoothing the measured R_x signal. Voltage drop U_x is measured continually and is treated as an indicator of the change of electrical resistance within the batch. This measurement is recorded through the data acquisition board installed in the personal computer, along with the batch (T_b) and furnace temperature (T_o). This method is not intended to accurately measure the absolute value of the conductometry, but to give an overview of the occurrences in the batch during heating. Fingerprints of the reactions occurred within the batch can be observed. Interpretation of the conductivity curve as a function of batch temperature can be seen in Figure 11.

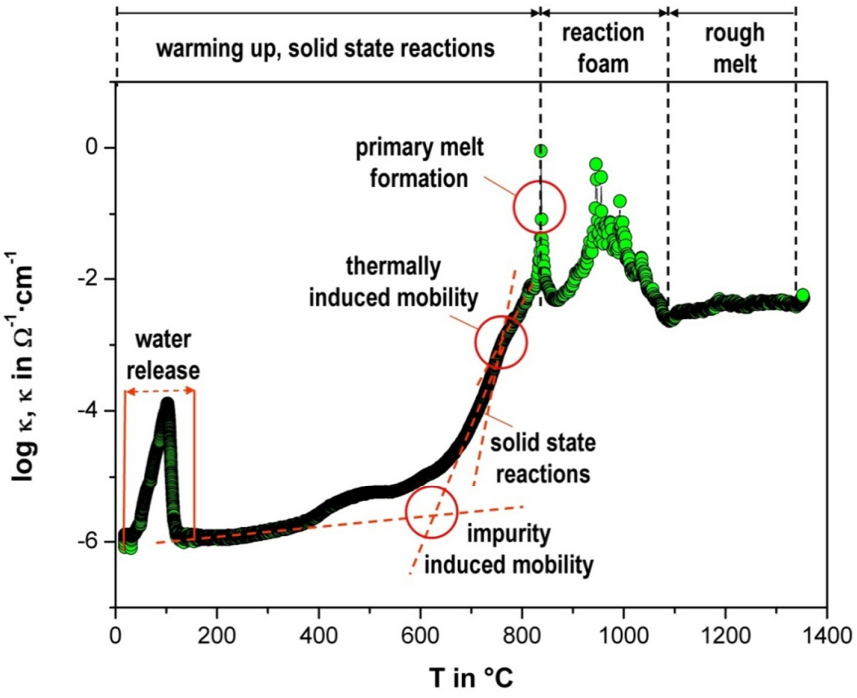

Fig. 11 Interpretation of the local batch melting reactions of soda-lime silicate glass via the conductometry measurement as a function of batch temperature

There is no change in the conductivity value at low temperatures due to very low ion mobility and insufficient grain-to-grain-contact reactions within the batch. Conductivity increases gradually as impurities via the vacancy diffusion mechanism induce ions to be more mobile. At higher temperatures, the ion mobility is thermally induced, which is indicated by the steep ascending conductivity curve. The formation of primary melt is unambiguously indicated by the conductivity jump up to three or four order of magnitude [CON 1994].

The conductivity sensor during the reaction foam measures portion of melt, bubbles as well as un-melted batch constituents rapidly, which leads to chaotic/up and down conductivity signal. The conductivity value becomes steady after a rough melt is formed within the batch. From this point, the batch melting process is solely a dissolution process of residual sand grains. The following figures show the combined graph of DTA and the conductometry (κ) signal as a function of batch temperature. This gives a comprehensive analysis of the batch occurrences of during melting under 10 K/min heating rate.

3.2.3 Observation furnace

The observation furnace method is another batch melting characterization in which batch occurrences is visually observed during the melting process. An experimental set-up is illustrated in Figure 12. A 50 cm-long special quartz glass, with 3 and 4 cm inner and outer diameter, respectively, is transparent and suitable for being used as a crucible in this method. The amount of charged batch is 30 g. The height of the crucible, with respective amounts of sample, should be adjusted to have an optimum observation, especially during the end of the foaming phase. All batch melting processes are conducted with the 10 K/min heating rate from room temperature to 1400 °C. Calibration of batch temperature was conducted prior to the test, in which the furnace temperature was compared to that of the temperature of the known melting point of substances, e.g. NaCl, K_2SO_4, among others. The batch melting process was captured by an analog video camera and directly recorded into DVD media.

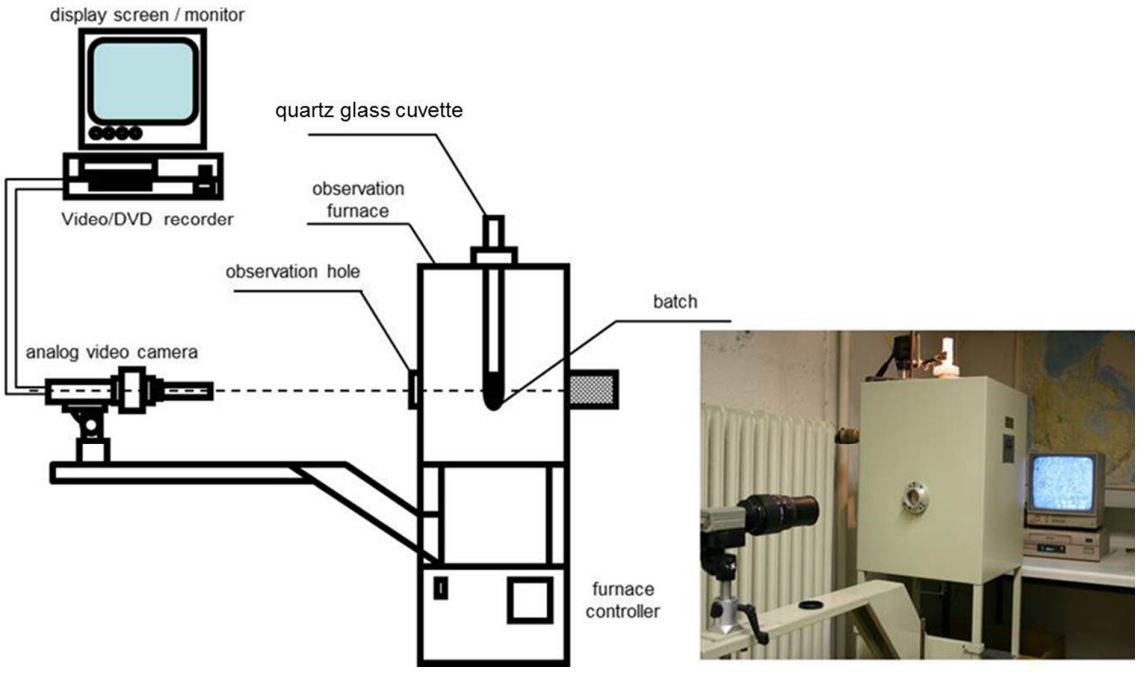

Fig. 12 Schematic diagram of an experimental set-up of observation furnace in which the batch melting process is optically observed through the analog video camera

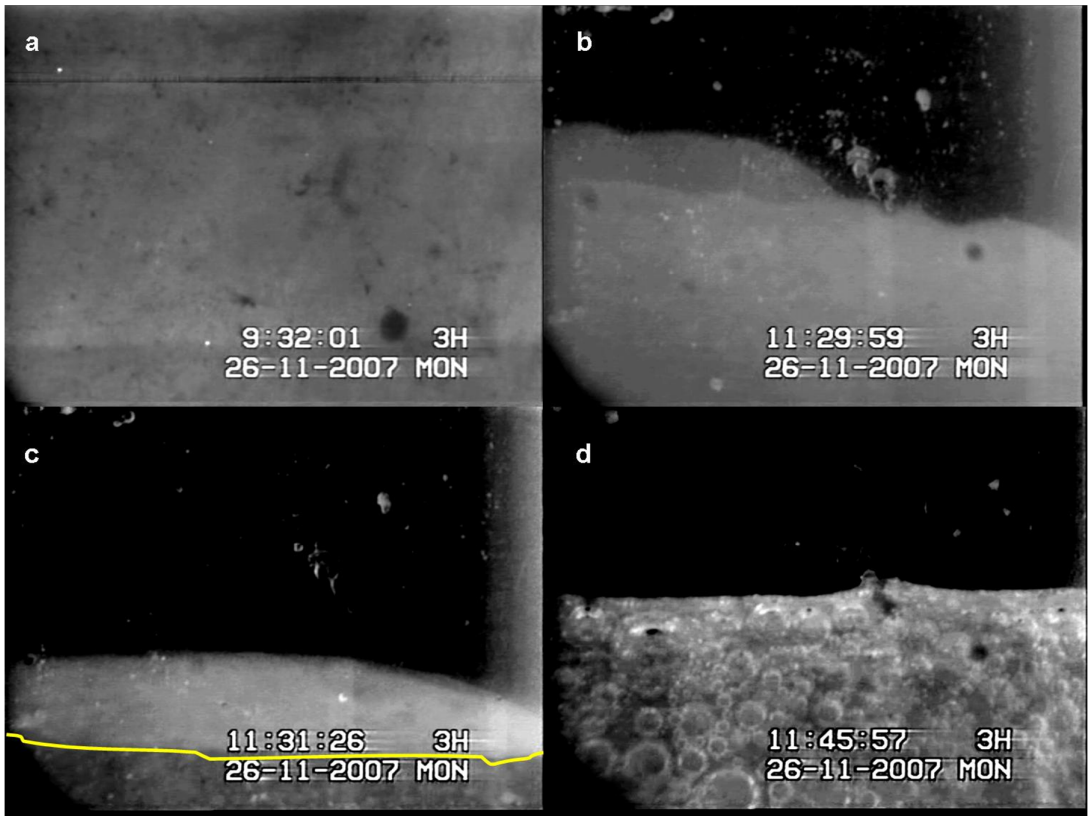

Fig. 13. Analysis of the results of analog video recorded during the observation experiment; a) starting condition; b) beginning of solid-state reactions (onset of melting); c) liquid phase formation (yellow line separates solid and liquid phase of the batch); and d) bubble followed by foam formation

3.2.4 Modified batch-free time (BFT)

Originally, batch-free time (BFT) is defined as the time required for a batch to melt or dissolved 98 % in molten glass melt [BUN 1969]. In the present study, BFT is modified to give immediate judgment on the melting behaviour of two or more batches.

Preliminary test using reference batch is usually performed for different time windows. The objective is to find suitable time frames, t_2 and t_3 which denotes time at which degree of batch dissolution in the melt is approximately 50 % and 100 %, respectively. The BFT experiments for the rest of the batch sample follow those t_1 and t_2.

To avoid the cracks that may develop due to internal stress during cooling, the BFT probe is annealed in another furnace. The annealing process is programmed

at around the glass transition temperature T_g , and then, it is cooled at a slow cooling rate of 2 K/min. Visual examination of the surface condition of the sample includes calculation of the percentage dissolution rate of the batch and identification of undissolved batch, such as foam, bubbles or crystalline matters, and crystalline scums.

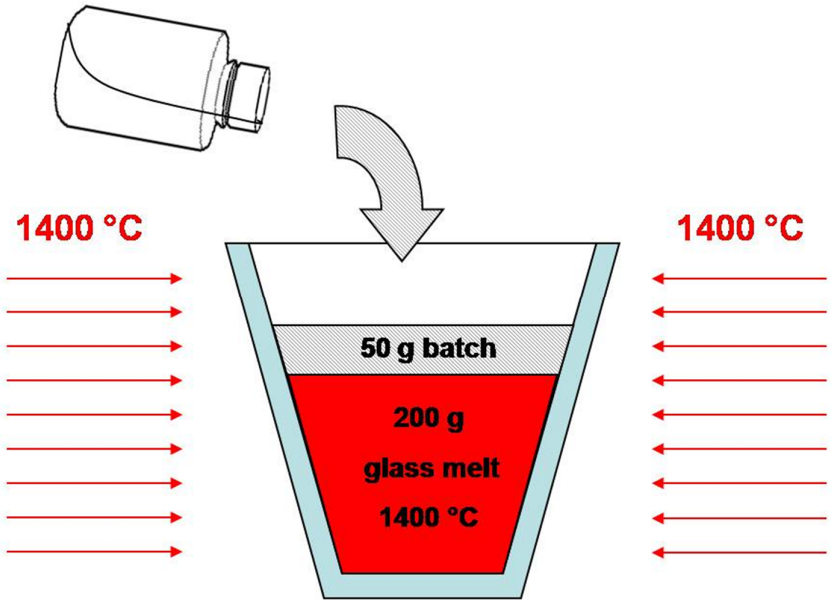

Fig. 14 Illustration of batch melting characterization via the batch-free time (BFT) test. The batch is charged into a pre-conditioned melt at 1400 °C; the modified BFT compares the melting progress of two or more batches, in which one of those batches is set as a reference batch

3.2.5 10 kg test

In the 10 kg range test, the type of the experiment becomes more realistic to the batch heap condition in a typical industrial tank. Different from the BFT test in which both radiation-conduction temperatures are kept constant (1400 °C), the 10 kg test utilizes 7 kg of molten glass kept at 1200 °C for several hours, and a 4 kg batch that is exposed to the radiation heat of 1400 °C as soon as the charging is completed. The progress of batch melting is observed by analysing five temperatures from type-K (NiCr-Ni) thermocouples, which were vertically set up with 1 cm distance between each of the thermocouples inside the batch (see Figure 14). Temperature profile obtained from the measurement (see Figure 15) gives an insight of the time required for the batch to finish endothermal reactions

(t_{endo}). At the end of the experiment, temperature differences (ΔT in K) between melt side position (T_2) and outer thermocouple on fire side position (T_5) is then calculated to see the heat distribution from melt and fire side after a particular melting time. Effective thermal diffusivity ***a*** can also be derived from this experiment by applying the second law of Fourier's heat transfer.

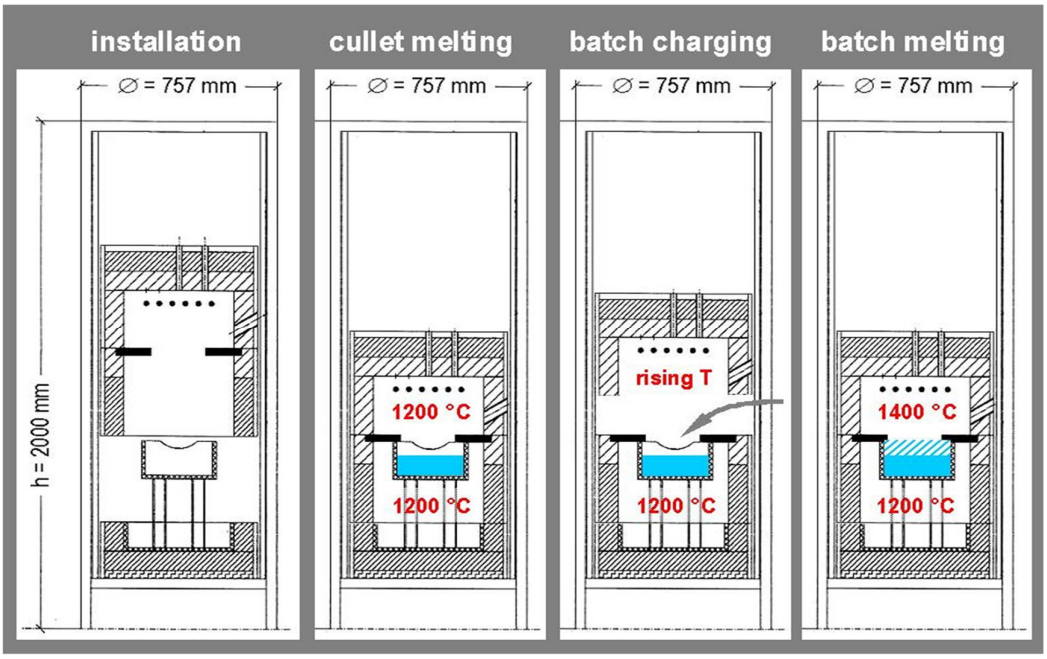

Fig. 15 Illustration of an experimental set-up for the 10 kg range test. In the beginning, 7 kg glass cullet is melted and conditioned at 1200 °C; batch charging is the next step, and temperature of the upper part of the furnace is increased to 1400 °C

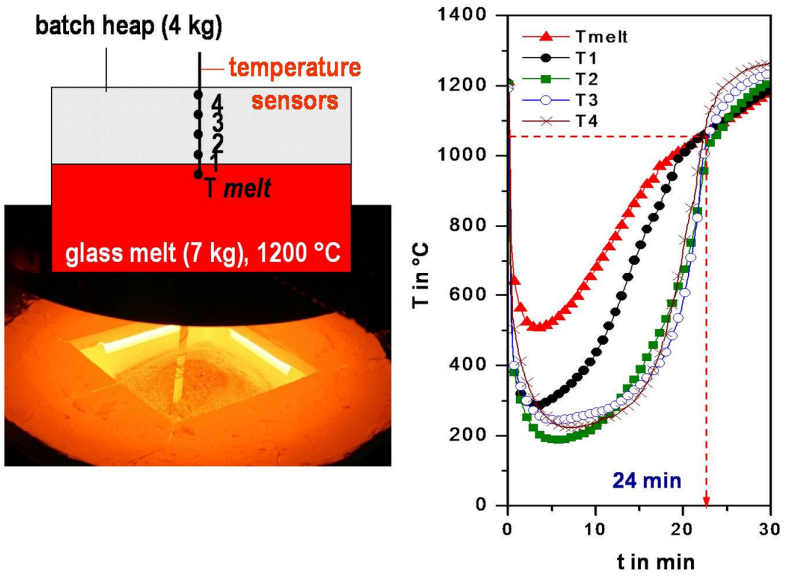

Fig. 16 Vertical set up of five thermocouple (T_{melt}, T_1, T_2. T_3, T_4, T_5) within the batch. The picture on the right shows the temperature distribution after the test

The possibility of uncertainty in measuring temperature field is higher under the high heat flux and electromagnetic field, compared to other methods. It is then necessary to assess its reproducibility by performing a double test. Table 8 shows the previous reproducibility tests in which the 10 kg test was applied twice to one type of batch with the same conditions (see Figures 17 and 18 for the double test results).

Table 8 Results of 10 kg duplicate test of six different batches

double test no.	$t_{endo} \pm 3\sigma$ **[s]**	$\Delta T \pm 3\sigma$ **[K]**
1	772 ± 7	45 ± 9
2	1506 ± 54	65 ± 11
3	1366 ± 1	62 ± 7
4	1304 ± 1	56 ± 8
5	1443 ± 5	69 ± 15
6	1066 ± 32	105 ± 8

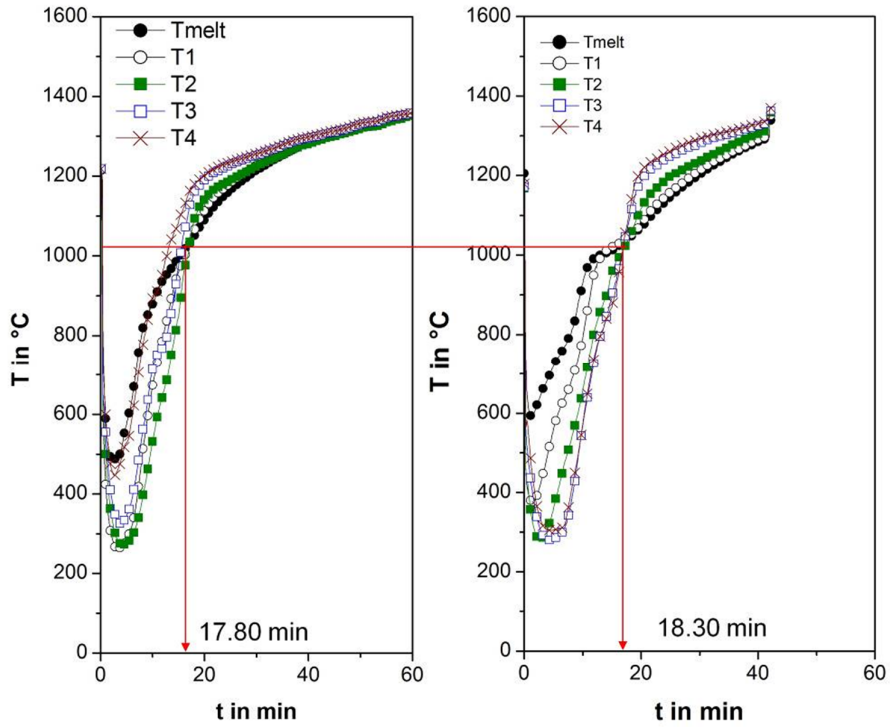

Fig. 17 Reproducibility of the 10 kg test of a particular batch. Only slight differences of t_{endo} of both batches were observed

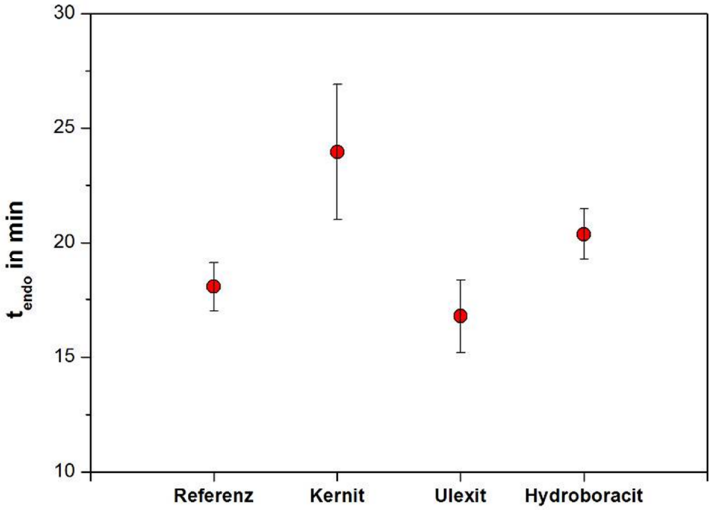

Fig. 18 Average value of t_{endo} in the double 10 kg tests; the error bar indicates upper and lower limit of three times standard deviation (± 3σ).

3.3 Phase equilibrium analysis

The additional phase equilibrium calculation is performed to provide a comprehensive analysis of the phase equilibrium of a particular glass oxide system. A commercial thermodynamic software, FactSage™, was utilized to calculate the phases of a given glass composition in equilibrium state, including the amount of liquid phase that may be formed from the cooling scenario. It is assumed in the calculation that the cooling scenario of glass melt forms a crystalline material, which, in reality, is not always the case. One can distinguish between the glassy and crystalline states from the energy point of view by considering an additional enthalpy unit, ΔH^{vit} , for the glass at lower than the glass transition temperature. This enthalpy difference can be used to calculate the enthalpy energy of the glass at room temperature. The thermodynamic calculation helps the batch melting technologist to understand the reactions (crystallization and phase transformation) prior to the primary melt formation, or liquidus temperature as in the present study.

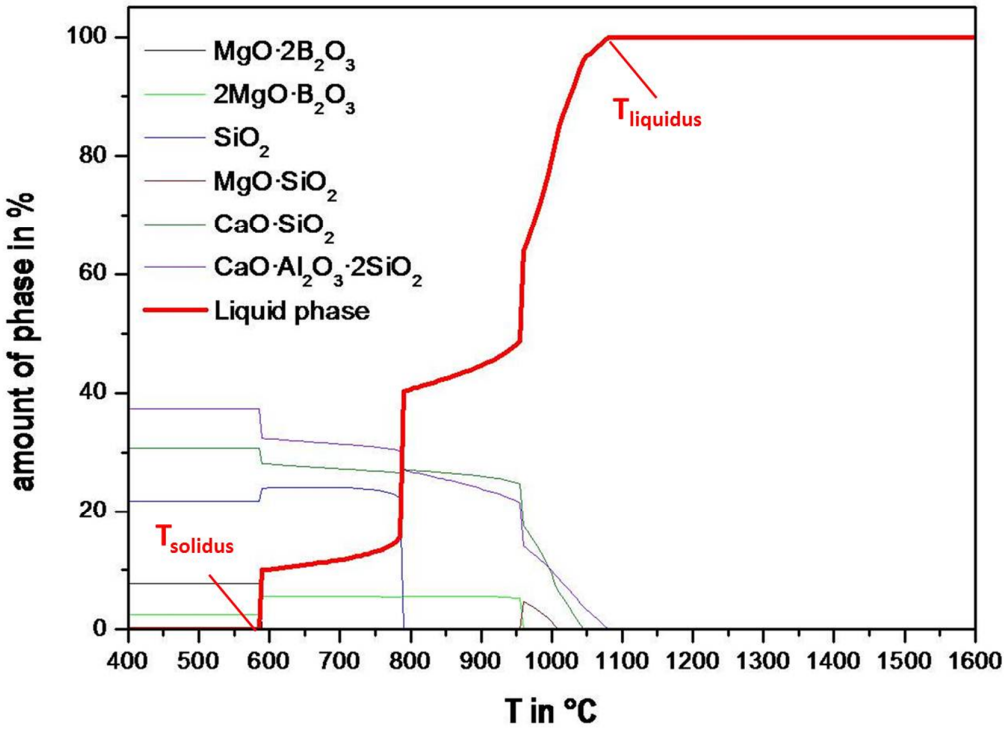

Fig. 19 An example of the equilibrium phase calculation by using the commercial thermodynamic software FACTSAGE™

4. Results and discussions

4.1 $CaO\text{-}Al_2O_3\text{-}SiO_2$ (CAS) and $CaO\text{-}MgO\text{-}Al_2O_3\text{-}SiO_2$ (CMAS) E-glass

It is the objective of the present study to characterize the batch melting of an alkali-free glass batch. The scope of batch melting experiments was limited to DTA-TG which represents the conventional method, while, for newly developed methods, conductometry and observation furnace were implemented. The experiment results are compared to the equilibrium phase calculation to obtain a comprehensive analysis of the batch melting behaviour.

4.1.1 DTA-TG

The total mass loss of the CAS system is relatively minor so as to be characterized as the gas evolution phenomena (0.61 wt. % of mass loss), and hence, the endothermal peak of quartz-crystobalite phase transformation at 581 °C in Figure 20 should not be interpreted as the mass reduction phenomena since it was not followed by a decreasing TG curve.

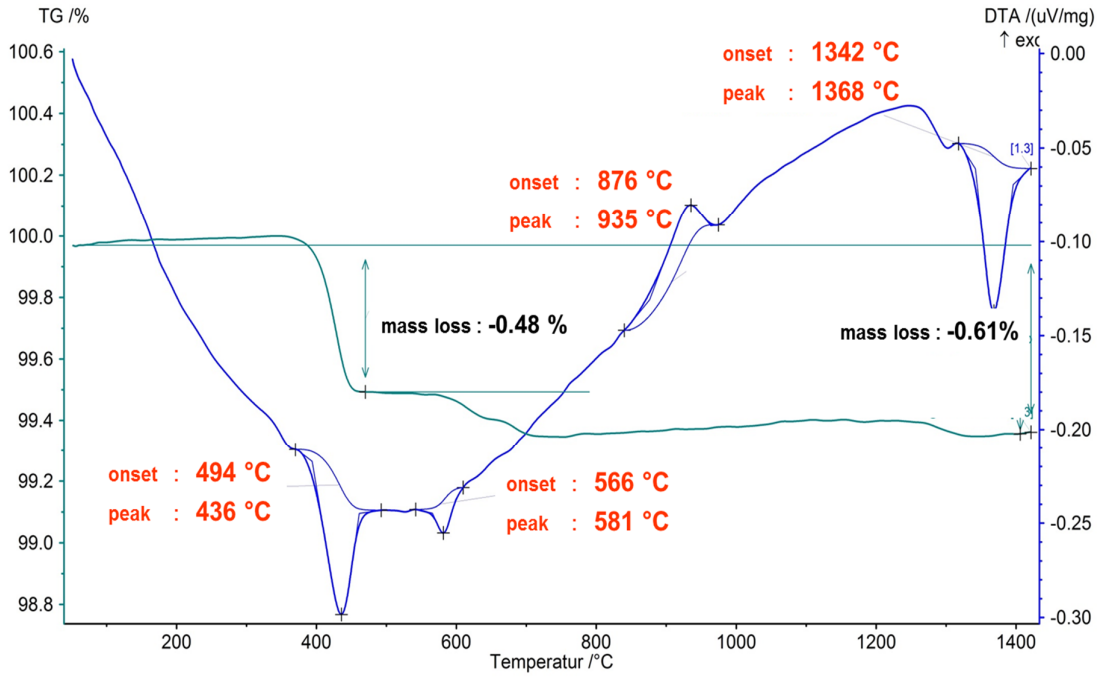

Fig. 20 DTA-TG results of the CAS system under 10 K/min heating rate.

Moisture content from the environment or water crystal in each substance might be the reason for the mass reduction observed by DTA-TG. An exothermal peak was also observed between 876 °C and 980 °C, which could be associated either with the crystallization phenomena or with the structural change in the sample. The endothermal peak in temperature range of 1340 °C and 1370 °C was denoted as the liquid phase formation. The formation of the liquid phase in the CAS system is strongly related to the eutectic reactions among the batch constituents; for, in the respective system, the melting point of individual oxide is higher than 1400 °C. Both the temperatures of onset and maximum peak were at 1342 °C and 1368 °C, respectively. These values, however, are significantly different to the liquidus temperature predicted by the respective phase diagram, 1170 °C.

Figures 21 and 22 show the DTA-TG curve of the CMAS systems. The quartz inversion is difficult to observe, and probably was superimposed by the broad dehydration endothermal peak from 470 °C to 600 °C. Different shapes and positions of the endothermal peak at 800 °C, which is followed by a higher amount of mass loss due to gas evolution, were observed for both the CMAS systems. The gas evolution is mainly outcome of carbonate decompositions from limestone ($CaCO_3$) and dolomite ($Ca,Mg(CO_3)_2$). Similar patterns for crystallization and melting peaks lie at temperatures beyond 1000 °C.

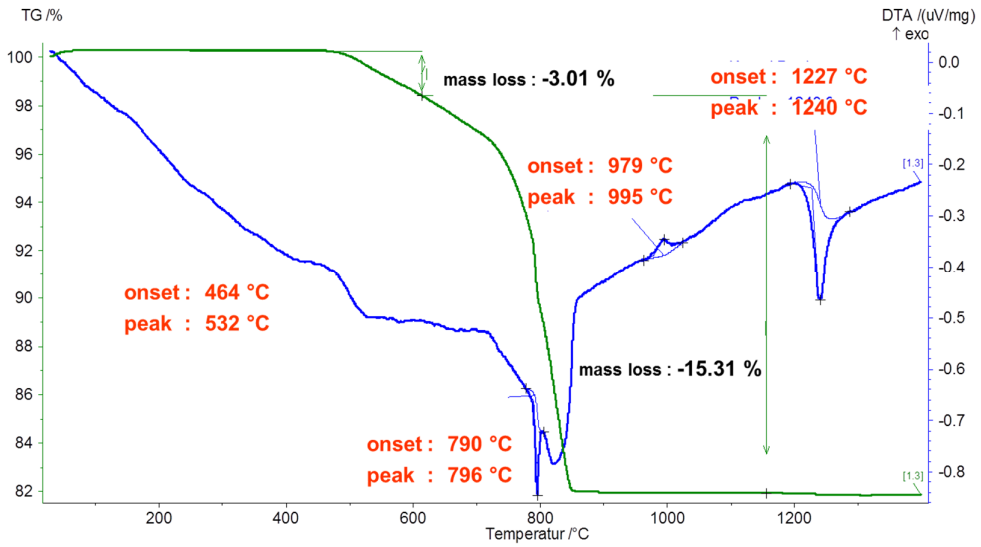

Fig. 21 DTA-TG of the CMAS system 1 (with 8.5 wt. % MgO) under 10 K/min heating rate

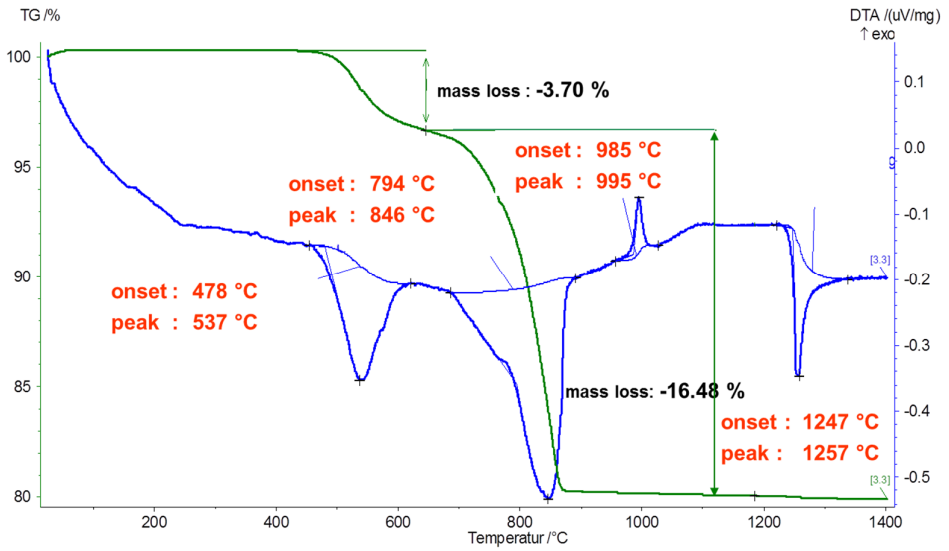

Fig. 22. DTA-TG of the CMAS system 2 (with 3.0 wt. % MgO) under 10 K/min heating rate

Identical to the CMAS systems, the endothermal peak for quartz inversion in the E-glass systems in Figures 23 and 24 was also obscured by another endothermal peak at temperatures between 400 °C – 600 °C. The gas release occurs at 800 °C for both the E-glass systems. However, crystallization and melting peaks in the E-glass with 1.5 wt. % B_2O_3 shift to higher temperatures, compared to the 5.0 wt. % B_2O_3 E-glass system.

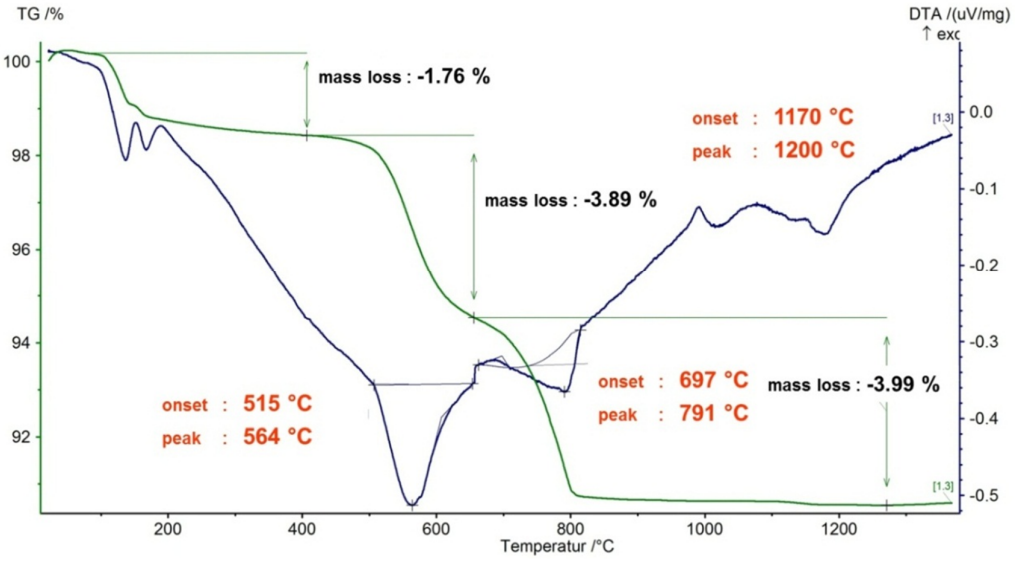

Fig. 23 DTA-TG of the CMAS-derived E-glass system 1 (with addition of 1.5 wt. % B_2O_3)

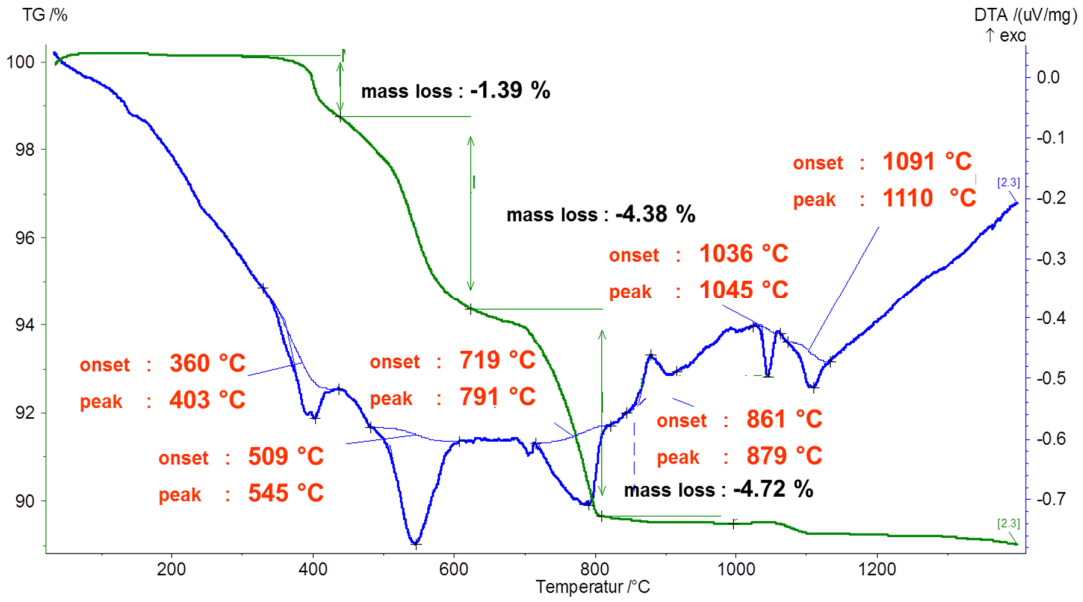

Fig. 24 DTA-TG of the CMAS-derived E-glass system 2 (with addition of 5.0 weight. % B_2O_3)

4.1.2 Conductometry

In the CAS system, there was no significant conductivity increase below 1200°C; however, the DTA curve shows two endothermal peaks, specifically at 430 °C and 580 °C and they refer to the release of structural water and quartz-to-crystobalite phase transformation. The onset of melting in the DTA curve, accompanied by the increase of κ signal and the κ jump at 1368 °C, coincides with the melting peak of the DTA signal.

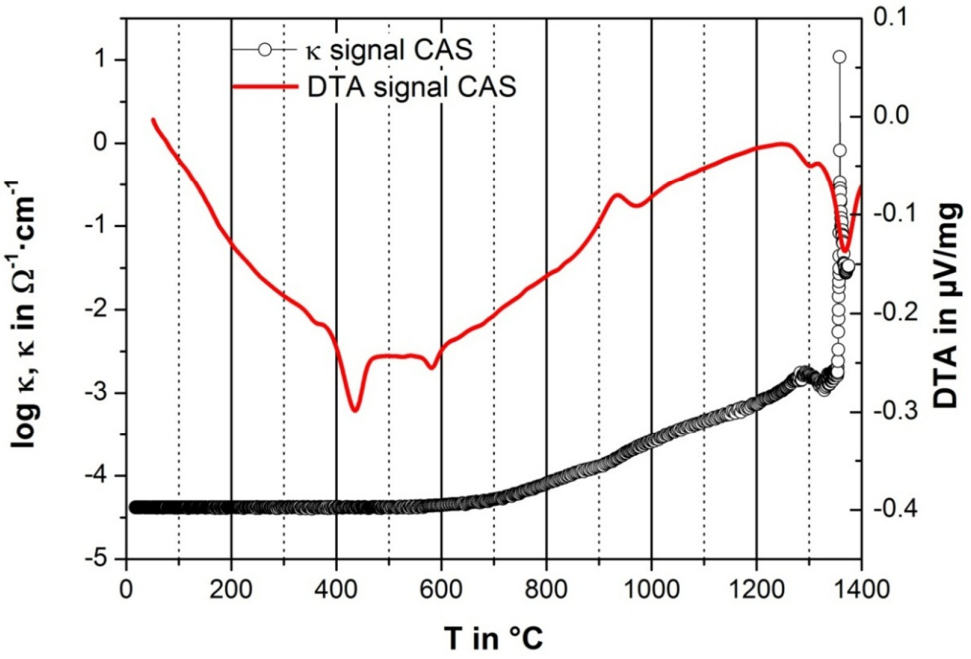

Fig. 25 DTA and the conductometry (κ) signal as a function of the batch temperature of CAS system

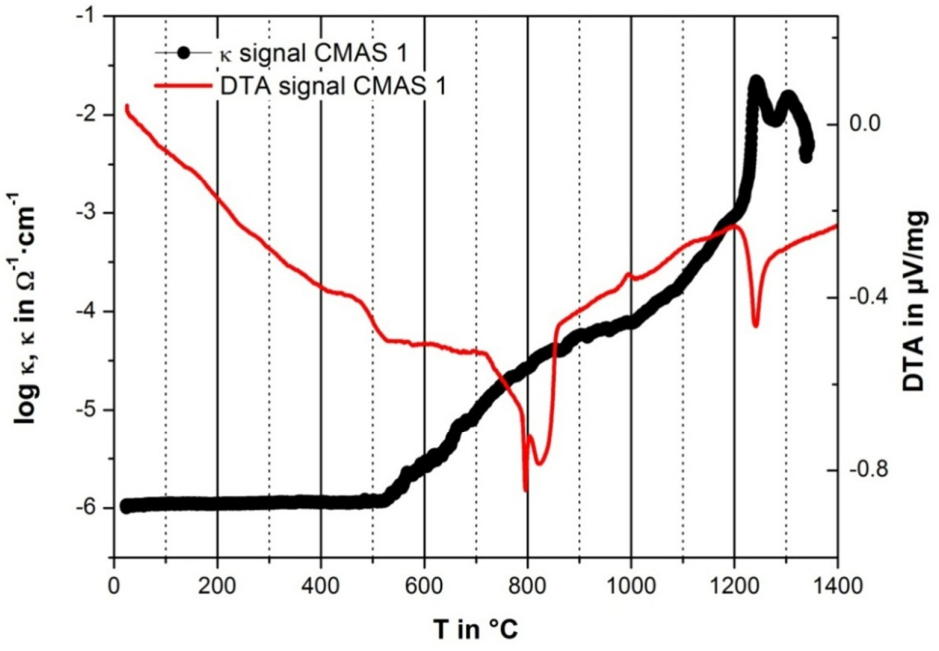

Fig. 26 DTA and conductometry (κ) as a function of the batch temperature of a CMAS system 1 (with 8.5 wt. % of MgO)

Figure 26 shows a CMAS system with 8.5 wt. % MgO. It is different from Figure 25 for the CAS system, solid state reactions as it is denoted by the gradual increase of κ, started at 500 °C, coincided with the DTA signal for the dehydration process. As the reactions within the batch occur, they are followed by the change of the κ signal. The gradient of κ shifts during the endothermal peak for the gas evolution observed by the DTA signal at 800 °C. During the exothermal process, indicated by the DTA signal at 1000 °C, the slope of the κ signal changed towards a higher conductivity value. Steep increase of the conductivity signal, associated with the onset of melting in the DTA curve, is consistent with the results of the CAS system. The melting peak in the DTA curve corresponds to the κ jump at 1240 °C.

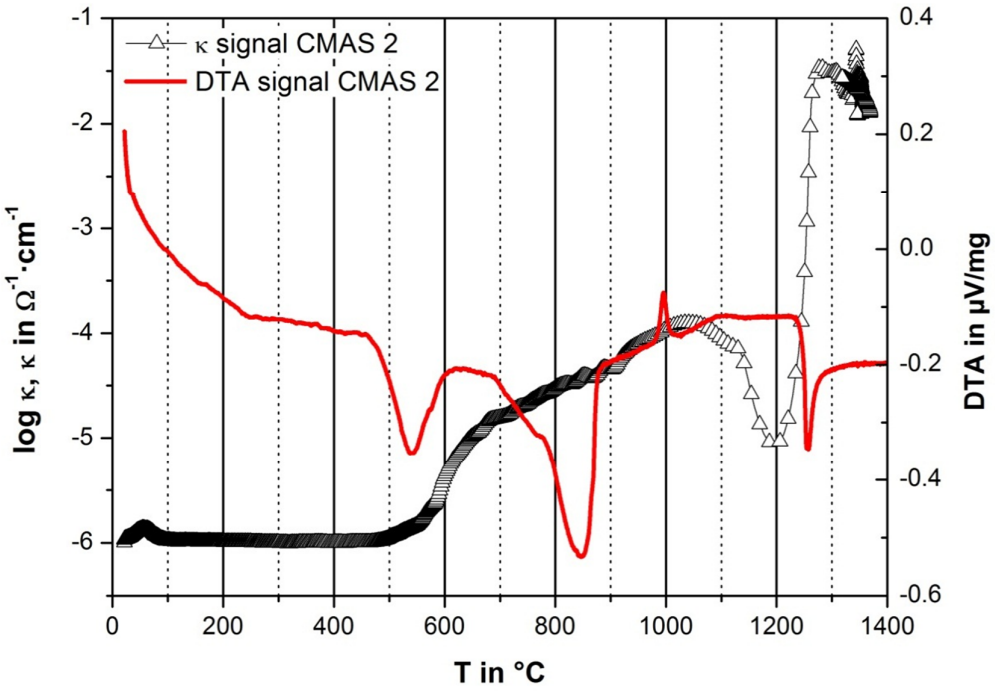

Fig. 27 DTA and conductometry (κ) as a function of the batch temperature of CMAS system 2 (with 3.0 wt. % of MgO)

Melting behaviour of CMAS 2 with 3.0 wt. % of MgO can be evaluated from Figure 27. Similar to CMAS 1, the conductivity change corresponds to the reactions detected by the DTA measurement. However, the κ changed towards more negative value after the completion of crystallization peak in the DTA signal. This

unexpected phenomena could be the effect of solid-state reactions occurred in the batch, e.g., shrinking or sintering process among the batch constituents in which the sensor could not detect the overall bulk solid (the value of the conductivity signal changed towards the starting value log κ = -6). However, as the batch begins to melt, steep increase in the κ signal is observed. This abrupt increase coincides with the DTA signal at 1274 °C and reaches its maximum at the same temperature of the maxima of the melting peak in DTA signal. Due to the lower amount of MgO than in CMAS 1, the peak temperature shifts to 15 °C higher. The addition of MgO into the CAS system gives significant impact on the formation of primary melt in the batch, by altering the liquidus temperature of the respective system.

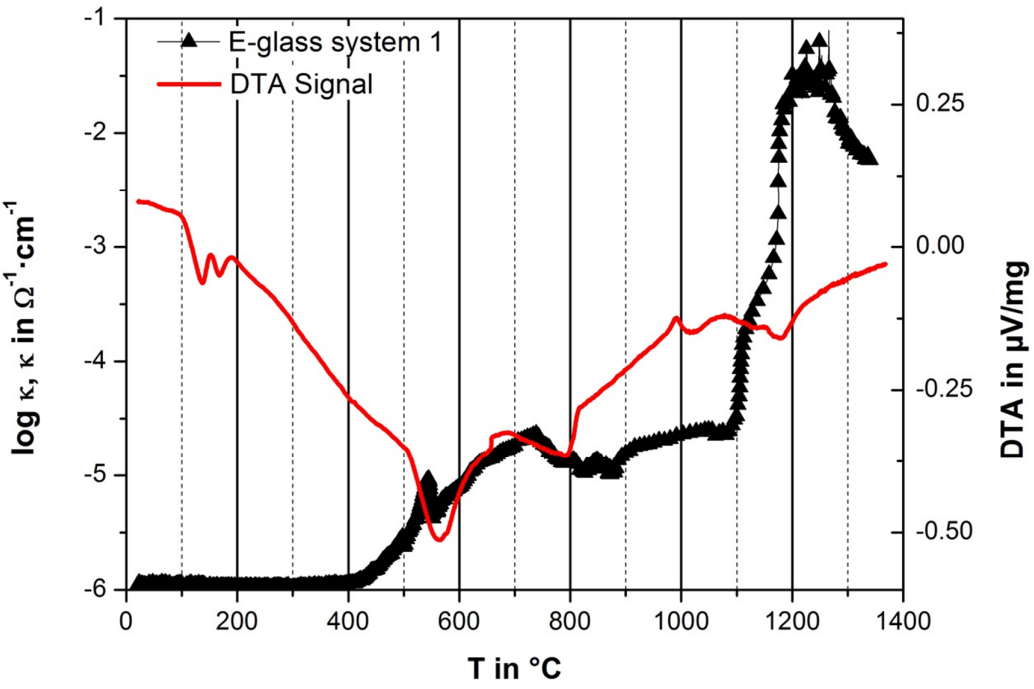

Fig. 28 DTA and conductometry of the CMAS-based E-Glass system 1 (with 1.5 wt. % B_2O_3)

Figure 28 shows the DTA and conductometry results of the CMAS-based E-glass batch, with an additional 1.5 wt. % B_2O_3. The quartz inversion and dehydration reactions were characterized by the endothermal DTA signal at 580 °C; however, the increase conductivity started at a lower temperature. The exothermal peak in

DTA signal refers to the crystallization phenomena within the batch. The significant increase of conductivity curve occurred at the same temperature as the onset of the melting peak of the respective DTA signal. Conductivity jump coincides with the melting peak of the DTA signal at 1200 °C.

In the high B_2O_3-containing E-Glass system (see Figure 29), a similar pattern can be observed that the reactions determined by the DTA measurement always correspond to the change of conductivity.

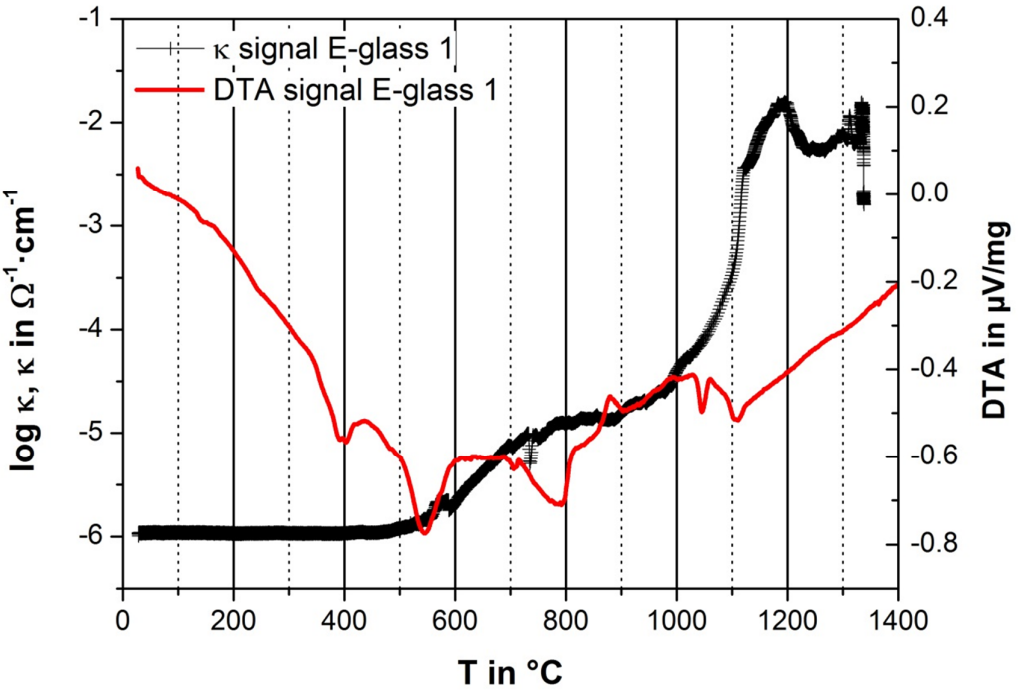

Fig. 29 DTA and conductometry of the CMAS-based E-Glass system (with 5.0 wt. % B_2O_3)

There are similarities in characterizing the melting process between the DTA and the conductometry of various CAS and CMAS glass systems. The gradual increase of conductivity corresponds to the solid-state reactions, quartz inversion, and crystallization as premised by Conradt et al. [CON 1994]. Only the evolution of the gas product is difficult, or even impossible to detect by the means of conductometry measurement. A rapid increase of conductivity signifies liquid phase formation in the system, and the conductivity jump coincides with the melting peak of the DTA signal.

4.1.3 Observation furnace

Figure 30 summarizes the experiment results of different types of alkali-free glass batch via the observation furnace method.

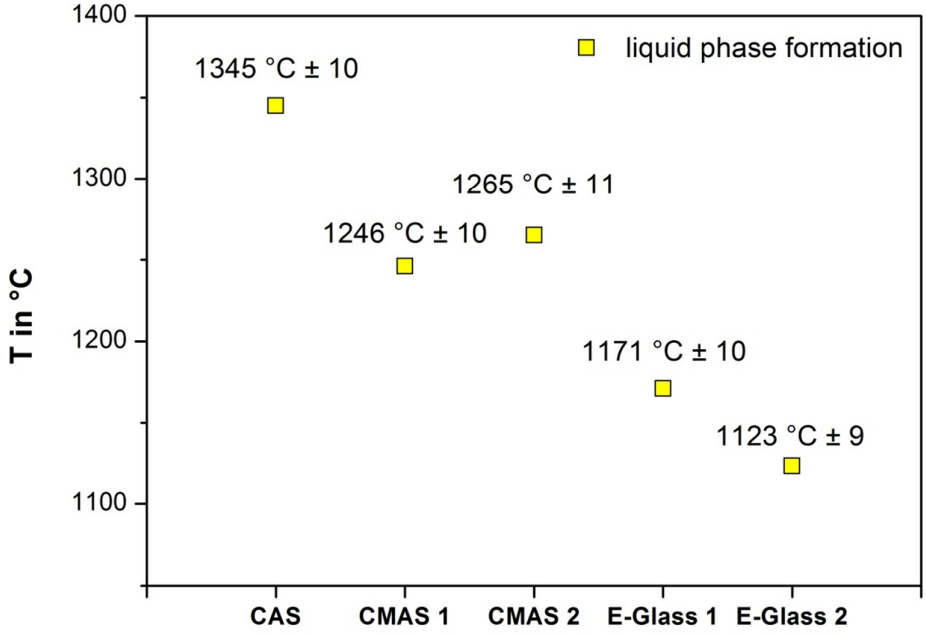

Fig. 30 Observation furnace experiment results of various types of alkali-free glass batches

The sign “±” behind the measured liquid phase formation temperature indicates the deviation of variation in determining the actual temperature during the video analysis. There is differences in temperature reading between the batch inside the quartz crucible and on display of the furnace controller. The solid-to-liquid phase transformation is characterized by endothermal reactions at certain temperatures, and it involves the latent heat, i.e. heat required for the completion of phase transformation. During the phase transformation, the temperature remains constant until the phase is completely changed, and then, it increases without following the heating rate of furnace temperature.

Table 9 Temperature summary in °C of the primary melt formation of various alkali-free glass batches

glass system	observation furnace		DTA-TG		conductivity κ jump
	onset of melting	liquid phase	onset of melting	melting peak	
CAS	1325	1345	1342	1368	1368
CMAS 1	1152	1246	1227	1240	1240
CMAS 2	1199	1265	1247	1257	1258
E-Glass 1	1058	1171	1170	1200	1200
E-Glass 2	981	1124	1091	1110	1115

Table 9 is a collective temperature data of the primary melt formation through three different batch melting characterization methods: DTA-TG, conductometer, and observation furnace. From Table 9, it can be seen that there is a good agreement between the results of DTA-TG and conductometry. Small deviations, however, are observed in the observation furnace method. This method is very useful to investigate the life-time of the bubble and foam that are formed during batch melting, which is not to be discussed in the present study.

4.1.4 Interpretation of results

From the previous studies done by Conradt et al. [CON 1990, 1994, 1997], it is known that the formation of liquid phase triggers the kinetic reactions of batch raw materials. One of the kinetic parameters that can have a great impact on the melting behaviour of a batch is the particle size of the batch. The finer the particle size, the faster is the kinetic reactions, especially in the dissolution of refractory materials, such as quartz and alumina in the glass melt. The thermal analysis evaluation, using DTA-TG, gives a good overview and the fingerprints of the occurrences within the batch under a particular heating rate. However, the amount of the sample requires only several milligrams in the form of very fine powder, lower than 63 µm in size. For that reason, the boundary and heat conductivity conditions of the sample are different from that of the industrial glass tank. Conductometer is another way of characterizing the batch under a specific heating rate similar to the DTA-TG. With larger and bigger sample size, i.e. 200 g, industrial grade batch materials with random particle size distribution and grain size can be characterized in a reliable way; thus it represents physical and chemical reactions occurring in the industrial glass tank.

The results of DTA-TG and conductometry measurement showed a good agreement in several aspects. Both endothermal and exothermal reactions, which occurred within the batch, were attributed to hydration, solid-solid phase transformation, gas evolution, crystallization, and melting. These typical reactions can be examined through a combination of the DTA and TG measurements, and it leads to the change of the diffusion path in ionic crystals. Conductometry is strongly related to the temperature-dependent diffusion coefficient of ionic oxide. As the solid-state reactions occur, the structure of the crystal is changed and so does the diffusion path, and therefore, an increase of conductivity can be detected.

Due to the lack of active mobile ions like alkali ions, a further increase is supressed. Monovalent sodium ion, Na^+, is the responsible species for charge carriers in soda-lime silica; while, in the CMAS system, divalent ions such as Ca^{2+} and Mg^{2+} are responsible for ionic conductivity within the solid body. The work of Natrup et al. [NAT 2005] stated that the conductivity of pure alkaline-earth silicate glass, $3CaO{\cdot}4SiO_2$, is governed by the migration of impurity charge carriers, which are likely to be Na^+ ions. The mobility of Ca^{2+} ion is clearly slower than Na^+ since

the diffusion speed of both the cations is also different. Diffusion is associated with the ability of an ion to jump into its neighbour site, and it involves a large dipole moment. In the case of no structural change in the local environment, Ca^{2+} ion draws very likely back to its original position due to this dipole moment. The presence of Na^{+} as impurities reduces the dipole moment since the Na^{+} ion occupies the vacated Ca^{2+} site. The higher the number of sodium ions as impurities in the system, the higher is probability for Ca^{2+} to jump successfully.

The relation between diffusion of the diffusing species (D_i) and conductivity (κ) of ion species is also described by the Nernst-Einstein equation. The conductivity is directly proportional to the atomic mobility of charge carrier species ($z_i \cdot e$) in the batch. The charges of ion is expressed by charge number ***z*** and elementary charge ***e***, while the concentration, Boltzman constant, and temperature are expressed by Ci, k_B, and T, respectively,

$$D_i = \kappa \cdot \frac{k_B \cdot T}{C_i \cdot z_i \cdot e} \qquad (28)$$

Additionally, from Stoke's Law, the ionic mobility is related to the viscosity of the medium, and further substitutions of the charges of ion into the Einstein relation gives the diffusion equation without any reference to the charge of the diffusing species. This expression is known as the Stokes-Einstein equation.

$$D_i = \frac{k_B \cdot T}{6\pi \cdot \eta \cdot r} \qquad (29)$$

where r is the radius of the diffusing species.

Figure 31 shows conductometry curves of conventional soda-lime silica and E-glass batch as a function of the temperatures. Below 600 °C, both batches have similar behaviour, i.e. conductivity remains unchanged because the ion mobility is limited by defect concentration. From the simple hopping mechanism, as previously discussed, the diffusion path for ion to be mobile depends on the

concentrations of defect or free volume in the solid. As the temperature increases, though it remains below the liquidus temperature, a thermally induced defect formation is observed which leads to an increase in the conductivity. At temperature 750 °C, the conductivity starts to increase rapidly followed by the jump of the conductivity value to three or four order of magnitude at 850 °C. This is the melting temperature of the soda ash as one of the batch constituents. In the E-glass batch, the increasing of the conductivity extends up to 1000 °C and it begins to increase rapidly until the eutectic temperature of the system is reached, i.e., at temperature 1170 °C. The conductivity jump, however, is different to that of soda-lime silica batch. Looking back to the previous Nernst-Einstein and Stokes-Einstein equations, alkali ion in the soda-lime is more mobile in the salt-like liquid identical to soda ash melt, in which the viscosity is very low. In the E-glass, the viscosity of the melt is already high at the eutectic ($\log \eta$ = 3.0 dPa·s), thus impede the ion mobility. The details of the mechanism of the alkali-deficient glass system will be discussed in the next paragraphs.

Most of the batches show an exhibited exothermal peak prior to the onset of melting. Similar to the solid-solid phase transformation, the structure of the sample changes, and this is followed by an increase of the conductivity value. Melting peak of DTA signal without any change in its TG curve indicates liquid phase formation. As the liquid phase is formed in the system, the diffusion of ionic species increases rapidly, and hence, initiates the rapid batch-to-melt at turnover rates.

Similar to the soda-lime-silica batch, the fingerprint of the liquid phase formation in the free alkali batches was indicated by the conductivity jump and it coincides with the maxima of the melting peak in the DTA-TG measurement. Figure 32 shows the summary of the DTA melting peak and conductivity jump.

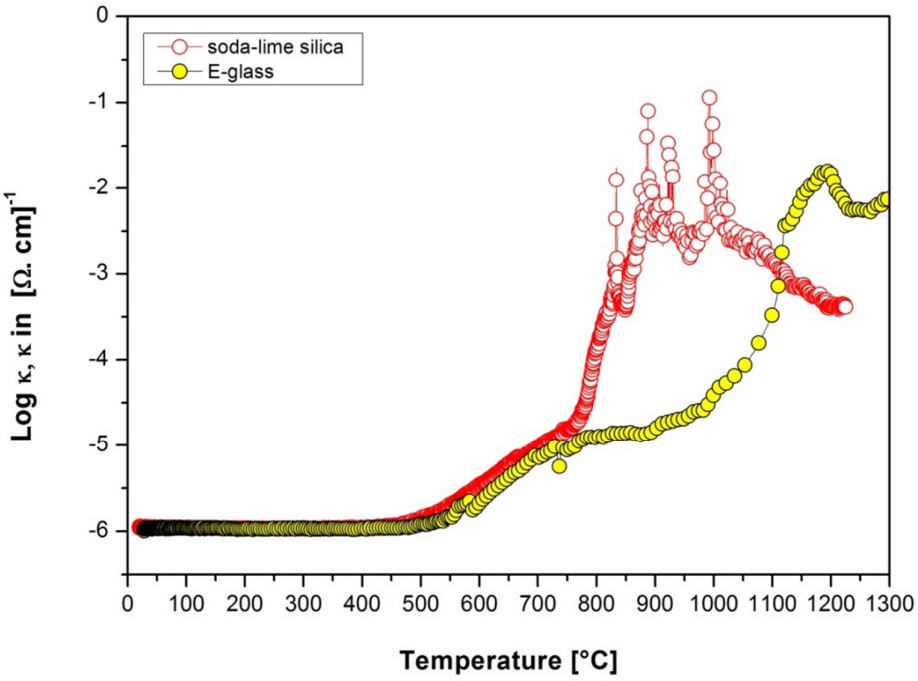

Fig. 31 Conductometry of a typical soda-lime-silica and E-glass batch as a function of temperature

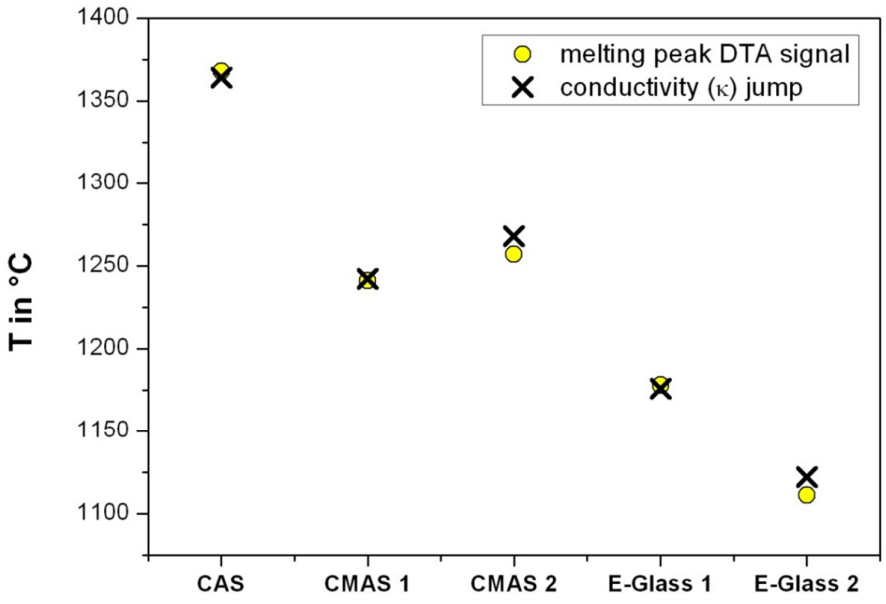

Fig. 32 Summary of melting peaks from the DTA measurement and conductivity jump from the conductivity test

Despite the fact that the maxima of the melting peak from DTA-TG and conductivity jump have identical temperatures, it does not agree with the CAS phase diagram as well as the FactSage™ thermochemical calculation (see Figures 33 and 34). This difference might arise due to different approaches in determining the liquidus temperature (T_{liq}) from the eutectic composition. In equilibrium, the liquidus temperature is determined by cooling the melt until the Gibbs formation of solid and liquid are in equilibrium, and in contrast, the melting process of the batch in the CAS system is followed by the batch-to-melt heating route. The lack of liquid phase formation at lower temperatures causes the segregation of batch raw materials—albeit the usage of fine and analytical-grade raw materials—and hence, sets the eutectic to a higher temperature, i.e. 1370 °C instead of 1170 °C, according to the phase diagram, number 630 [PHA 1998].

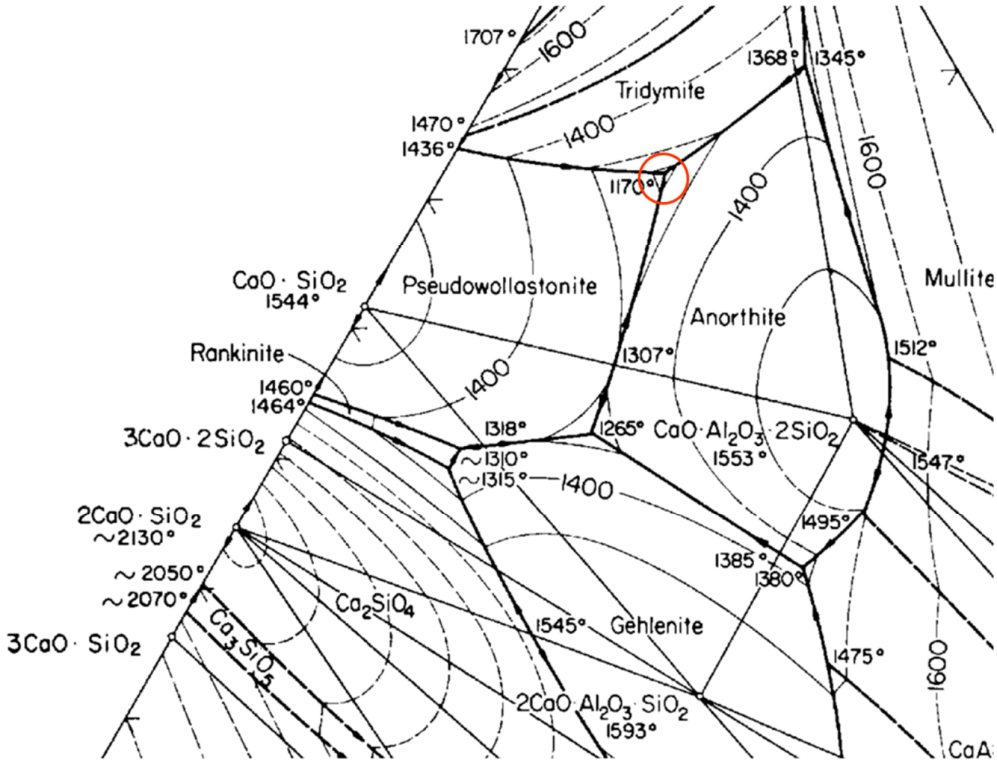

Fig. 33 Partial phase diagram of the system CAS [No. 630] at which the composition of CAS lies on the eutectic point at 1170 °C (red circle) [PHA 1998]

Addition of other oxides, such as MgO and B_2O_3, into this CAS eutectic system lowers the liquidus temperature. This addition modifies the alumosilicate glass structure by lowering the network connectivity, and therefore, reduces the viscosity and liquidus temperature of the glass since they are a function of the glass structure.

Another way to evaluate the relationship between the experiment results and theoretical thermodynamic, is by performing thermodynamic calculation in equilibrium state. A commercial thermodynamic software, FactSage™, was again used for determining both the crystalline and liquid phases that occur upon cooling at high temperature. The following series of figures show the conductivity signal as combined with the equilibrium liquid phase and effective viscosity calculated from the amount of the solid-liquid fraction.

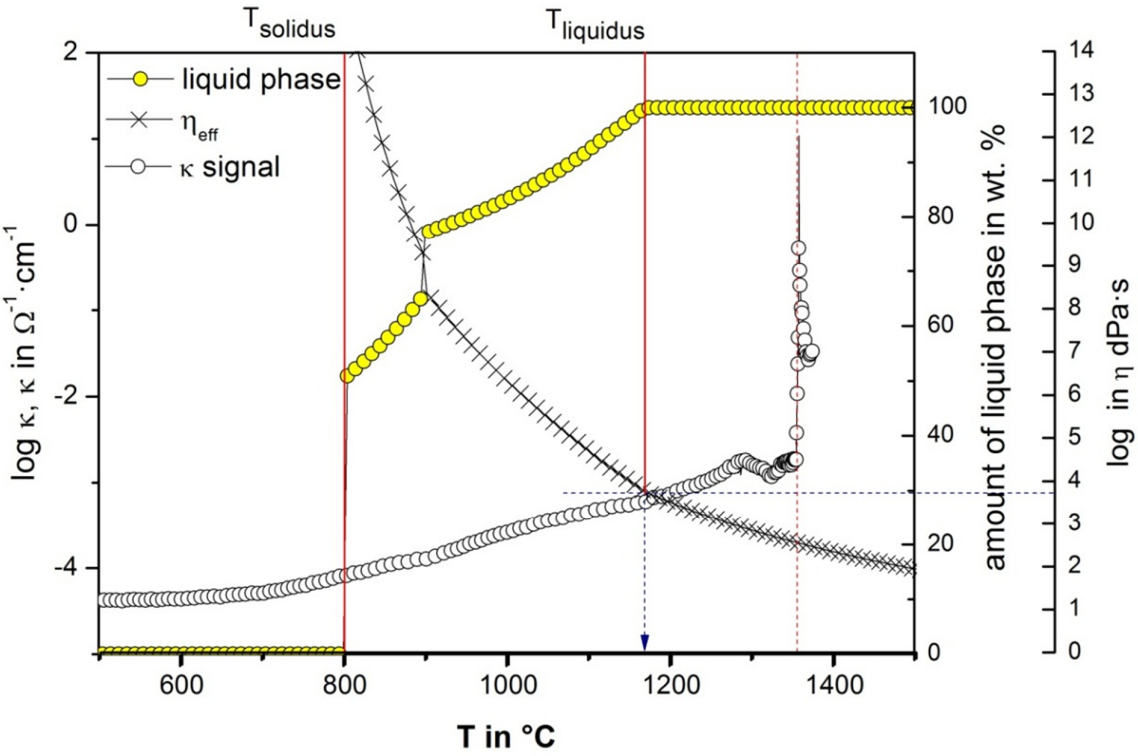

Fig. 34 A comprehensive analysis of the conductivity curve (κ signal) and calculated equilibrium liquid phase formation as well as effective viscosity as a function of the temperature in the system CAS

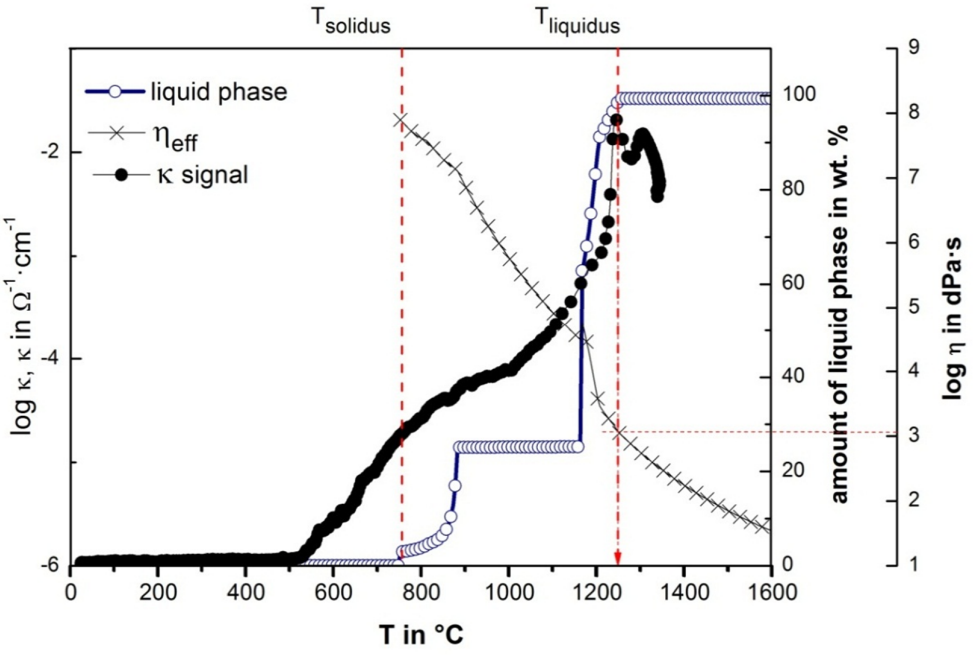

Fig. 35 A comprehensive analysis of the conductivity curve (κ signal) and calculated equilibrium liquid phase formation as well as effective viscosity as a function of the temperature in the CMAS 1 system

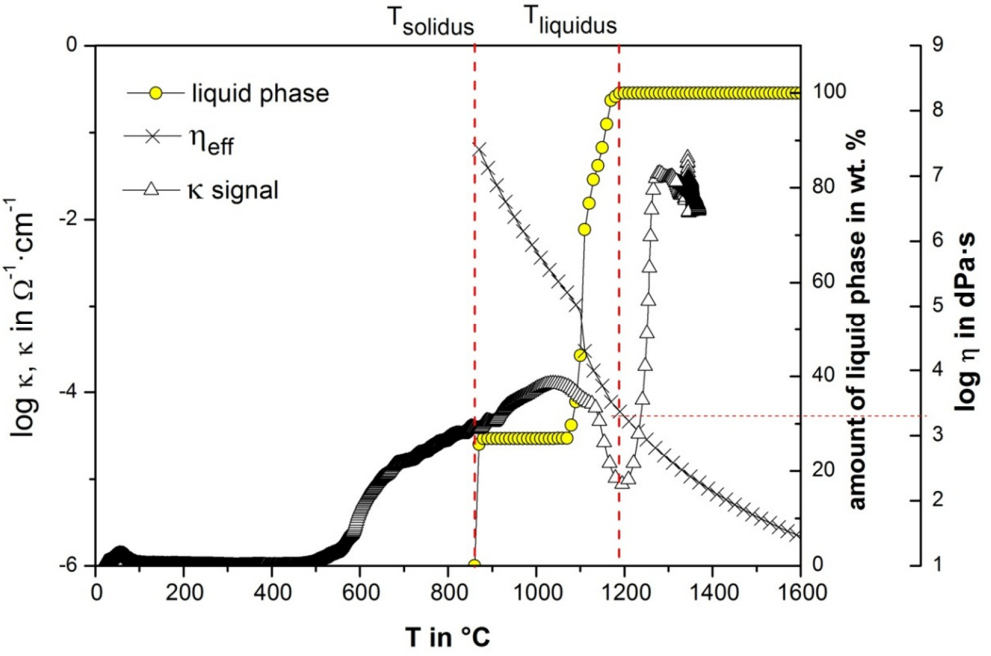

Fig. 36 A comprehensive analysis of the conductivity curve (κ signal) and calculated equilibrium liquid phase formation as well as effective viscosity as a function of the temperature in the CMAS 2 system

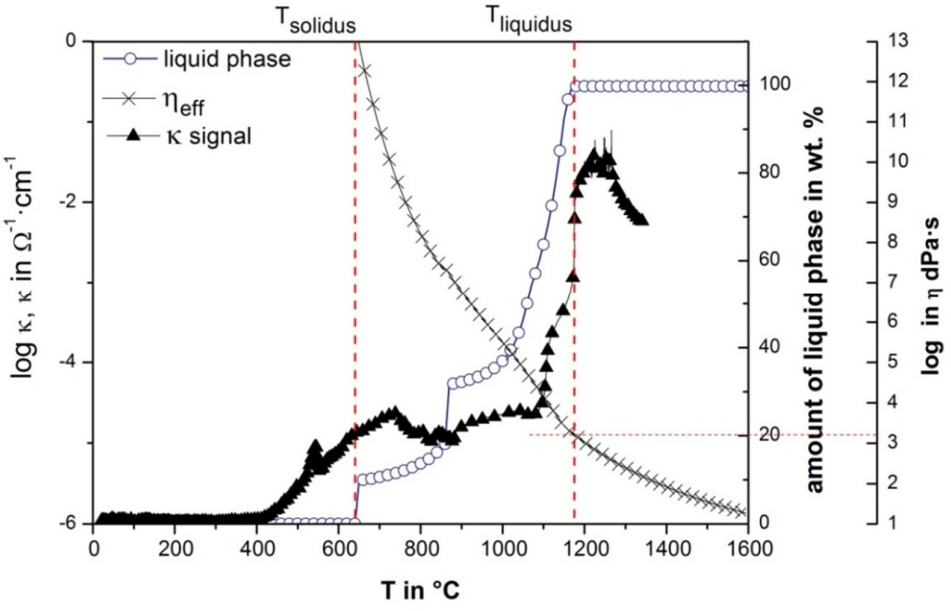

Fig. 37 A comprehensive analysis of the conductivity curve (κ signal) and calculated equilibrium liquid phase formation as well as effective viscosity as a function of the temperature in the E-glass batch 1 (with 1.5 wt. % B_2O_3)

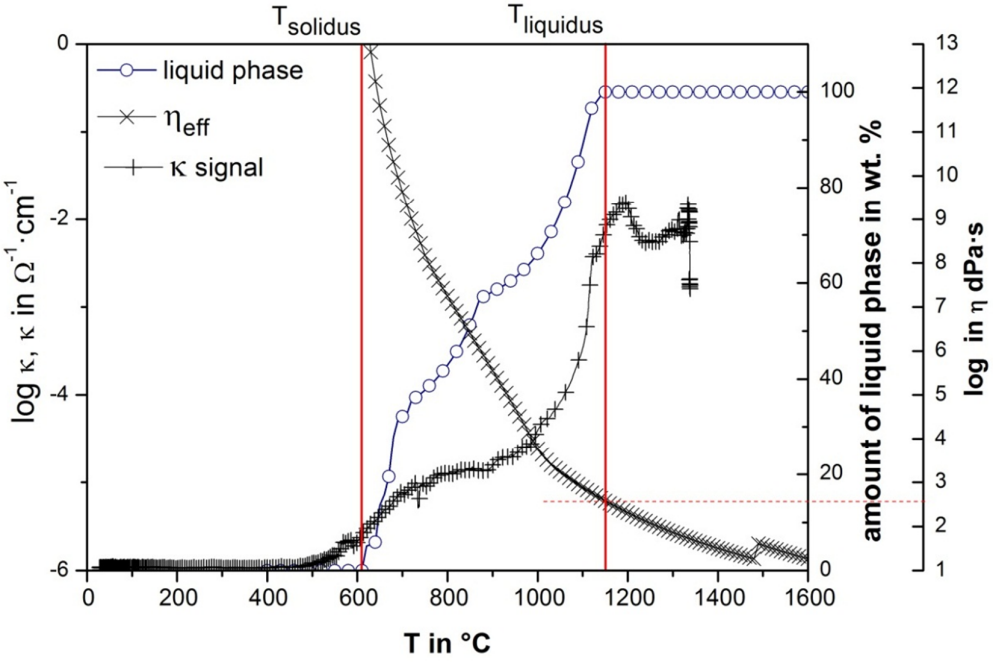

Fig. 38 A comprehensive analysis of the conductivity curve (κ signal) and calculated equilibrium liquid phase formation as well as effective viscosity as a function of the temperature in the E-glass batch 2 (with 5.0 wt. % B_2O_3)

Different from the results of batch melting in the CAS system, the CAS-based systems, after addition of MgO (CMAS) and B_2O_3 (CMAS-B), shows good agreement between the thermodynamic calculations and results, especially at the points where the κ signal increases significantly, i.e. the liquid phase formation. The liquid phase formation indicated by the jump of the conductivity signal is not yet observable at lower temperatures, even though the respective calculated liquid phase was already formed. This conductivity jump was detected as the amount of the liquid generated at a significant amount, i.e. at reaction points or liquidus temperature. The above series of figures show that the primary melt formation, indicated by the conductivity jump, indeed coincides with the liquidus temperature of the equilibrium system. As previously discussed, an exception has to be made for the CAS system.

The utilization of FactSage™ for thermodynamic calculation of the respective systems leads to the calculation of liquid composition formed in the equilibrium state. Therefore, it can also be combined by the effective melt viscosity which is calculated empirically as a function of the glass composition. A combination of Lakatos and self-developed model calculation (UNIGLASS) is used as a tool to predict the viscosity of the liquid phase η_{liq} at a particular temperature and composition. The solid fraction below the liquidus temperature should also be taken into account for predicting the viscosity in the multiphase systems, known as effective viscosity, η_{eff} , as proposed by Krieger-Dougherty [KRI 1959] (see Equation 30)

$$\eta_{eff} = \eta_{fluid} \cdot \left[1 - \frac{\emptyset_{solid}}{\emptyset_{max}}\right]^{-2.5} \qquad (30)$$

The effective viscosity η_{eff} is a function of the liquid phase viscosity η_{fluid} and solid phase fractions Φ_{solid} in the mixture. It is assumed that the batch powder is random close packing with approximated value of Φ_{max} is 0.64.

4.2 Batch melting behaviour of varied B_2O_3 content in E-glass batch

E-glass composition for general purpose is usually derived from the eutectic composition of the CaO-Al_2O_3-SiO_2 (CAS) or CaO-MgO-Al_2O_3-SiO_2 (CMAS) system with several additions of melting fluxes. According to the ASTM, the maximum amount allowed for alkali oxides in E-glass is 1.0 wt. % maximum. It has a great impact on the production process since liquidus and the fibrization temperature ($T_{\log \eta} = 2.5$), i.e. the temperature at which glass melt is drawn to produce glass fibre becomes very high. Therefore, the process becomes very costly, and possesses high energy demand. Addition of B_2O_3 into the E-glass system is a common practice since other melting fluxes used for lowering liquidus and viscosity are mostly alkali-containing oxides. However, B_2O_3 is easily vaporized at high temperature and shorten the lifetime of the furnace refractory. Much efforts have been made to optimize the E-glass composition in terms of energy saving and devitrification problems. It is then a necessity to test all the modified E-glass compositions in laboratory, prior to putting them into operation in the large industrial tank. One of the strategies that represent the real batch melting behaviour in large scale is scaling-up laboratory experiments from the milligram to kilogram range. Most of the conventional methods, such as DTA-TG, Hot-Stage Microscopy (HSM), and High Temperature X-ray Diffractometer (HT-XRD), are classified into the milligram or small scale methods. Other means of batch melting characterization involve larger amounts of sample, and most of them are either self-developed (conductometry, BFT, 10 kg test) or specific-purposed instrument (thermo-optical, observation furnace)

The last study case (sub-chapter 4.1) with various alkali-free glass batches showed that conductometry can be also applied for alkali-free glass batches. In the present study case, batch melting characterization methods, ranging from the milligram to kg scale, are utilized to investigate the batch melting behaviour of the E-glass model system with varied B_2O_3 content. The raw materials and glass compositions are given in the chapter of materials and methods (Chapter 3).

4.2.1 DTA-TG

Decomposition peak pattern as seen in Figure 39 of DTA-TG results is likely a finger print of decomposition of dolomite and limestone. The results are summarized in Table 10 below. Note that small decomposition peaks below temperature 600 °C, i.e. 150 °C and 580 °C, are associated with water release and the SiO_2 phase transformation, respectively, and they are not included in the respective table. Only the onset, peak and end set of the melting DTA signal are different. The increase of the amount of B_2O_3 content in the CMAS system gave a significant impact on the liquid phase formation at lower temperatures.

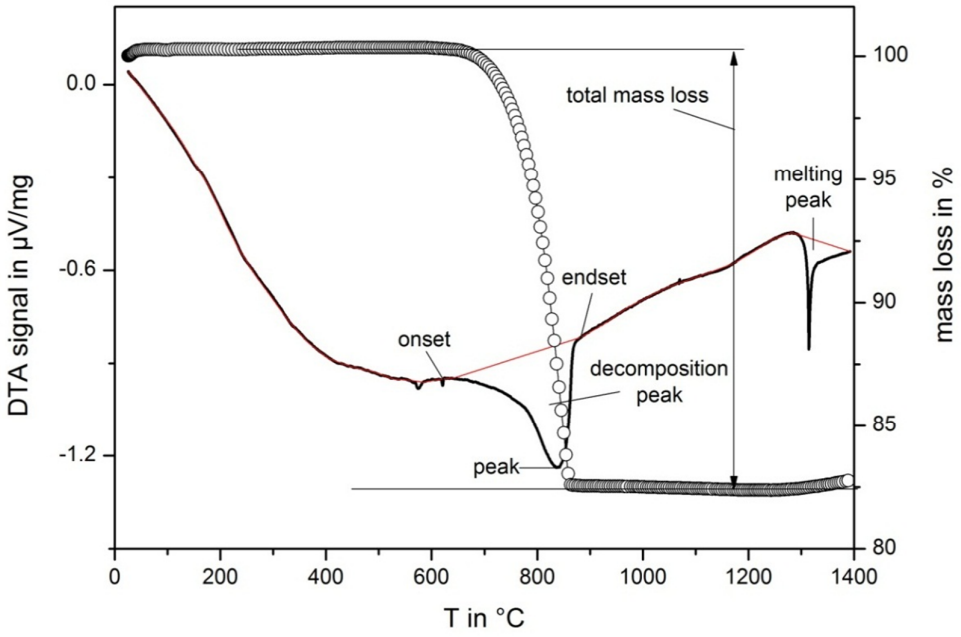

Fig. 39 A typical DTA-TG result of batch raw material under 10 K/min heating rate,from room temperature up to 1400 °C. DTA signal refers to either physical or chemical reactions within the batch, while TG shows mass change due to the respective reactions

The boron oxide-containing samples 3B, 5B, and 7B lead to the dehydration process denoted by the endothermal peak at temperatures lower than 200 °C (see Figure 40). Most of the boron oxide carriers contain several water molecules attached to their structure, and at a certain temperature, vaporize by consuming heat (endothermal reaction). The release of water molecules within the batch was

quantitatively summarized in Table 10. The B_2O_3-containing batch samples 3B, 5B, and 7B had obviously higher mass loss than that of the 0B sample.

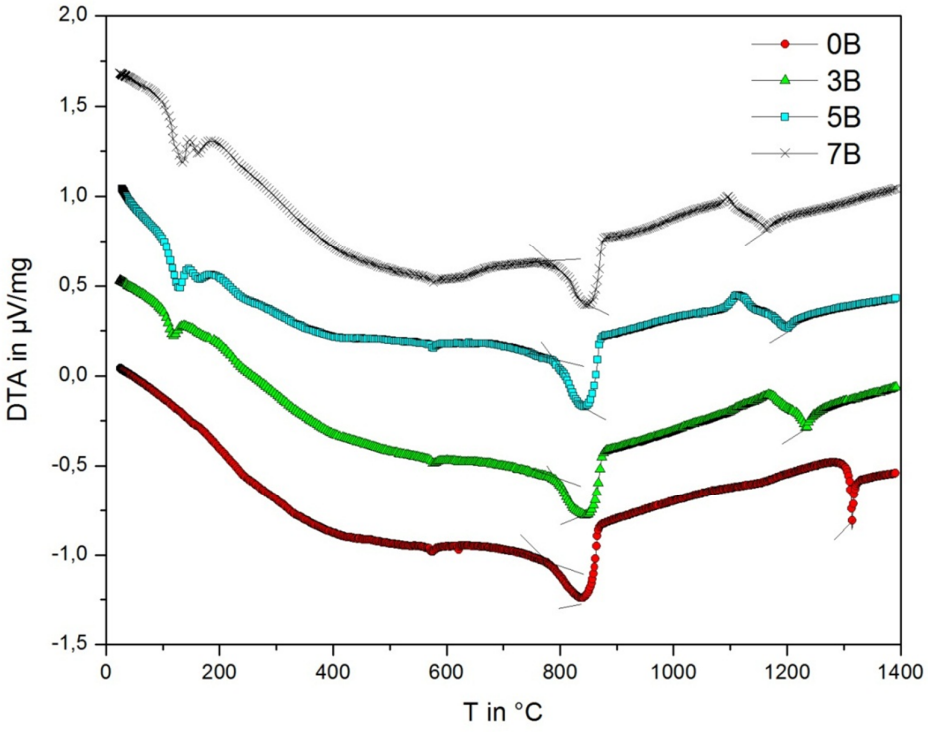

Fig. 40 DTA signal of the CMAS E-glass batch with different amounts of boron oxide

Table 10 Results of DTA-TG of the CMAS glass batches with varied B_2O_3 content

batch type	decomposition peak		melting peak		total mass loss
	onset	max. Peak	Onset	max. peak	
0B	640 °C	840 °C	1294 °C	1314 °C	17.92 %
3B	655 °C	845 °C	1209 °C	1233 °C	18.94 %
5B	679 °C	842 °C	1142 °C	1200 °C	19.59 %
7B	750 °C	850 °C	1122 °C	1163 °C	20.78 %

The small endothermal peak without reduction of the sample mass in the temperature range of 550 °C and 650 °C is associated with the inversion of quartz. Large endothermal peaks, followed by a significant mass loss, represent unambiguously a CO_2 decomposition, which, in the present case, was from dolomite

and limestone. The release of gas started and finished at 650 °C and 900 °C, respectively, which corresponds to the onset of the decomposition temperature for both dolomite and limestone The effects of additional B_2O_3 in the CMAS batch are not only lowering the melting peak, but also creating small exothermal peaks associated with the crystallization prior to melting. As predicted by the equilibrium thermodynamic calculation, showed in Figure 41, the respective crystal that may be formed are wollastonite $CaO{\cdot}SiO_2$ and anorthite $CaO{\cdot}Al_2O_3{\cdot}2SiO_2$. The molten borate formed at lower temperatures acted as a solvent which assist the liquid state diffusion, and thus enhance the crystal formation and melting of the system. The lower melting of boron oxide might be absorbed or reacted with other oxides, and form a new crystal structure which leads to lower liquidus temperature of the system.

4.2.2 Conductometry vs. thermochemical calculation

Several phenomena difficult to observe in the DTA-TG can be observed through the conductometry. In soda-lime silica glass batch, mobile Na^+ ions are responsible for ionic conductance in the glass. Mobility of such ions is an indicator of the particular reactions that may occurr in the glass batch. Figure 11 in the previous chapter shows the interpretation of temperature-dependence of the measured conductometry related to the events in the batch during heating, e.g. water release, solid-state reactions, primary melt formation, foaming phase, and rough melt formation.

Conductometry experiment results of various B_2O_3 content in the CMAS glass batch can be seen in Figure 43. The conductivity curve remains steady at temperatures below 1000 °C, and thus there are no significant reactions leading to the batch-to-melt turnover. The conductivity curve of 0B batch decreases up to two orders of magnitude and increases abruptly in three or four of orders magnitude at 1316 °C, which coincides with the maximum peak of melting in the DTA signal (1314 °C). The jump of conductivity in an alkali-free glass batch, as discussed in the previous chapter, is correlated to the eutectic melting of the respective system. This statement is supported by the calculated liquidus temperature at 1300 °C of the respective system by using FactSage™ (see Figure 42).

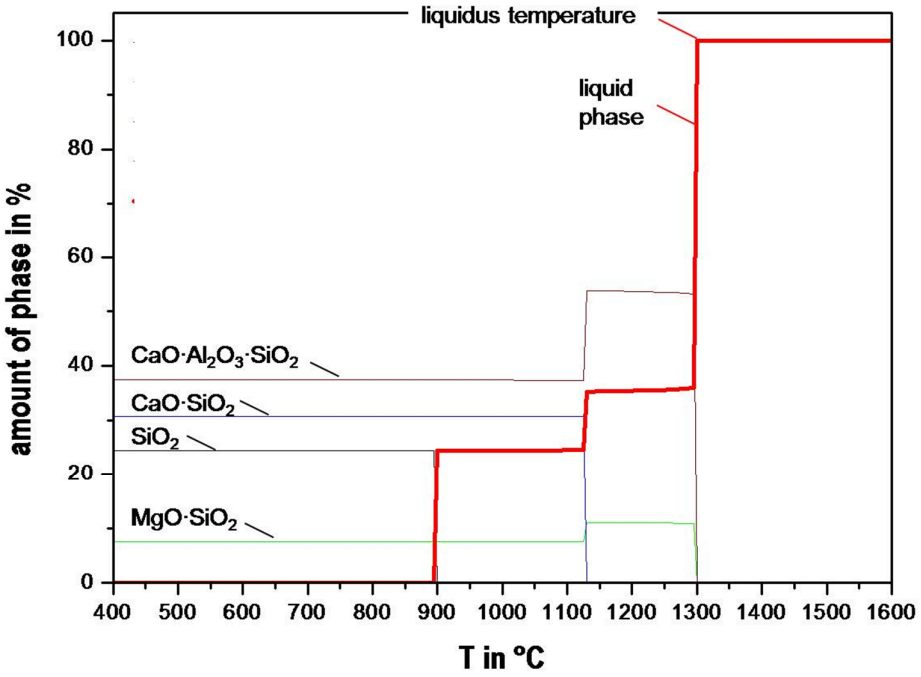

Fig. 41 Equilibrium phase calculation of the system CMAS with 22 CaO, 3 MgO, 13.5 Al_2O_3, and 60 SiO_2 in weight percentage. The red line is the calculated liquid phase that is formed during cooling from high temperature. The liquidus temperature is denoted as the temperature at which the equilibrium lies between 100 wt. % liquid phase and formation of $CaO{\cdot}Al_2O_3{\cdot}SiO_2$-$MgO{\cdot}SiO_2$ i.e. at 1300 °C

A strong deviation from the batch melting characteristics occurred for the B_2O_3-containing batch. Small increase of conductivity for 3B, 5B, and 7B were observed at temperatures around 700 °C, and the conductivity signal became steady at 900 °C for the 3B batch. Further solid state reactions were detected for 3B at 1170 °C, and it reached ultimate conductivity jump at 1275 °C. In 5B and 7B, the conductivity signal decreased slighlty before it started to increase till formation of the liquid phase. The conductivity jump at 1230 °C and 1200 °C for the 5B and 7B batches, respectively, was observed.

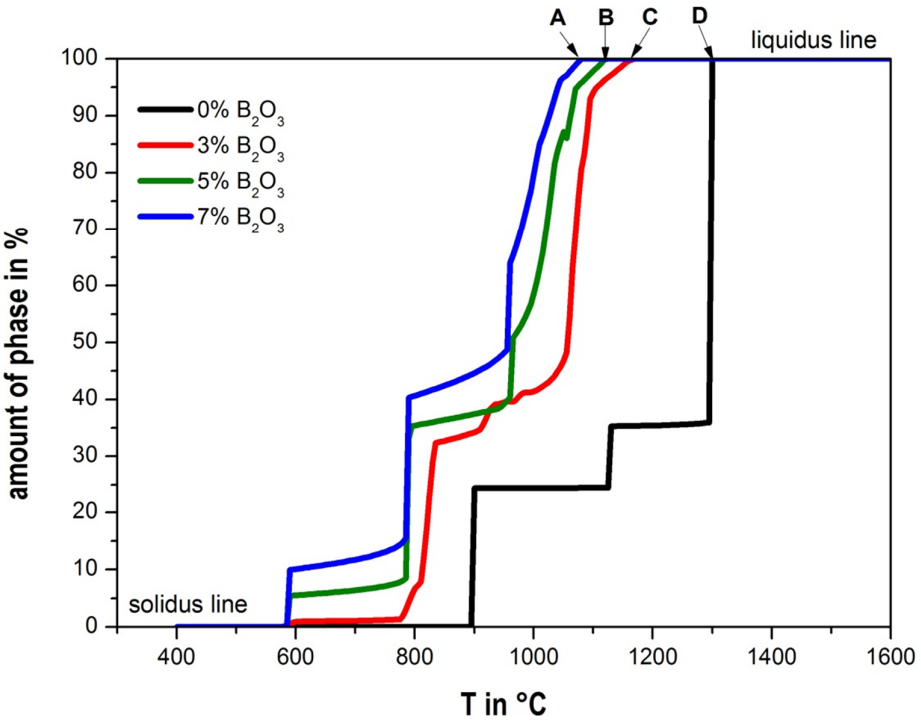

Fig. 42 Calculated liquidus temperature (T_{liq}) of various B_2O_3-containing glass batches in the system CMAS, as described in Table 6. The capital letters on the graph denote the glass type and its liquidus temperature, **A** (7B; 1085 °C), **B** (5B; 1125 °C), **C** (3B; 1165 °C) and **D** (0B; 1300 °C)

In comparison to the thermochemical calculation of the relevant glass systems, the liquidus temperatures did not agree with the conductivity jump, but coincided with the change of conductivity prior to the jump. This occurrences might be attributed to the difference between thermodynamic equilibrium of the system and the real batch condition under a particular heating rate in the experiments. As the liquid phase formed within the batch, the reaction progress increased as it is denoted by the significant increase of the conductivity signal. The conductivity jump takes place, as the quantity of the melt formed is sufficiently high.

Additional B_2O_3 in the CMAS system leads to the solid-state reactions, including the eutectic melting as indicated by the changes of the conductivity curve prior to the formation of liquid phase in the batch. The higher the amount of B_2O_3 added into the system, the earlier is the liquid phase formation.

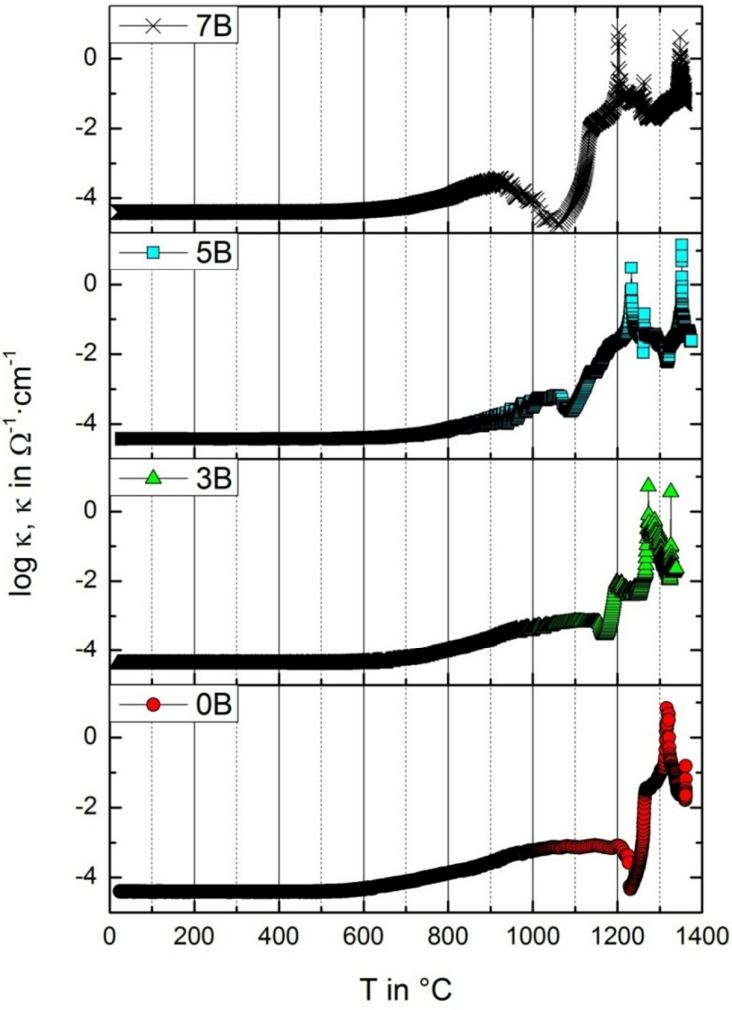

Fig. 43 Conductometry results of different amounts of B_2O_3 content in the CMAS batch as a function of batch temperature

4.2.3 Observation furnace

Temperatures of the liquid phase formation by means of DTA, conductometry, thermodynamic calculation and observation furnace are summarized in Table 11. Direct observation of occurrences of the batch during heating under a particular heating rate can be carried out by the observation furnace. However, determination of the accurate temperature of the corresponding occurrence within the batch was very difficult to perform. This is because the batch temperature was

not directly measured in the batch, but solely depended on the calibrated value of the furnace-batch temperature conducted before the experiment.

Table 11 Summary of the liquid phase formation temperature through evaluation of the results of DTA, conductometry, thermodynamic calculation (FactSage™) and observation furnace

sample	DTA peak	conductivity jump	FactSage™	observation furnace
0B	1314	1362	1300	1289
3B	1233	1337	1165	1199
5B	1199	1270	1125	1135
7B	1165	1230	1085	1099

The furnace temperature was programmed at a constant heating rate, i.e. 10 K/min, and so was the batch temperature. However, this is unlikely to have happened in the batch because the batch reactions increase significantly as the liquid phase is formed. Figure 44 shows the batch temperature profile in the batch from conductometry experiments. At lower temperatures, both the batch and furnace temperatures have similar pattern in a particular heating rate. At the melting temperature, the curve becomes plateau (difficult to recognize in the given example) as the result of latent heat required to complete phase transformation. This point is characterised by constant temperature and changes in time to allow the phase to transform completely. Therefore, the observed temperatures of liquid phase formation via the observation furnace were comparatively lower than that of the results of DTA and conductivity measurement.

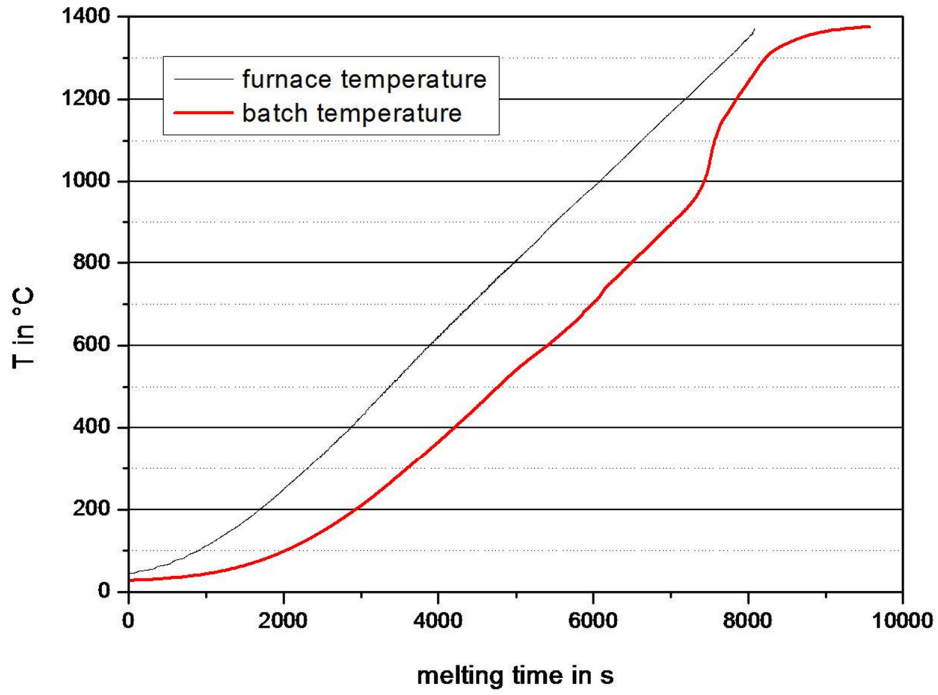

Fig. 44 Batch and furnace temperatures denoted by red and black lines, respectivley, from conductometry measurement

4.2.4 Modified batch-free time

Evaluation of the melts in this experiment was based on solely visual appearance of surface and cross-section of the sample. In the first case, the amount of the reacted batch and un-dissolved batch materials was also analysed quantitatively by counting black and white pixels relative to the pre-defined calibrated picture with either 100% of clear melt or unreacted batch. In this case, the black pixels within the circle which resembles the top view of the crucible refer to the amount of free surface or clear melt. In contrast, the white pixels are denoted as the amount of undissolved batch materials.

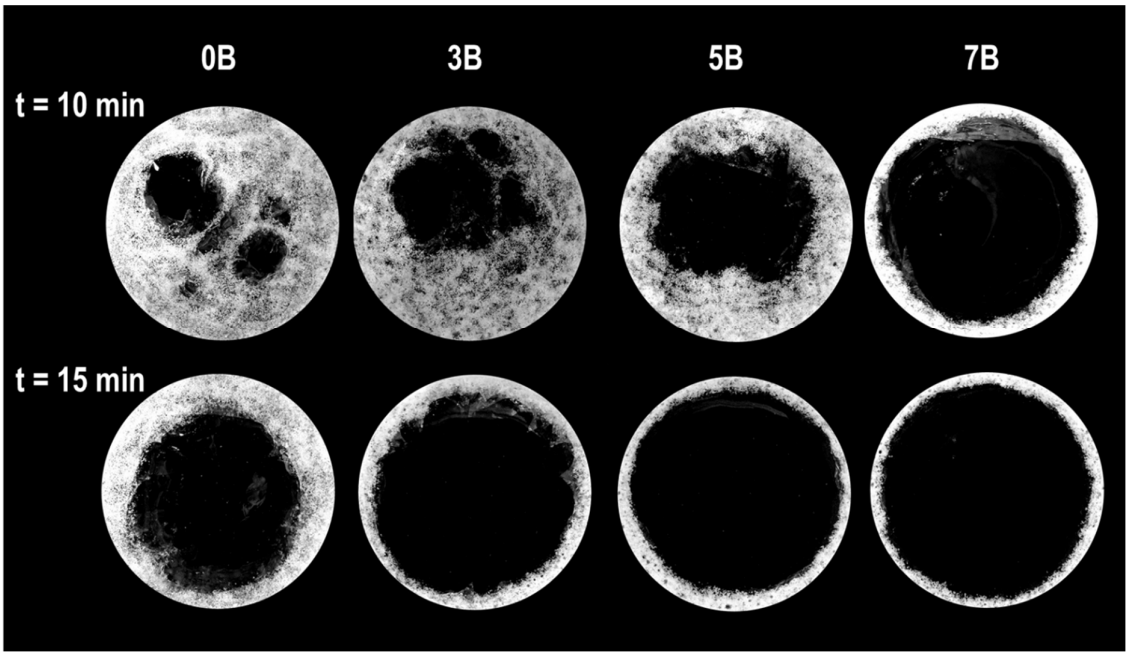

Fig. 45 BFT results of various B_2O_3 content in the system CMAS. The original images have been converted into a black (free surface) and white (undissolved batch) mode. This is then utilized to count the amount of black and white pixels with respect to the amount of melt and undissolved batch, respectively

The amount of free surface that was formed during the experiment can be determined quantitatively by calculating the amount of black and white pixels by utilizing image processing software, such as Gimp™ and Image J™. Figure 45 shows the surface appearance of the BFT test of the CMAS glass system with various B_2O_3 content. Early liquid phase formation in the batch gives significant contribution of the kinetic aspect of batch melting progress, as discussed in the previous section.

Without adding B_2O_3, the CMAS system has higher liquidus temperature; therefore, the liquid phase within the batch was inhibited or delayed at a high temperature. In isothermal process or arbitrary heating rate situation, the batch was exposed to radiation heat from the top and convection from the molten glass. The liquid phase formation might occur at a lower temperature. The batch temperature was then homogenized for a particular melting time, and the melting progress was solely based on the ability of the batch component to dissolve into the existing melts. The addition of B_2O_3 into the CMAS glass system promoted the

liquid phase formation during the earlier stage of melting; hence, the batch melting progress increased gradually as more B_2O_3 was added into the batch. The liquid phase of the B_2O_3-containing batch has low viscosity and surface tension, which easily spread throughout the batch materials, thus promoting further reactions.

For a quantitative analysis, Table 12 shows the estimated result of the analysis of the amount of black and white pixels which correspond to the amount of free surface (batch-to-melt turnover) and undissolved crystalline materials, respectively.

Table 12 Quantitative evaluation of BFT tests

	% of free surface	
sample	t = 10	t = 15
0B	22.11	54.20
3B	35.41	73.16
5B	44.65	78.55
7B	69.19	81.94

Cross-sectional analysis of those samples revealed that there were neither bubbles nor crystalline relics in the bulk sample even at below 1 cm from the surface. The convection heat transfer between the molten glass and the batch prevailed, while the radiation heat transfer from the furnace heating elements into the batch was relatively slower. The convection current in the molten glass melt strongly depends on the temperature of the molten glass, which also affects other properties like viscosity, and hence, heat transfers units The molten E-glass with 5.0 wt. % B_2O_3 had quite a low viscosity level at 1400 °C; however, in the present study, there was not sufficient evidence that the batch-to-melt conversion is directly related to the convection current. In an earlier study by Beerkens [BEE 1992-1], the measurement of five different temperatures in the batch, which was exposed to radiationheat from the top and convection-conduction under the batch pile, showed that heat conduction from the glass melt was faster, and hence, played an important role in the process of the batch-to-melt conversion.

Bunting and Bieler [BUN 1969] studied the correlation between the batch-free time and volume of the corresponding crucibles. They found that there was no significant effect of convection current in the batch melting process for the volume of crucible up to 3 l, while, in contrast, the work from Berkeens utilized 40 l of ceramic pot. Depending on the furnace design, the bigger the crucible, the higher was the temperature variation along the crucible, which generates more convection current.

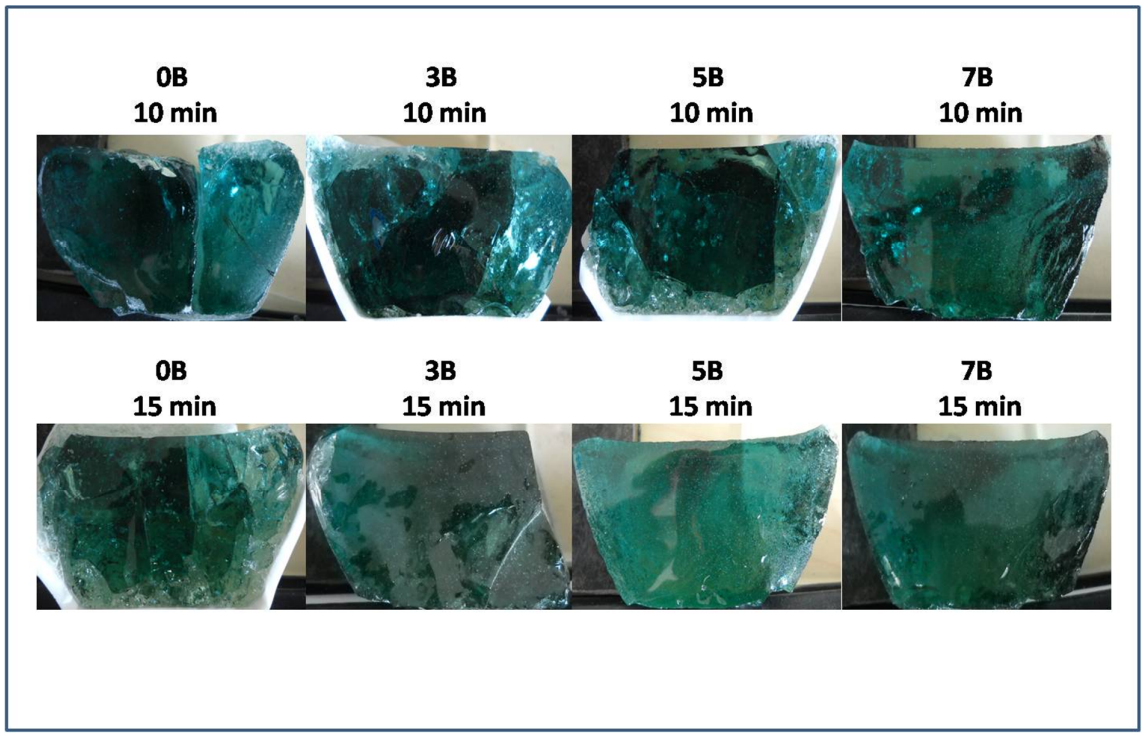

Fig. 46 Cross-sectional view of the CMAS batches with varied B_2O_3 content melted at 1400 °C for 10 and 15 min of soaking time; The numbers in front of alphabet B refer to the weight percentage of B_2O_3 added into the batch

4.2.5 10 kg test

In the present study, 3 kg batch was applied, instead of 4 kg, since the industrial grade raw materials used in this experiment were very finely grounded. The larger amount of fine batch has a very large surface area that cannot be compensated by the crucible size. Five temperatures were set up in each thermocouple, which were placed vertically in 1 cm distance from each other, within the batch. The measured temperatures gave information of the batch melting behaviour under the

exposition of heat radiation, influence of heat convection from the molten glass, and intrinsic heat conductivity of the batch.

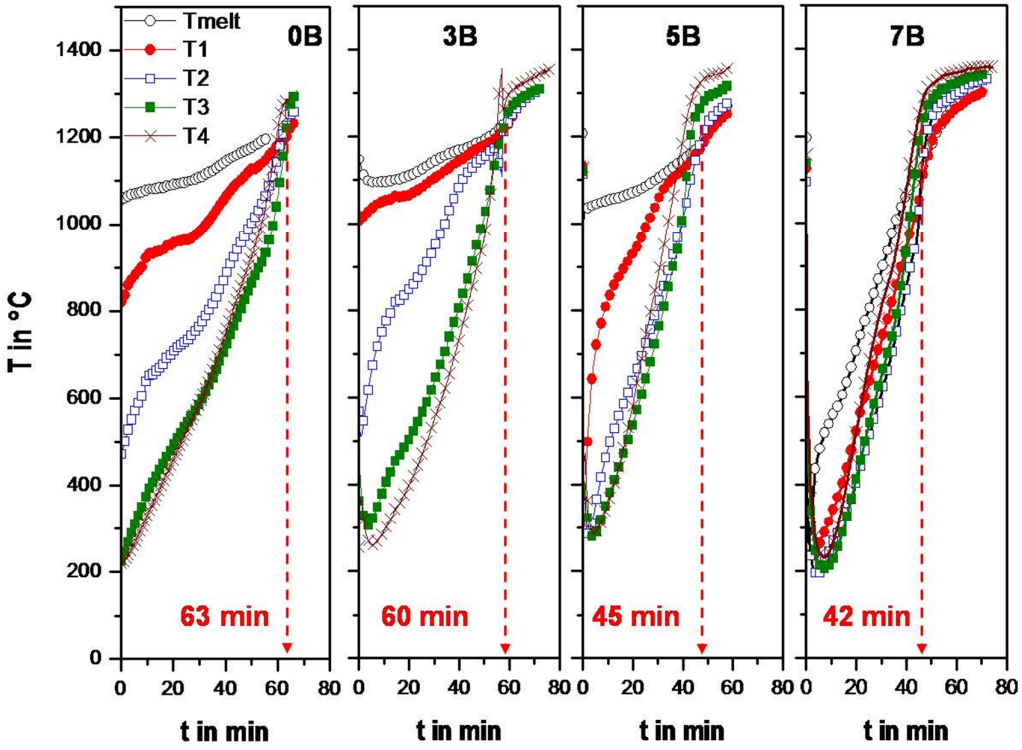

Fig. 47 Vertical temperature distribution in the kg range experiment; temperature in the melt and fire side are denoted as T_1 and T_5, respectively; while T_2 is the temperature at the interface between melt and batch; the number indicated by the bold red indicates t_{endo} of the respective 10 kg result, i.e. the time required to complete endothermal reactions

Figure 47 shows temperature distribution after the batch was charged. Several minutes after the batch charging, the temperatures of the melt side, i.e. T_1, T_2, and even T_3, were already high due to the influence of convection heat flowing from the molten glass. Temperatures in the fire side increased gradually until the point of the completion of endothermal reactions occurred in the batch. It is the point in which all the temperature curves become plateau and it is a typical curve for identifying the occurrence of endothermal reactions at any particular time and temperature.

Figure 47 shows the results of the kilogram test of the CMAS batch with varied B_2O_3 content. The temperature distribution among the batches was quite similar among the batch samples. The heat transfer from the molten glass melt was obviously better than that of the fire/combustion side. Temperatures of T_1 and T_2 were higher than that of the fire side T_3 and T_4. It was difficult for the heat radiation from combustion space to penetrate the batch due to the formation of foams and crystallization scums. Foam and scums have relatively lower heat conductivity, thus the temperatures T_3 and T_4 were relatively 'cold'. As soon as the foaming reactions were finished, heat conductivity from the fire side showed a rapid increase.

The plateau of the temperature curves at a particular melting time is signified as the time required for the batch to complete the overall reactions in the batch. This plateau was hardly seen for the 0B batch since the thermocouples were broken beyond 65 min of melting. All the temperatures in the highest B_2O_3-containing batch were low after the charging process. This can be occurred as the batch raw materials penetrate several cm depth into the melt, thereby affecting the heat conduction from the molten glass melt into the batch. However, the increase of T_3 and T_4 were faster than other batches as the result of the higher content of B_2O_3 that influences the foam stability in the batch. The better the heat conduction within the batch, the faster the reactions within the batch, thus the t_{endo} of 7B was the fastest. This result was in agreement with the evaluation of BFT in the previous chapter.

At the end of the test, it is also necessary to measure the temperature difference which denotes if the batch has melted homogenously. However, in the present study, this could not be performed because the end time of temperature distribution among the 0B, 3B, 5B and 7B batches were not in the same timeframe. As seen in Figure 47, the thermocouples of the 0B batch beyond its t_{endo} were broken, and thus, the evaluation of heat distribution could not be realized.

Utilizing arbitrary heating rates for investigating the batch melting behaviour, as shown in the BFT and 10 kilogram tests, had similar tendencies as the batch melting experiment with a particular heating rate (DTA-TG, observation furnace, and conductivity tests). Early formation of the liquid phase in the batch is the rate-

determining factor for the batch-to-melt turnover, regardless of the applied heating rate to the batch.

To give a comprehensive analysis of the behaviour of batch melting, a thermodynamic calculation in equilibrium state on the CMAS system with an addition of B_2O_3 was conducted. As shown in Figure 41, the formation of the B_2O_3-containing phases whose melting points are lower than the melting point of $CaO{\cdot}SiO_2$ might act like a solvent which change the silicate and calcite reaction route. The reaction proceeds, first, through the dissolution of SiO_2 into the borax melt from 800 °C, and formation of $MgO{\cdot}2B_2O_3$ from 700 °C. This enables the liquid state diffusion of SiO_2 and CaO, and rapid first order formation of $CaO{\cdot}SiO_2$ which dissolves into the melt above 900 °C andsimultaneously dissolves the rest of quartz. As the result, the system was completely in the liquid form at 1170 °C for the 7B batch.

4.3 Alternative boron oxide carriers in glass industry

The European Union (EU) has issued a new regulation to lower the environment and health risks of chemical substances under REACH—which stands for Registration, Evaluation, Authorization of Chemical Substances—specifically, chemical substances derived from chemical treatments. Exemptions can be applied for those substances beneficiated or treated through the physical process (grinding, crushing, milling, drying). The chemical substances strictly limited to this regulation are boric oxide (B_2O_3), boric acid (H_3BO_3), and borax pentahydrate ($Na_2O{\cdot}2B_2O_3{\cdot}5H_2O$) which are mainly used in borosilicates, insulation wool, and E-fibre glass industries. Substitution of B_2O_3 in glass composition is not a wise decision since it requires long and complicated research and development. The most economic and feasible way to overcome this problem is to replace the conventional boron oxide carriers with alternative borate minerals.

The present study suggests more research on the occurrences and physical properties of borate minerals as the first step to find suitable B_2O_3 carriers. The available borate minerals are characterized by their particle distribution and chemical analysis either via X-Ray Fluorescence (XRF) or titration, phase analysis through X-Ray Diffractometer test and observation of their reactions under heating by means of the DTA-TG. The chemical analysis data of individual borate minerals

are applied to adjust the batch and glass composition of the target glass. The boron-containing glass batches used for the present study are borosilicate laboratory ware, lamp, wool, and E-glass. The present study is a process-oriented study which focuses on the influence of alternative borate minerals in boron-containing glass batches in terms of batch melting behaviour. The main objective is to make sure that the application of the alternative borate minerals is safe in terms of the melting process and emission to be transferred to industrial tanks. This project is financially supported by the German government public funded organization through The German Federation of Industrial Research Association (AiF), German Glass Society (DGG-HVG) and industrial partners.

In the previous paragraphs, natural borates are said to contain other phases and large amounts of impurities and gangue that cannot be applied directly into the glass production process. Another problem is the commercial availability of natural borates to be accessed for mass production. Only five types of alternative borates were successfully made available in the present study, e.g. colemanite (CB_3H_5), ulexite ($NC_2B_5H_8$), hydroboracite (CMB_3H_6), tincal (NB_2H_5), and kernite (NB_2H_4). The first two borates are already commercially available. Colemanite has been widely used as a boric acid replacement in the E-glass fibre production, albeit small amounts of borax pentahydrate are added to introduce a few Na_2O into the E-glass composition. Even though a deposit of ulexite is sufficient for mass production, it is rarely used as a boron oxide carrier for insulation wool and E-glass producers as per the writer's knowledge.

4.3.1 Particle size distribution, phase, and chemical analysis

The characterization of natural borates is relatively complicated since they may have variation in either the chemical composition or the phase composition in different particle sizes. The first step of characterization of individual natural borates is an analysis of the particle distribution of as-received borate minerals from the supplier. The size range of every particle was analysed to find out oxide and phase compositions through a combination of X-Ray Fluorescence (XRF) and volumetry for oxides and boron content. The phase composition was analysed by X-Ray Diffractometry (XRD). The Sieve analysis method was applied to analyse particle sizes between 63 µm and 2000 µm. Fine raw materials can only be characterized by the means of laser granulometry. Except kernite and tincal, other

natural borates are available as very fine powders; hence, they may contribute to high amounts of carryover and emission problem.

Getting such fine powders cannot be avoided during the boron up-grading process. After the sieve analysis, the phase analysis of main borate minerals and its impurities in every particle size range was conducted via XRD. It is then found that the borates are mixtures of different types of mineral. Boron oxide content in natural borate minerals is very difficult to be determined either via XRF or Inductive Couple Plasma (ICP)/Atomic Absorption Spectrometry (AAS). In the XRF measurement procedure, it is necessary to fuse the sample together with Lithium tetraborate as a melting flux in a glass or platinum bead, in order to diminish the mineralogical and particle effects. The content of boron oxide may evaporate along with the melting flux and other volatile matters. ICP/AAS is actually suitable for determining boron oxide; however, it is only valid for the sample that contains only small amounts of B_2O_3. Wet chemistry or titration method is the solution to determine the content of boron oxide in borate minerals. However, skilled and experienced laboratory assistants are required for this measurement to be performed. The results of the characterization of borate minerals are summarized in Table 13 and 14.

Table 13 Particle size distributions, boron oxide content, and phase analysis of raw materials from the sodium borate mineral group [CON 2012a]

borate mineral and phase composition		**particle size distribution**		**main oxide composition in wt. %**	
Borax-Pentahydrate		< 1200 µm	100.0%	B_2O_3	48.5
		> 600 µm	91.2%	Na_2O	21.6
		> 500 µm	16.4%	H_2O	29.9
		> 315 µm	11.6%		
		< 250 µm	***2.54%***		
Tincal		< 3000 µm	100.0%	B_2O_3	36.1
Tincalconite (NB_2H_9)	48 – 52 %	> 2000 µm	99.5%	Na_2O	16.4
Borax decahydrate (NB_2H_{10})	48 – 52 %	> 1200 µm	55.6%	H_2O	44.8
Kernite (NB_2H_4)	2 – 5 %	> 600 µm	49.9%		
		< 500 µm	***5.0%***		

borate mineral and phase composition (cont.)		particle size distribution		main oxide composition in wt. %	
Kernite		< 5000 µm	100.0%	B_2O_3	54.8
Kernite (NB_2H_4)	80 – 90 %	> 4000 µm	96.3%	Na_2O	23.8
Tincalconite (NB_2H_9)	10 – 20 %	> 3000 µm	96.9%	H_2O	20.3
		> 2000 µm	79.0%		
		> 1200 µm	70.2%		
		> 600 µm	63.8%		
		< 500 µm	***6.2%***		

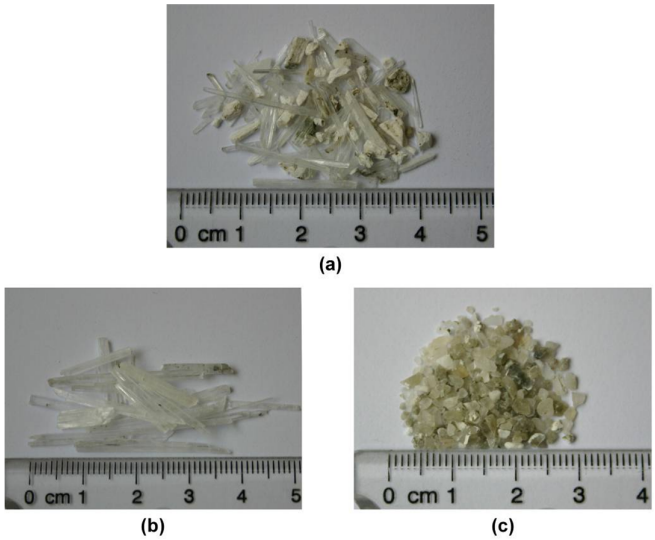

Fig. 48 (a) Natural kernite consists of a mixture of borate mineral phase, i.e. kernite and tincalconite; (b) kernite-rich fraction; and (c) tincalconite-rich fraction

Table 14 Particle size distributions, boron oxide content, and phase analysis of raw materials from the sodium-calcium-magnesium borate mineral group [CON 2012a]

borate mineral and phase composition		particle size distribution		main oxide composition in wt. %	
Ulexite					
Ulexit ($NC_2B_5H_8$)	85 – 95 %	< 500 µm	100.0%	B_2O_3	37.7
Colemanit ($C_2B_3H_5$)	3 – 5 %	> 315 µm	99.8%	CaO	16.7
Meyyerhofferit ($C_2B_5H_7$)	2 – 5 %	> 250 µm	99.7%	Na_2O	6.4
Quarz(SiO_2)	2 – 4 %	> 160 µm	97.4%	H_2O	18.6
Calcite ($CaCO_3$)	8 – 10 %	> 90 µm	87.3%		
		> 63 µm	90.2%		
		< 63 µm	***74.4%***		

borate mineral and phase composition (cont.)		particle size distribution		main oxide composition in wt. %	
Colemanite					
Colemanite ($C_2B_3H_5$)	70 - 80 %	< 160 µm	100.0%	B_2O_3	43.1
Meyyerhofferite ($C_2B_3H_7$)	15 – 20 %	> 90 µm	99.6%	CaO	26.7
Quartz (SiO_2)	2 – 5 %	> 63 µm	96.8%	H_2O	21.3
Calcite ($CaCO_3$)	5 – 8 %	***< 63 µm***	***96.4%***		
Hydroboracite					
Hydroboracite (CMB_3H_6)	70 – 80 %	< 250 µm	100.0%	B_2O_3	37.2
Quartz (SiO_2)	8 – 12 %	> 160 µm	99.8%	CaO	12.7
Anorthite (CAS_2)	5 – 10 %	> 90 µm	94.8%	MgO	8.1
Gismondine (CAS_2H_4)	3 – 5 %	> 63 µm	85.2%	H_2O	16.2
Dolomite (Ca, Mg $(CO_3)_2$)	4 – 8 %	***< 63 µm***	***79.8%***		

Tincal and kernite have the same origin and can be found as a mixture of sodium diborate, NB_2H_x, such as natural borax (NB_2H_{10}), tincalconite (NB_2H_9), and kernite (NB_2H_4) in which N, B and H stand for Na_2O, B_2O_3, and H_2O, respectively; while the subscript denotes the number of moles of the corresponding oxide. In the previous phase diagram (see Figures 6, 7 and 8), the difference among the sodium diborate minerals lies on their amount of water molecules. The physical appearance of up-graded and as-received natural kernite from the borate producer (Rio Tinto) can be seen as flake-rand and round-grain-form (see Figure 48), The flake-rand fractions consisted of kernite phase as their main phase, while other fractions contained the mixture phases of natural borax and tincalconite. The other groups of borate minerals are very fine raw materials, as reflected by the results of particle size distribution in Table 14, of ulexite ($NC_2H_5B_8$), colemanite ($C_2B_3H_5$), and hydroboracite (CMB_3H_6).

The chemical analysis of individual borate mineral was performed by a combination of the following methods: X-Ray flourescence (XRF), loss of ignition (LOI), and wet chemistry (volumetry). Different from Table 13 and 14, Table 15 shows a complete analysis of the oxide contents. Kernite has relatively high amount of B_2O_3 content with the lowest amount of water H_2O as anticipated in its oxide formula. In contrast, tincal has the lowest B_2O_3 content, compared to that of borax pentahydrate; thus more tincal is required to replace borax pentahydrate in

the batch calculation. Sodium bearing borate minerals can only be used for borosilicate glass due to the earth alkaline's constraint. The batch calculation for both borosilicate glasses, (laboratory ware and lamp glass) showed a slight excess of MgO and CaO; however, they are still in the allowed level.

The natural borate minerals always contain impurities regardless of whether they physically undergo the beneficiation process. Depending on the glass type, the iron oxide, alkali, and earth alkaline content should be considered. Borosilicate glass, as previously discussed, is restricted in earth alkaline, and in contrast, E-glass fibre is limited to the content of alkaline oxide. The main concerns could be the fact that most natural borate minerals consist radioactive and hazardous components, such as Strontium Sr, Barium Ba and Arsenic As, in the oxide form.

Table 15 Chemical analysis of individual borate minerals normalized to 100 wt. % by means of X-ray fluorescence (XRF); the single asterisk symbol (*) denotes that B_2O_3 content was analysed by titration; the double asterisk symbol (**) signifies the amount of H_2O determined by the loss of ignition method (LOI)

	borax penta-hydrate	***tincal***	***kernite***	***ulexite***	***colema-nite***	***hydro-boracite***
SiO_2	0.00	1.74	0.43	2.90	4.40	12.12
Al_2O_3	0.00	0.39	0.16	0.08	0.20	1.01
$B_2O_3^*$	48.55	35.89	54.79	37.73	43.18	37.37
Fe_2O_3	0.00	0.14	0.06	0.30	0.08	0.51
Cr_2O_3	0.00	0.00	0.00	0.00	0.00	0.00
TiO_2	0.00	0.03	0.02	0.00	0.00	0.06
MnO	0.00	0.00	0.00	0.00	0.00	0.05
BaO	0.00	0.00	0.00	0.00	0.00	0.01
CaO	0.00	0.41	0.21	16.71	26.75	12.62
MgO	0.00	0.27	0.11	1.42	1.88	8.08
K_2O	0.00	0.14	0.05	0.03	0.00	0.30
Na_2O	21.52	16.31	23.76	6.4	0.08	0.30
SO_3	0.00	0.00	0.00	0.00	0.65	1.31
As_2O_3	0.00	0.00	0.00	0.00	0.00	0.12
SrO	0.00	0.00	0.00	0.61	1.43	0.09
H_2O	29.93	44.68	20.39	33.85	21.34	26.10
sum	**100.00**	**100.00**	**100.00**	**100.00**	**100.00**	**100.00**

4.3.2 Thermal analysis of borate minerals

Figures 49, 50, and 51 show the results of the DTA of individual sodium borate minerals (borax pentahydrate, tincal, and kernite) in which all sodium borate minerals display similar behaviour under 10 K/min heating rate. The first relatively wide endothermal peak refers to water molecule (H_2O) hydration at temperatures below 200 °C. Subsequently, there is re-crystallization to anhydrous borate ($Na_2O{\cdot}2B_2O_3$) within the borate structure as water molecules hydrate completely. The last endothermal peak at 740 °C is narrow and sharp, which is associated with the melting point of the anhydrous sodium borate minerals.

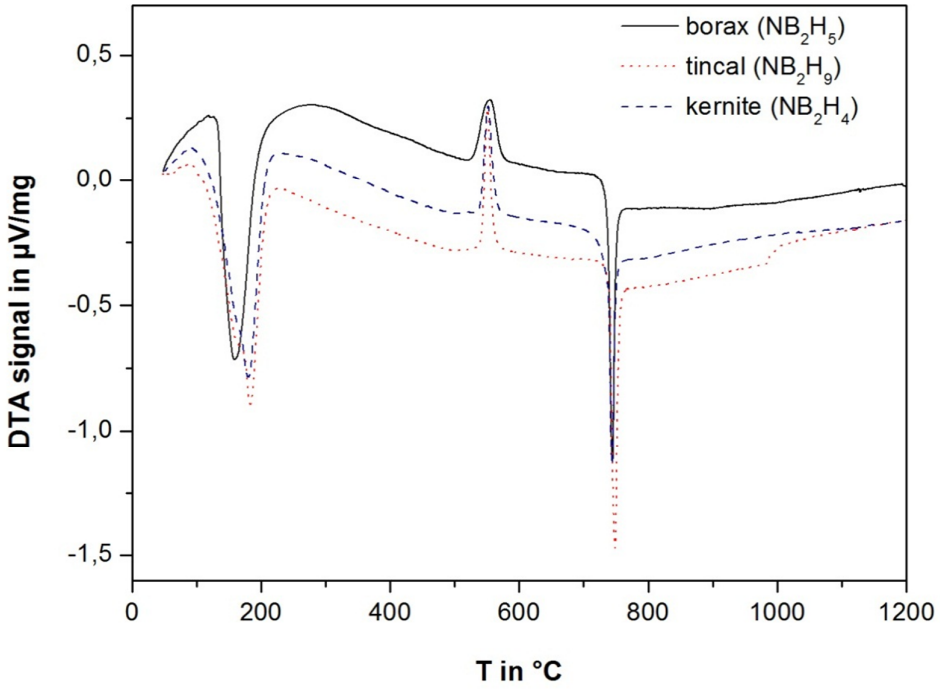

Fig. 49 Results of thermal behaviour of individual sodium borate mineral group by means of Different Thermal Analysis (DTA) under 10 K/min heating rate. The upper case of N, B, and H designated to Na_2O, B_2O_3 and H_2O

In contrast to that of sodium borate minerals, the DTA-TG results showed that the sodium-calcium and calcium-magnesium borate minerals have different melting behaviour. The peaks in the DTA signal can be categorized into three distinctive peaks. The first endothermal peak, accompanied by mass reduction, was an indicator of the dehydration process of water molecules within the structure. The

second peak observed was an exothermal peak which is associated with the new crystal structure formation. Shallow endothermal peak at high temperatures was ambiguously interpreted as a melting peak of the respective borate mineral. According to Celik [CEL 1995] and Demirci [DEM 2000], this shallow endothermal peak at a temperature region between 800 °C and 900 °C is denoted as either the continuation of the calcination process or the melting point of amorphous structures developed during the formation of new crystal.

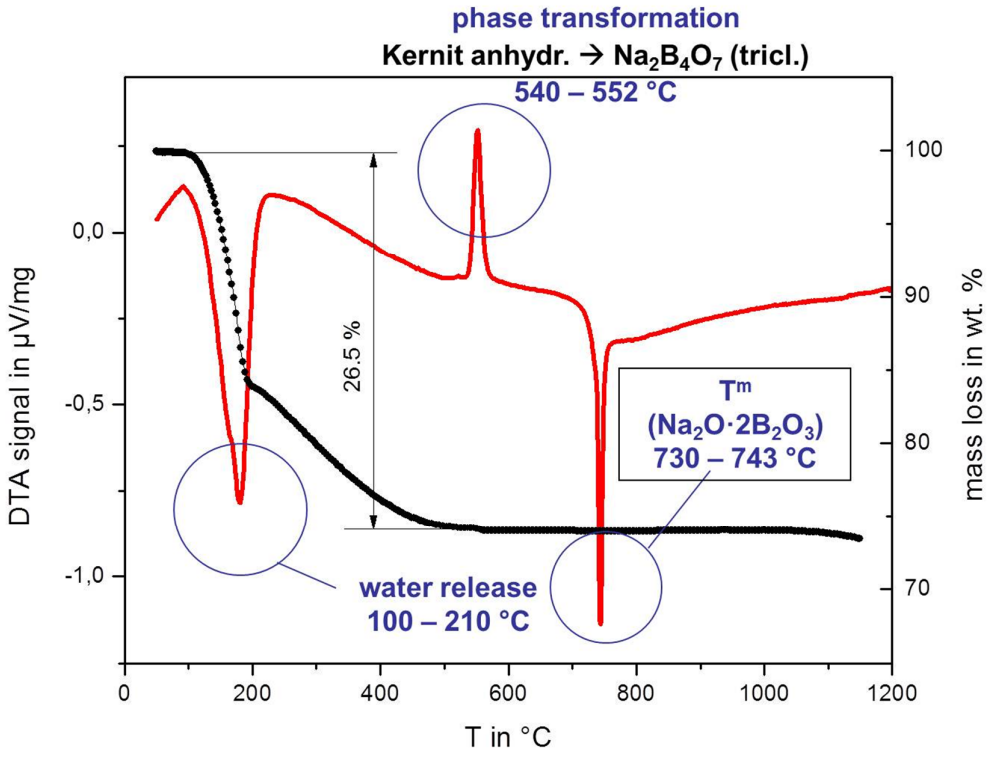

Fig. 50 General interpretation of the DTA signals associated with physical reactions of the hydration of water molecule (*Entwässerung*), crystallization/solid state phase transformation (anhydrous formation), and melting point (T^m)

The dehydration of water molecules of individual borate minerals is indicated by the endothermal peaks below 400 °C occurred at different temperatures. The onset temperature of water dehydration of ulexite, hydroboracite, and colemanite lie at 65 °C, 180 °C and, 300 °C, respectively. Ulexite undergoes gradual decomposition in a wide range of temperatures, up to 800 °C. Ulexite releases water molecules at different steps upon heating as indicated by the TG signal in Figure 51. The hydration process can be discriminated by two different

mechanisms. The first is the release of free H_2O molecules at temperatures below 120 °C, and left the –OH group attached to the main borate structure as the second mechanism. The bond strength between the cations and the –OH group determines the temperature of further dehydration processes. The higher the bonding energy between cations and –OH groups, the higher is the temperature. Compared to that of ulexite, the dehydration temperature of colemanite and ulexite shifted at higher temperatures and occurred at a relatively narrow temperature region.

Sharp exothermal peaks related to recrystallization phenomena can be observed obviously for ulexite at 650 °C. The melting point of these borate minerals in the present study is somewhat beyond the experiment temperature window. The melting area can be theoretically defined by determining solidus ($T_{solidus}$) and liquidus temperature ($T_{liquidus}$). The theoretically calculated value of melting area temperature i.e. $T_{solidus}$, $T_{liquidus}$ [°C], and solid phase at the liquidus temperature of the anhydrous form of colemanite C_2B_3 are 1262 °C (solidus), 1371 °C (liquidus) CaB_2O_4 (phase at liquidus temperature). In anhydrous ulexite NC_2B_6, solidus temperature is at 834 °C, while liquidus temperature is 1176 °C, with CaB_4O_7 as the phase at liquidus temperature. In hydroboracite CMB_3, the solidus, liquidus temperatures are 1180 °C, 1273 °C, (phase at liquidus: Mg_2B_5), respectively.

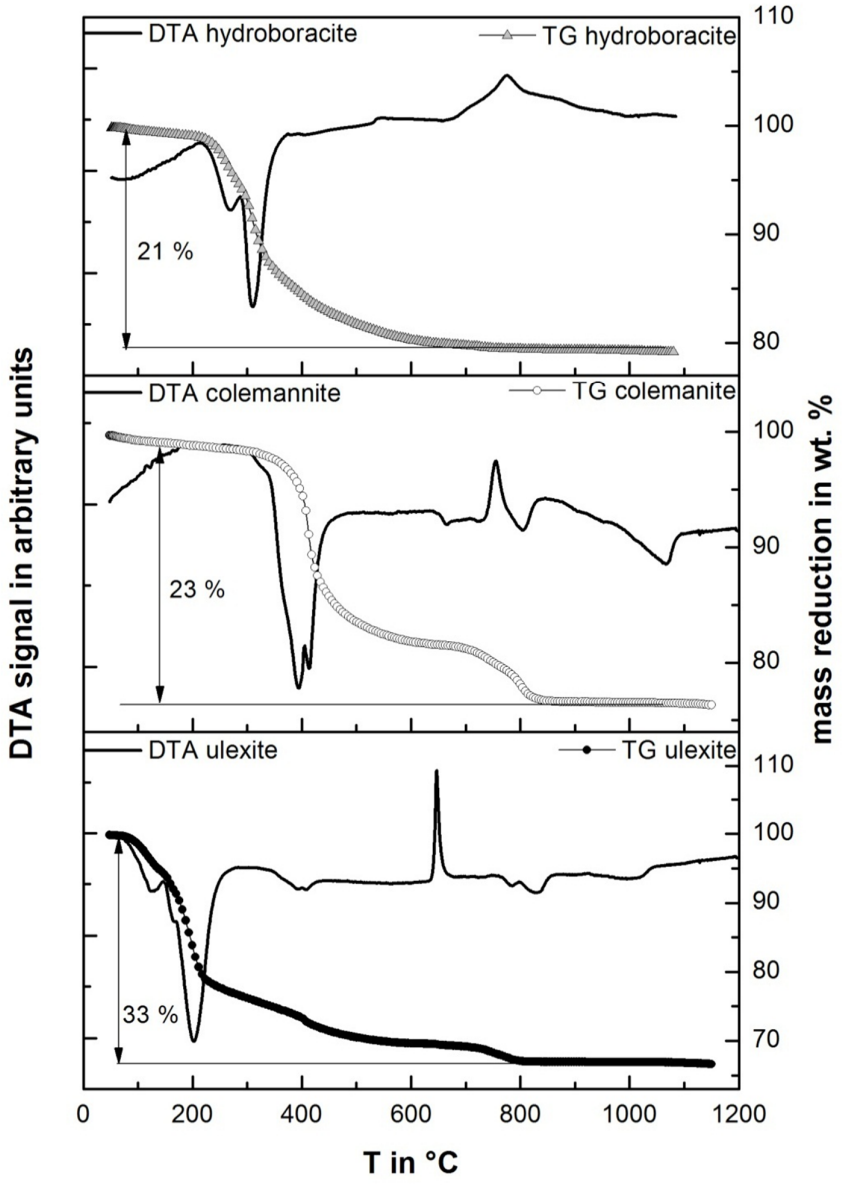

Fig. 51 Results of the DTA experiment of magnesium-calcium-sodium-borate mineral group; N = Na_2O, M = MgO, B = B_2O_3, and H = H_2O.

4.3.3 Selection of boron oxide carriers and batch calculation

The characterization of individual borate minerals—specifically, phase and chemical analysis—is a very important step for determining the suitable boron oxide carriers for particular boron oxide-containing glasses. Based on the chemical analysis, not all borate minerals can be applied in certain types of glasses. For instance, the laboratory glassware batch requires a restricted amount of alkaline

earth oxide, CaO and MgO; so, borax pentahydrate (NB_2H_5) can only be replaced by the alternative sodium-borate group, tincal (NB_2H_9) and kernite (NB_2H_4). Another example is the E-glass batch in which alkali oxide content should not exceed 2.0 wt. % of total oxides. In a recent development, small amounts of Na_2O are allowed in the E-glass composition, and both colemanite and borax pentahydrate are used as B_2O_3 and Na_2O carriers, respectively. The possibility of replacing colemanite and borax pentahydrate can be achieved by hydroboracite. However, complete B_2O_3 carriers replacement in E-glass decreases the amount of Na_2O slightly. In general, a combination of two or more alternative B_2O_3 carriers can be performed to find the optimum composition. However, due to technical and economic constraints of procurement of silos that might be required for two or more alternative B_2O_3 carriers, the scope of study is limited to only one alternative carrier for particular glass batch types.

Batch calculation is the next step to determine not only the amount of required alternative B_2O_3 carriers, but also the deviation of non-linear composition-properties relationship between reference and modified batch i.e. viscosity and liquidus temperature. Viscosity was calculated by a combination of Lakatos and self-developed model, while the liquidus temperature was calculated by using the commercial thermodynamic software FactSage™. Due to the confidential issues between industrial partners for the present study, the following glass composition of lamp, laboratory ware, wool, and E-glass can only be expressed in the composition range.

There were no significant deviation of viscosity in all temperature ranges by alternative borate minerals, even though natural borates contain impurities. As previously stated, not all available borate minerals can be applied to all glass types due to the constraints of maximum impurities allowed for the particular glass type. Borosilicate glasses, such as lamp and laboratory glassware, can only adopt the sodium borate mineral group (tincal and kernite) as the boron oxide carrier due to the alkaline earth constraint. The conventional borax pentahydrate in the E-glass batch can be replaced by tincal, kernite, and ulexite; while in the wool glass batch, all available borate minerals—tincal, kernite, ulexite, colemanite, and hydroboracite—can be applied. Hydroboracite is the only B_2O_3 carrier used for substituting colemanite since Na_2O content might exist as the trace element.

However, significant amounts of MgO and B_2O_3 content in hydroboracite may influence the viscosity level at fibrization and liquidus temperature; so, the application of hydroboracite in E-glass should be carefully taken.

4.3.4 Conductometry

4.3.4.1 Laboratory glassware batch

Figure 52 shows the conductivity result of laboratory glassware batch between reference batch in which the conventional borax pentahydrate was applied and alternative batches with tincal and kernite as B_2O_3 carriers. The primary melt formation indicated by the conductivity jump of the alternative B_2O_3 carrier-containing batches shifted to higher temperature compared to the reference batch.

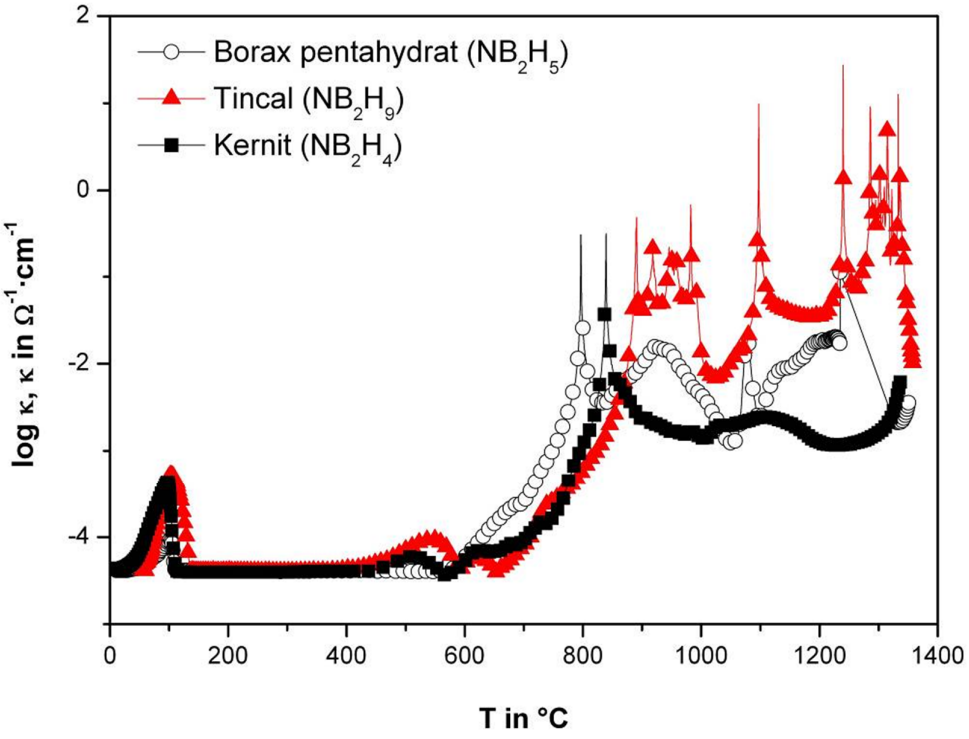

Fig. 52 Conductometry κ of the laboratory glassware batch with various B_2O_3 carriers as a function of temperature with 10 K/min heating rate

The temperatures of the primary melt formation of reference, kernite, and tincal batch are 800 °C, 844 °C, and 890 °C, respectively. Below 500 °C, all the batches showed similar behaviour characterised by the increase of conductivity signal

within the range of physical batch water removal. The conductivity signal was slightly changed at temperature range between 500 °C and 550 °C. Fluctuation of the signal was observed in the alternative B_2O_3-containing batches, while the reference batch showed relatively smooth transition. This point indicates the beginning of solid-state reactions as the mobile ion species within the batch starts to be active.

From the previous chapter, this phenomenon is related to the theoretical solidus temperature calculated by FactSage™ of the batch ($T_{solidus}$ = 550 °C), as shown in Figure 51. As the amount of local occurrence of the bulk primary melt increases, the conductivity signal jumps three to four order of magnitude, and compared to that of the calculated phase equilibrium in Figure 53, it is correlated to the liquidus temperature ($T_{liquidus}$ = 800 °C) of the corresponding system. Cullet content up to 50 wt. % influenced the behaviour of the laboratory glassware batch melting.

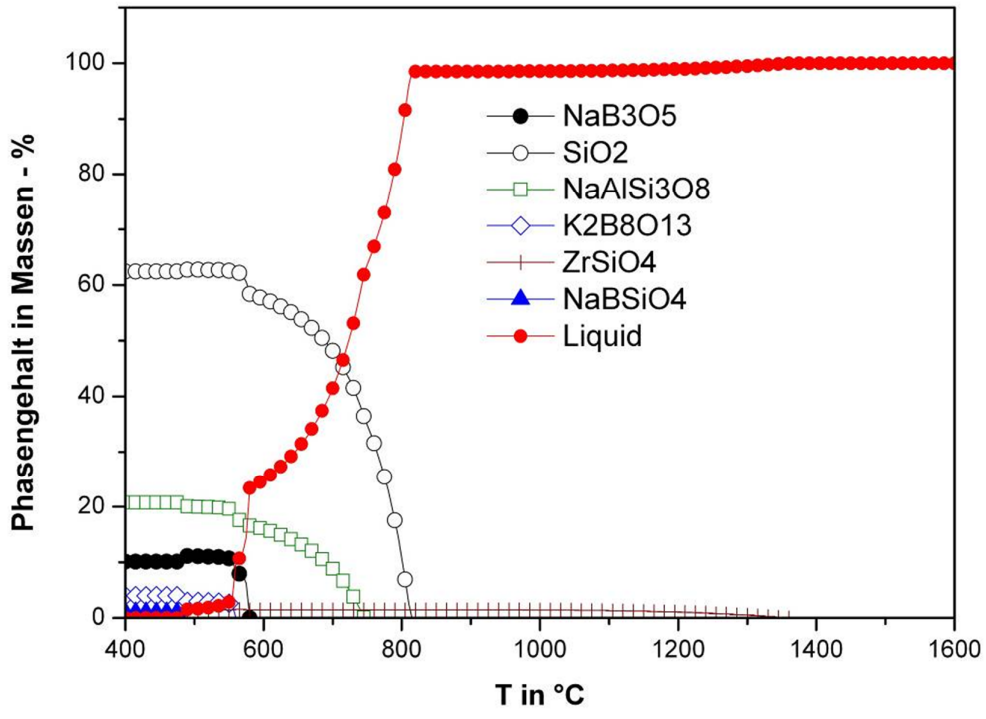

Fig. 53 Thermodynamic calculations of phase equilibrium via FactSage™ [GTT] of the commercial laboratory glassware. Liquidus temperature is 810 °C; phase: Quartz

The difference of conductivity jump temperature can be explained in terms of the grain-to-grain interaction in which the particle size of raw materials—in this case borate minerals— play a significant role. Tincal and kernite have relatively large particle size and elongated form, as seen in Figure 48, compared to borax pentahydrate. Large particle size slowed down the reactions; even though the beginning of the solid-state reactions at 550 °C were relatively similar among the batches, the temperature of the conductivity jump were shifted by 50 °C.

Tincal and kernite used in the conductivity experiment were in the as-received form, as seen in Figure 48, thus kinetic aspects, which were influenced by particle size, played a major role in determining the batch melting behaviour. These events, in contrast, cannot be observed in the DTA measurement because the sample should be prepared in fine powder (lower than 63 µm) in order to diminish the heat transfer problem between sample and Pt-crucible. For that reason, the effect of particle size in characterizing the batch melting behaviour in the small experiment scale is neglected; thus there is a significant difference between the DTA and conductivity results.

4.3.4.2 Lamp glass batch

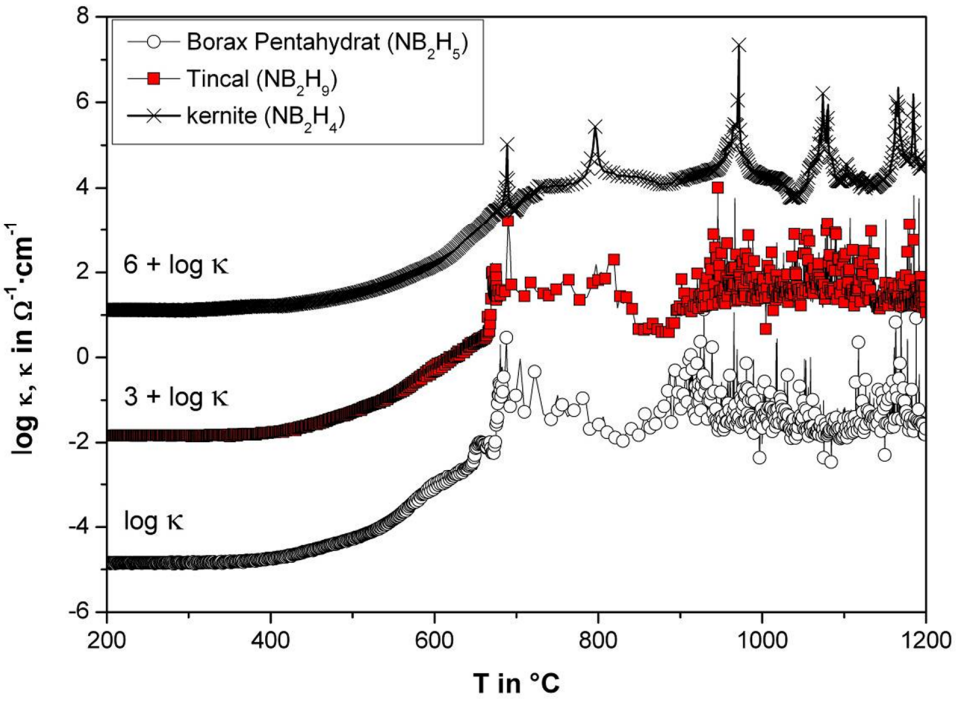

Fig. 54 Conductometry of various B_2O_3 carriers-containing batches against the batch temperature of 10 K/min heating rate

The above figure showss the results of conductometry of various B_2O_3 carriers in the lamp glass batch. It is shown that there was no significant impact of the application of the alternative B_2O_3 carriers in lamp glass batch. The batch contains 40 wt. % of glass cullet and differs to the previous borosilicate glass batch in which Na_2O and B_2O_3 carriers originated from borax pentahydrate. The lamp glass batch utilizes soda ash (Na_2CO_3), potassium carbonate (K_2CO_3), and barium carbonate ($BaCO_3$) as raw material carriers for Na_2O, K_2O, and BaO, respectively. Therefore, the conductivity jump similar to that of the soda-lime-silica glass batch represents the physical melting of the carbonates or eutectic reactions of the salt-like melt. The batch components developed the primary melt formation at the temperature 680 °C as predicted by the phase diagram in Figure 55.

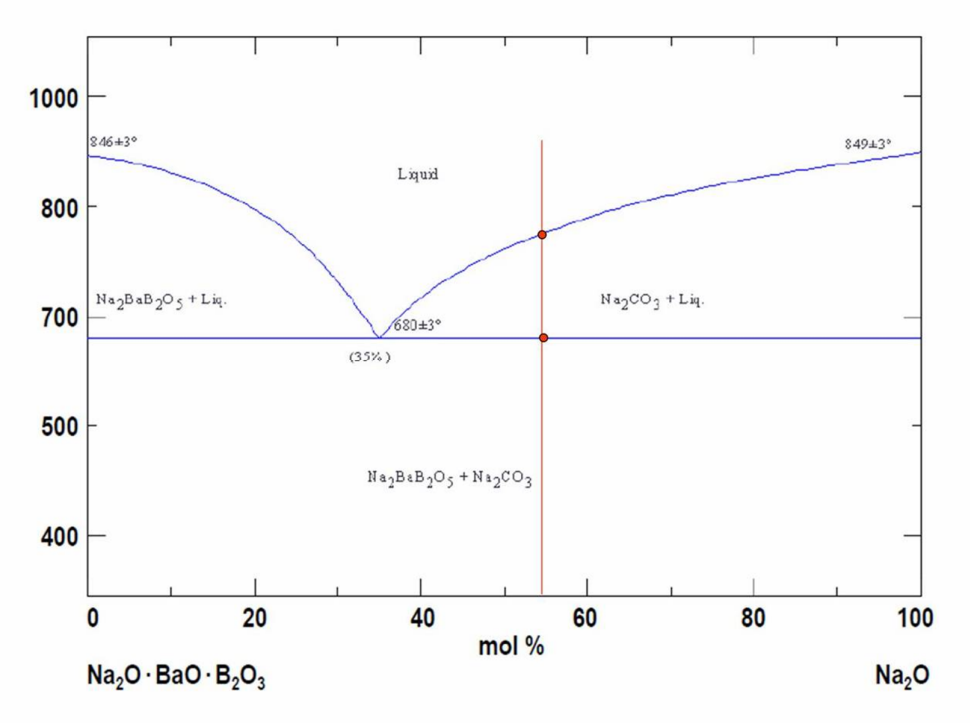

Fig. 55 Phase diagram of the system $Na_2O \cdot BaO \cdot B_2O_3$ – Na_2CO_3 [PHA 1998]. The thin red line indicates the temperature and actual composition in the glass batch

4.3.4.3 E-glass batch

Figure 56 shows the results of the conductometry of E-glass batches with various boron oxide carriers. Reactions turnover do not achieve significant turnovers at temperatures below 1000 °C. At higher temperatures, solid-state reactions, and eventually, the primary melt formation can be observed by the increase of the conductivity curve and conductivity jump, respectively. In the E-glass batch, however, the relatively weak conductivity jump is detected, compared to that of the two previous borosilicate glasses. In the alkali-poor E-glass batch, the change of the conductivity signal is solely dependent on the amount of mobile ion species, which, in this case, is Na^+. The temperature, where the conductivity jump occurs, coincides with the liquidus temperature of the system in the equilibrium as it is calculated theoretically by FactSage™ (see Figure 57).

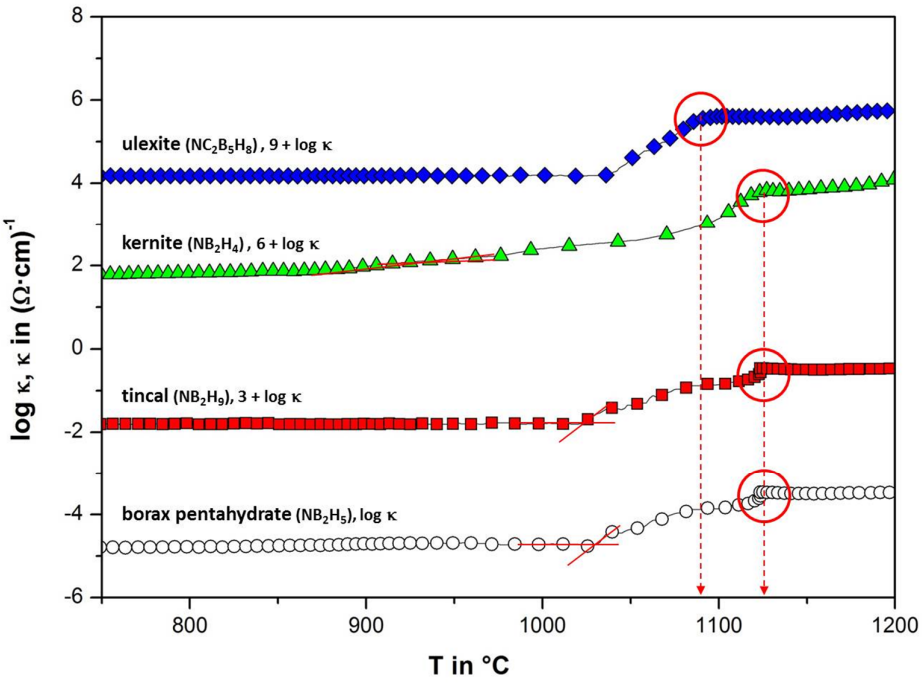

Fig. 56 Conductometry signals of E-glass batches with various types of boron oxide carriers

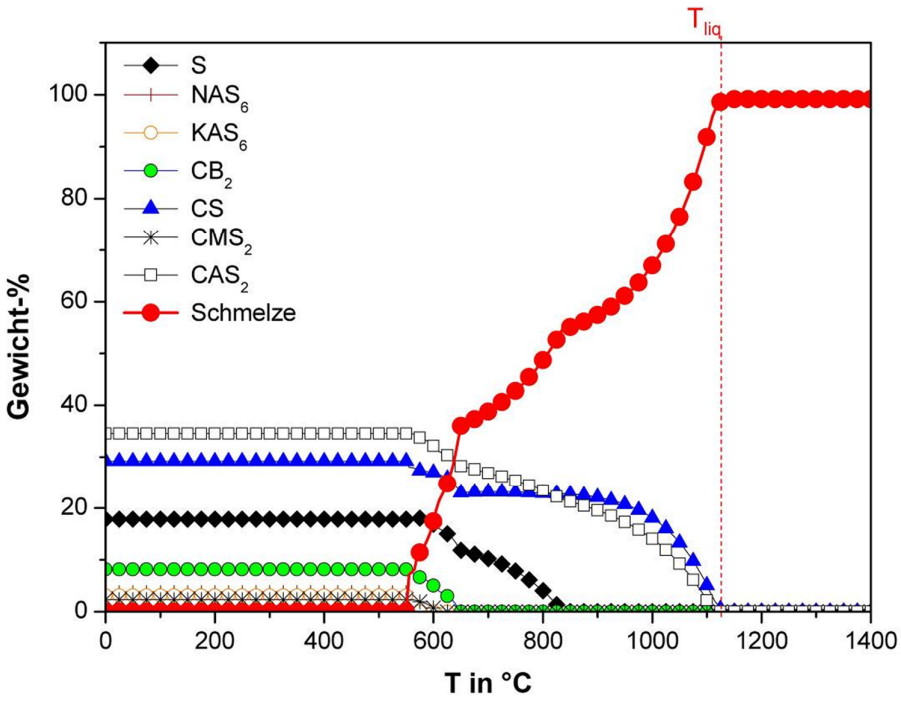

Fig. 57 The thermochemical calculation of the phase equilibrium for the E-glass by system using FactSage™; The liquiuds temperature is 1120 °C with Wollastonite (CS) as the predicted phase prior to melting

The melting progress among the batches show the similar behaviour as indicated by the similar conductivity curves, except for the ulexite batch, in which the primary melt formation associated with the conductivity jump shifted to a lower temperature of 1095 °C, instead of 1120 °C, for the other batches. The ulexite batch, however, has obviously larger amounts of Na_2O content than the other batches, thus lowering the liquidus temperature of the system.

4.3.4.4 Insulation glass wool batch

In this particular batch, the melting behaviour of kernite, tincal, and hydroboracite as the alternative boron oxide carriers. The conductometry results are similar for all the batches, and they can be seen in Figure 58. The temperature at which the primary melt formation occurred in the hydroboracite-containing batch (755 °C) is slightly higher than that of borax pentahydrate and kernite batch (750 °C), but slightly lower than the ulexite batch (800 °C). The ulexite batch showed relatively shorter foaming phase than the others, since several parts of the the raw material which contribute to the gas decomposition is partly replaced by the ulexite.

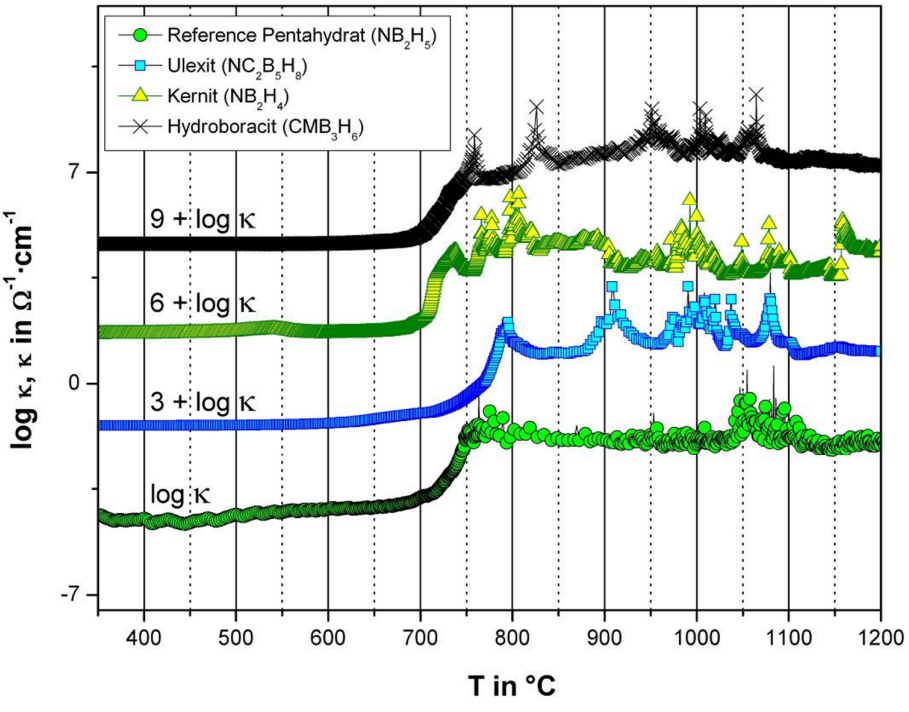

Fig. 58 Conductometry of the insulation glass wool batches by applying various types of boron oxide carrier

The behaviour of the conductometry signal in this batch is similar to that of the lamp glass batch, in which salt-like melt formation of the raw materials determine the mechanism of primary melt formation. Large amounts of soda ash, utilized as the Na_2O carrier in the respective batch, contribute to the lower primary melt formation temperature. Interactions of raw materials within the batch lead to a lower eutectic melting that can be detected by the conductometry method.

4.3.5 Modified batch-free time (BFT)

Different than conductometry and other thermal analysis methods, in which the heating rate is set as a constant value (10 K/min) from room to final temperature, the batch-free time (BFT) test is a method to observe the dissolution rate of the batch under the influence of both glass melt and radiation heat at a constant experiment temperature (1400 °C), thus at an arbitrary heating rate. The definition of BFT is literally the time required for the batch to dissolve into molten glass at a particular temperature. However, in the present paper, the method is modified as it is intended to compare the batch melting behaviour between the designated reference and tested batches at a particular temperature; therefore, instead of determining the dissolution rate, a qualitative comparison of the batches is analysed in at least two window timeframes. One of the timeframes should be defined as the time required for the reference batch to dissolve completely in the molten glass. From that point, one can determine the other timeframes for all batches, and compare them, mostly in the qualitative way.

4.3.5.1 BFT of laboratory glassware batch

Figure 59 shows the surface appearance of the laboratory glassware batch after the BFT test after 30 and 60 minutes of exposure time at 1400 °C. In the first time window, 30 min, the batch melting behaviour of the tincal-containing batch has better melting progress than that of the reference (borax pentahydrate) and kernite batches. Both the borax pentyhdrate and tincal batches do not show different appearances by longer melting time, while the kernite batch has similar appearances between 30 min and 60 min of exposure time and more foams than the others.

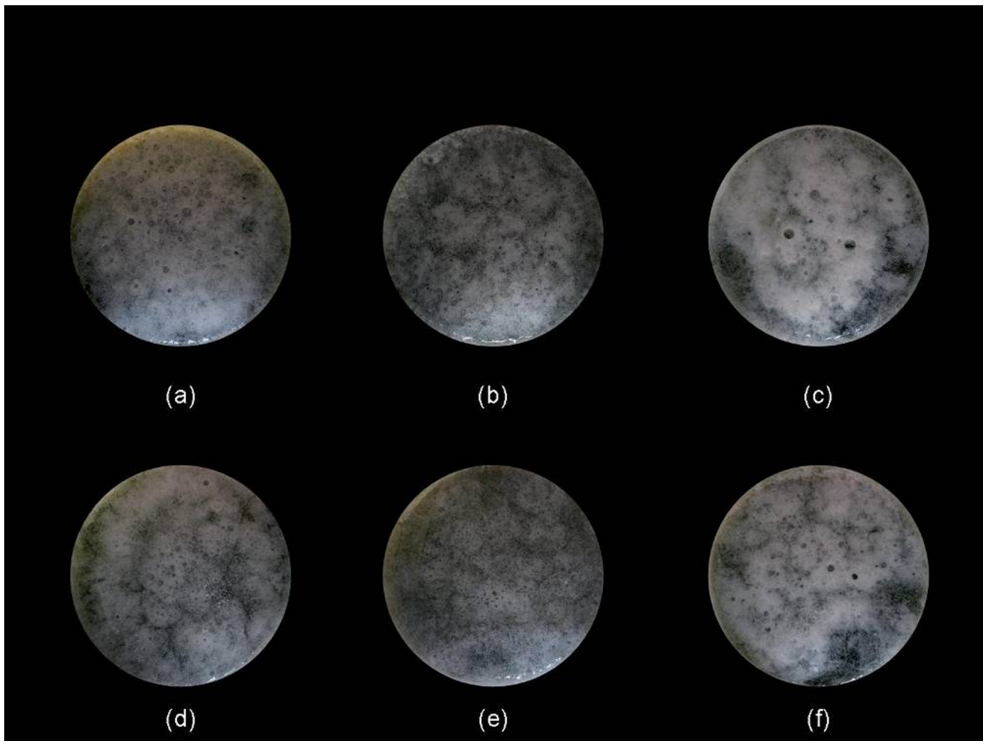

Fig. 59 BFT results of the laboratory glassware batch; (a), (d): reference batch (Borax Pentahydrate); (b), (e): Tincal batch; (c), (f): Kernite batch; The series of pictures (a-c): 30 min of exposure time, (d-f): 60 min of exposure time

4.3.5.2 BFT of lamp glass batch

The behaviour of batch melting with various types of boron oxide carriers in the lamp glass batch show no significant differences. In the respective batch, two exposure times were chosen, namely 10 and 40 min. The surface appearance of the BFT result (see Figure 60) shows that the application of tincal and kernite as the alternative boron oxide carrier in the lamp glass batch is not critical during the melting progress. The melting formation of carbonate raw materials shown in the conductometry tests may contribute in the melting progress under an arbitrary heating rate.

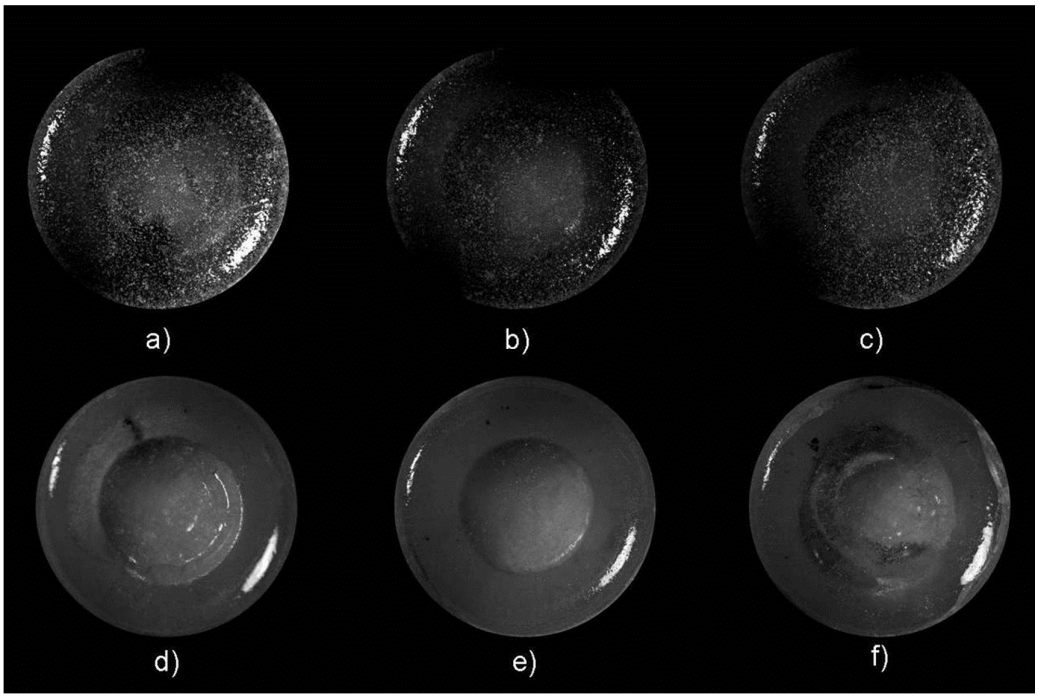

Fig. 60 Surface appearance of BFT results of the lamp glass batch; (a), (d): Reference batch; (b), (e): Tincal batch; (c), (f): Kernite batch; Upper (a-c) and below (d-f) picture series corresponds to 10 min and 40 min at 1400 °C, respectively

4.3.5.3 BFT of E-glass batch

Similar tendencies of the batch melting behaviour are also observed in the E-glass batch (see Figure 61). Two exposure times, 15 and 40 min, were chosen as the BFT time-windows. The role of alternative boron oxide carriers has an insignificant impact on the melting behaviour of E-glass batch. The ulexite-containing batch is the best batch in terms of the batch melting behaviour, and it is consistent with the conductometry results. In 15 min of exposure time, the area of free volume of the ulexite batch at the surface is the largest, thus the melting progress is obviously faster. No significant impact can be observed for other batches, since only small amounts of the sodium-bearing borate minerals (tincal and kernite) were added to the batch. Recently, colemanite ($C_2B_3H_5$) has been considered, indeed, as the conventional B_2O_3 carrier in the E-glass production. The alternative boron oxide carriers in the present study were used for substituting the borax pentahydrate of limited Na_2O in the E-glass composition.

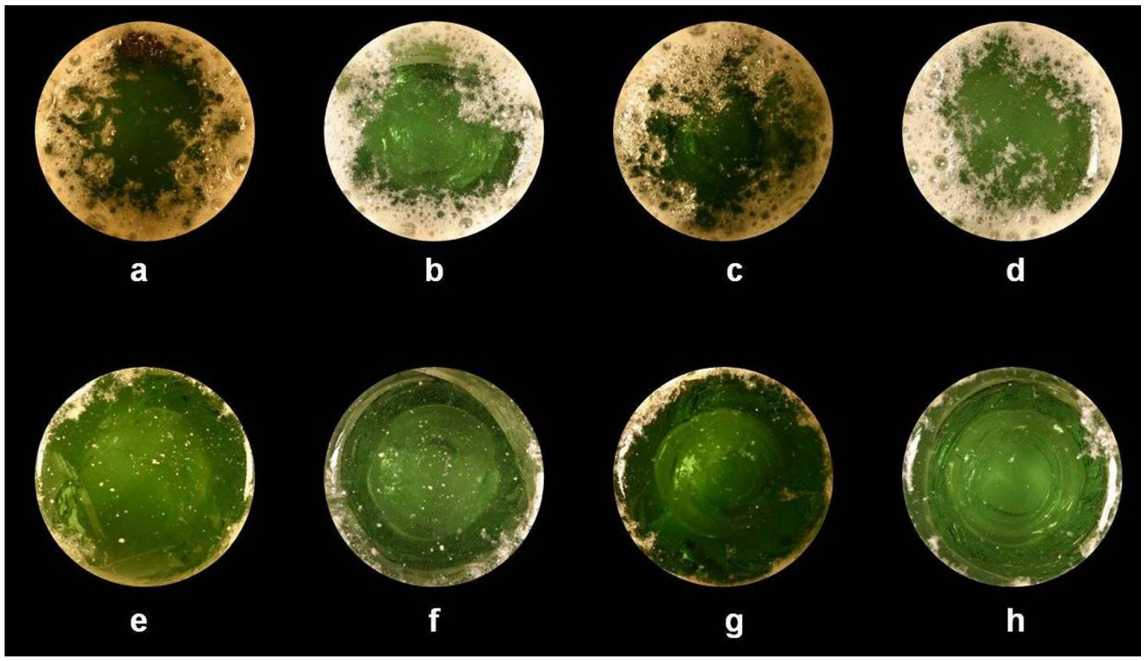

Fig. 61 Surface appearance of the BFT results of the E-glass batch; (a), (e): reference batch; (b), (f): tincal batch; (c), (g): kernite batch; (d), (h): ulexite batch. Upper (a-d) and below (e-h) are picture series correspond to 15 min and 40 min at 1400 °C, respectively

4.3.5.4 BFT of wool glass batch

The complete melting progress of all batches in the insulation glass wool batch is achieved after 15 min of BFT, as shown in Figure 62, because the wool glass batch composition in the present study contains 50 wt. % cullets. Evaluation of the surface appearance can be carried out in 5 min of exposure time, and based on that result, ulexite has a slightly better melting progress than the other batches using borax pentahydrate, tincal and kernite.

Similar to that of the lamp glass system, melting reactions are faster due to a combination of reactions between cullets and other raw materials. However, this behaviour cannot be observed in the laboratory glassware batch in which 40 wt. % of cullets are added into the batch. The cullets are melted at its liquidus temperature, i.e. 800 °C. Due to the lack of salt-like-melt bearing raw materials like soda ash, the high viscosity reached at lower temperatures impedes the sand dissolution progress. As a result, the laboratory glassware batch has a slow melting progress in comparison to that of other glass batches.

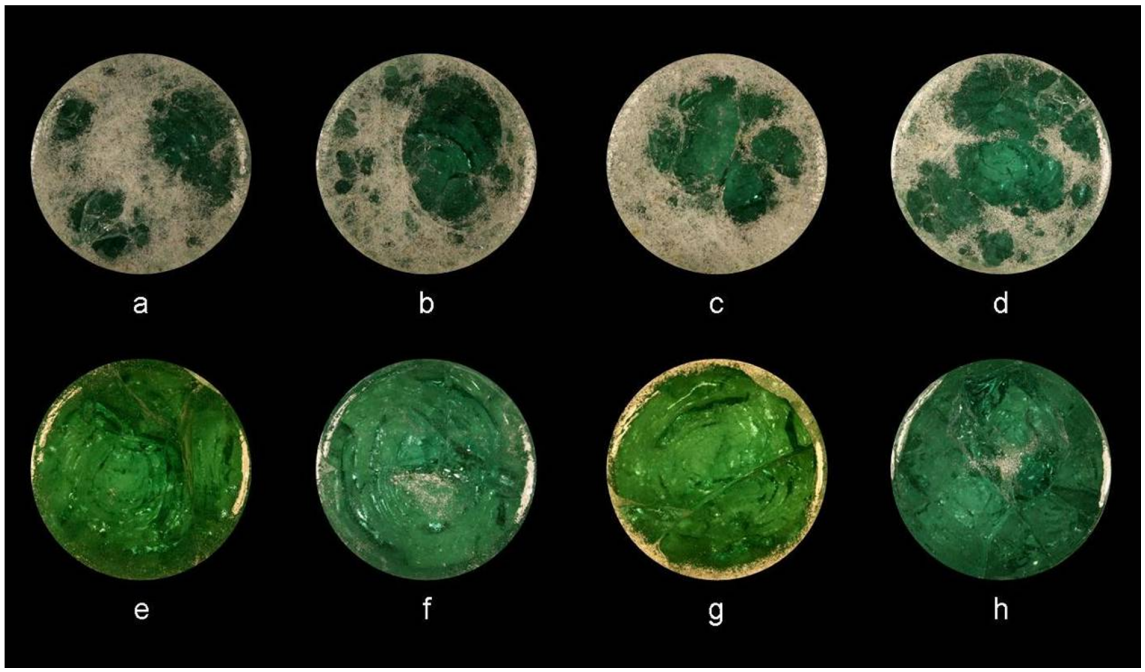

Fig. 62 Surface appearance of the BFT results of the wool glass batch; (a), (e): reference batch; (b), (f): ulexite batch; (c), (g): kernite batch; (d), (h): hydroboracite batch. Upper (a-d) and below are (e-h) picture series correspond to 5 min and 15 min at 1400 °C, respectively

4.3.6 10 kg tests

4.3.6.1 10 kg test of laboratory glassware batch

The substitution of the conventional borax pentahydrate with tincal and kernite does not significantly alter the time required to complete endothermal reactions in the batch, t_{endo}, of the laboratory glassware and lamp glass batches. In the laboratory glassware, temperature profiles are similar between reference and tincal-containing batches. Figure 63 shows that Temperatures in the melt side, T_1 and T_2 for kernite batch is obviously colder than the reference and tincal at the same temperature positions. As the 1400 °C radiation heat was supplied by the upper compartment of the hood furnace, the melting progress in the kernite batch is the fastest among the others. At the end of the experiment (after 40 min of melting), the heat penetration, expressed by ΔT, of the kernite batch is slightly higher than that of reference and tincal batches. Based on the modified BFT results of the laboratory glassware batch in Figure 59, the degree of the amount of surface crystallization (scum) in the kernite batch is also slightlyhigher than in the

reference and tincal. The scum and foam formation at the glass melt surface obstructs the radiation heat transfer from combustion space to the batch.

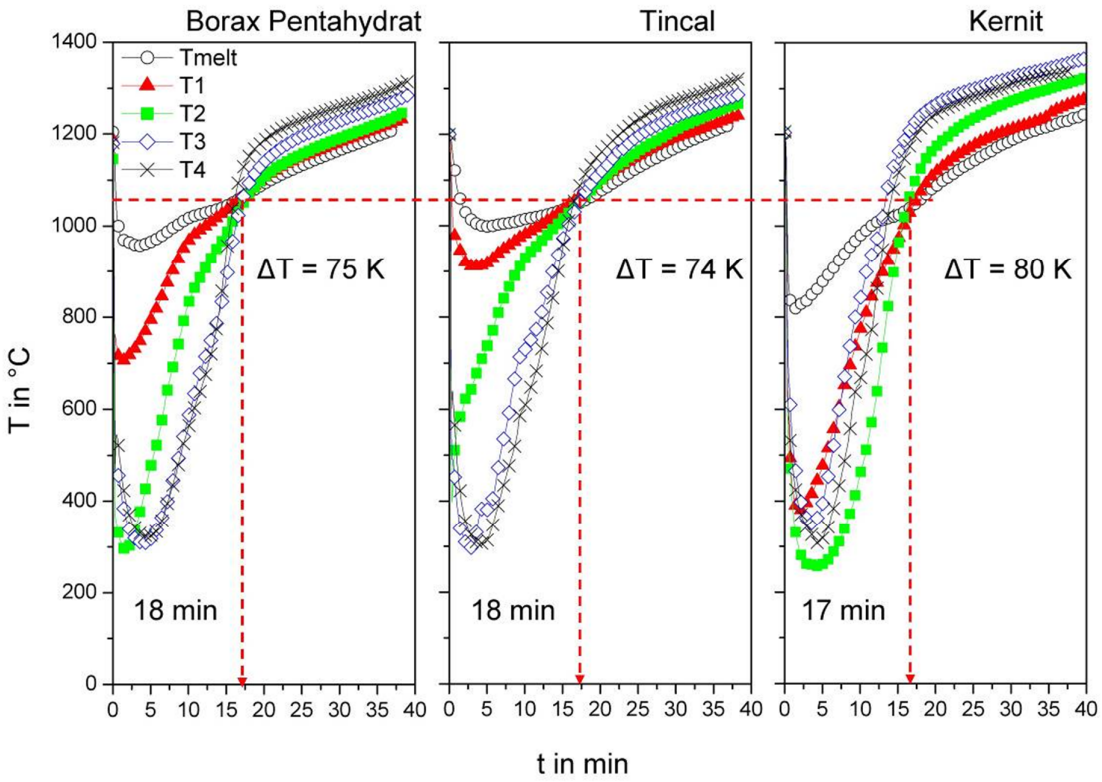

Fig. 63 Temperature profile of the laboratory glassware batch in the 10 kg test.

4.3.6.2 10 kg test of lamp glass batch

Despite the small variance of t_{endo} among the reference, tincal and kernite batches in the lamp glass batches, the temperature profiles are slightly different, specifically for the kernite batch (see Figure 64). Both the temperatures in the melting and fire side in the kernite batch were already high at the beginning of the warming phase (0 to 15 min), in which the progress of the reaction is relatively slower than that of the reference and tincal batch within this range. Significant increases of temperature in the middle of the batch (T_3) of the kernite batch indicate that heat transfer in the batch from below and combustion space improves significantly. At the end of the experiment, the reference batch has the largest ΔT value than the other batches.

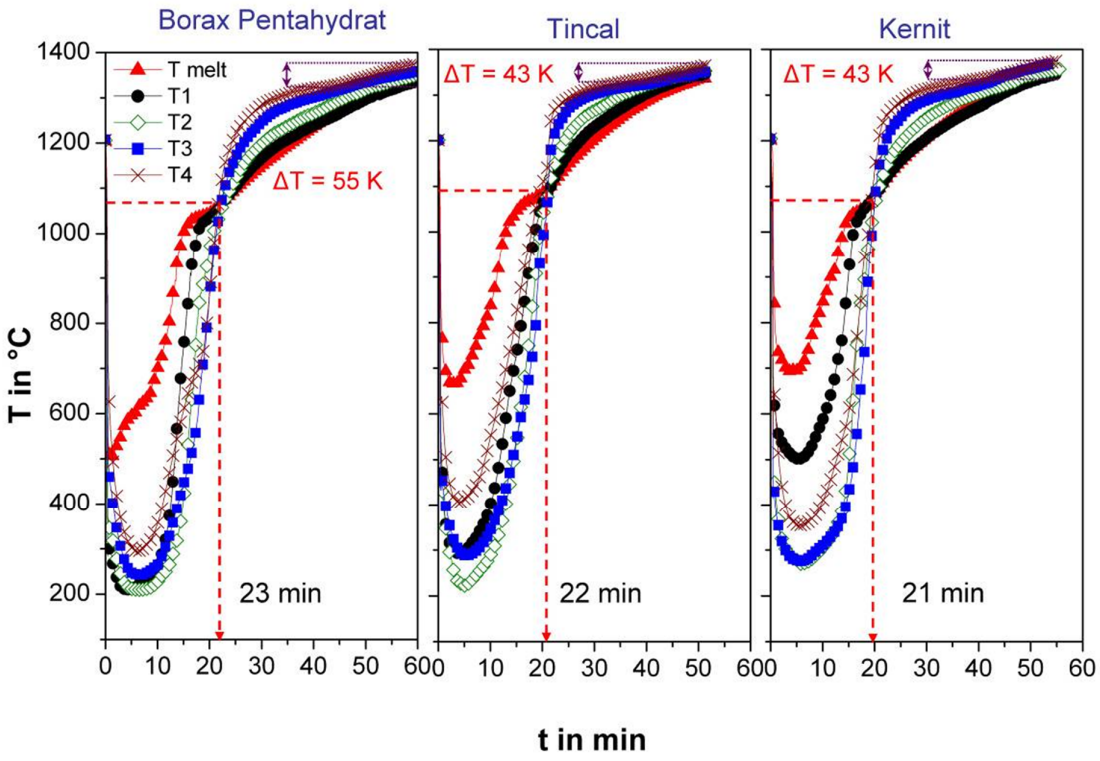

Fig. 64 The temperature profile of lamp glass batch after the 10 kg test

4.3.6.3 10 kg test of E-glass batch

In E-glass batches, the excessive amount of Na_2O in the ulexite-containing batch brings about faster t_{endo} than the other batches, while the other batches show similar behaviour in terms of t_{endo}. Higher amount of Na_2O from ulexite decreases the eutectic points of the raw batch materials in the E-glass system. The E-glass system has different mechanisms of melting, compared to the conventional soda-lime silica glass batch. According to the evaluation of the results of conductometry, the turnover reactions became faster after 1000 °C under the 10 K/min heating rate. Figure 65 shows the rapid temperature increase, specifically T_2 and T_3, occurred at lower temperatures because the heating rate is obviously higher in the 10 kg test than in the conductometry. The influence of convective motion from molten glass and radiation heat transfer from combustion space is the same; it indicates the small temperature differences between T_1, T_2, T_3, and T_4. The heat transfer of the other batches were mainly contributed by the convectional motion from glass melt. The application of alternative borate minerals in the E-glass batch gives a better heat transfer by convection, radiation, and even conduction.

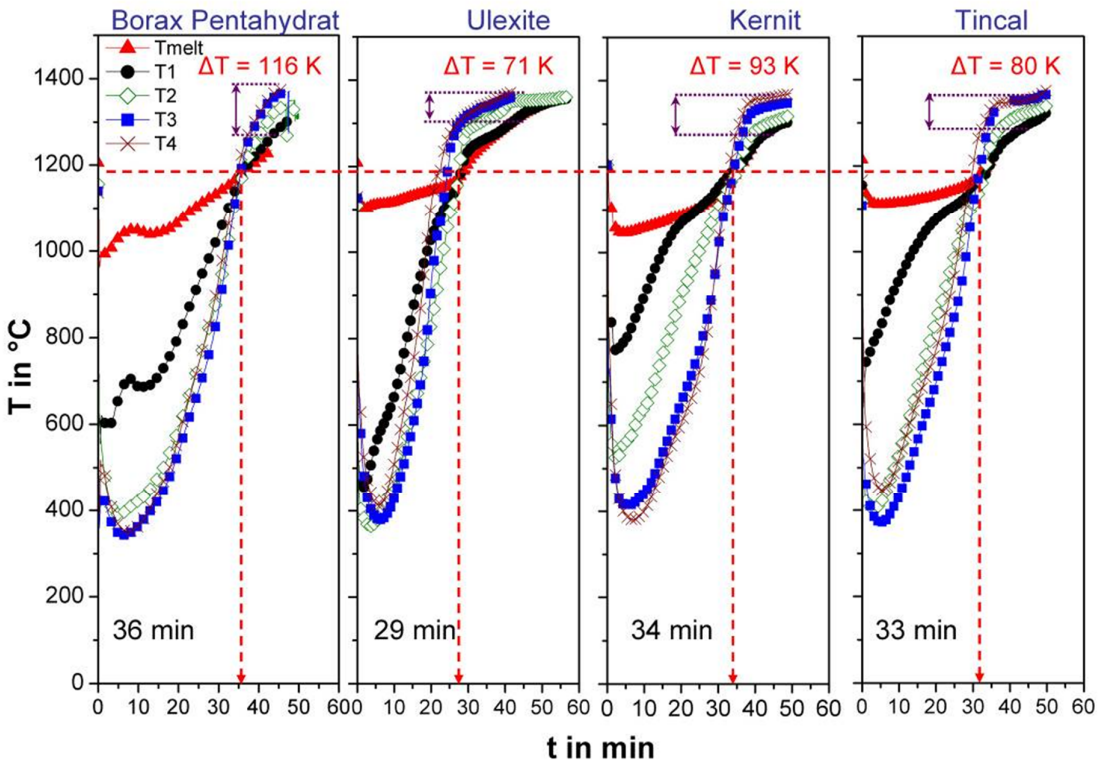

Fig. 65 The vertical temperature profile of E-glass batch in 10 kg test

4.3.6.4 10 kg test result of wool glass batch

In contrast to the E-glass batch, t_{endo} for the ulexite batch in the wool glass batch is the slowest, as shown in Figure 66. The amount of ulexite in the wool glass batch is obviously higher than that of in the E-glass; therefore, ulexite plays a major role in the batch reactions. In the ulexite batch, the endothermal reactions involved during melting, such as the hydration, hydroxylation, and CO_2 decomposition processes, require longer time and higher temperature which are indicated by the higher value of t_{endo} and its respective temperature. However, the ΔT value after 50 min of melting are similar for all batches; thus the ulexite batch requires longer time for the endothermal reactions to be completed, but as soon as the batch-to-melt turnover point is reached, the reaction progress increases to the same extent to other batches.

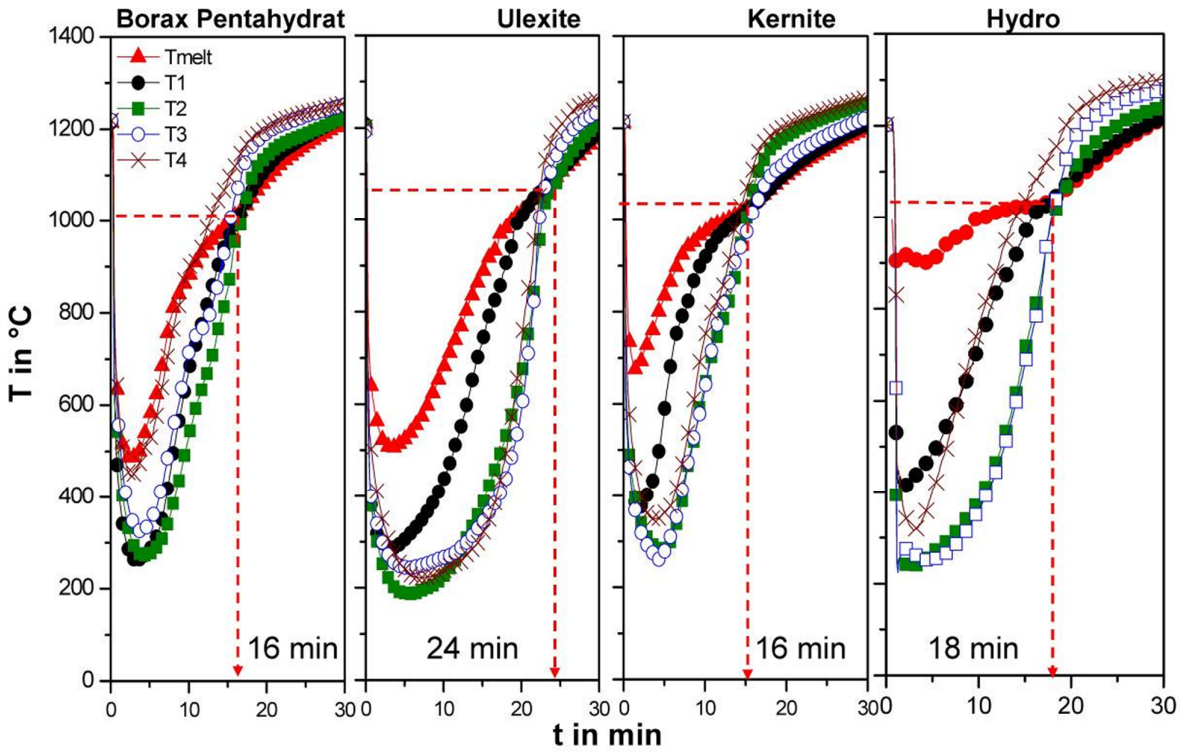

Fig. 66 The vertical temperature profile of 10 kg test result of the wool glass batch.

For a better understanding of this occurrence, there is, in fact, an interaction between the batch-to-melt turnover as indicated by the formation of primary melt in the batch and thermal diffusivity ***a*** [cm^2/s]. The effective ***a*** value can be derived from the temperature profile of the 10 kg test results by applying the Fourier's equation for heat transfer in the steady state. Figure 67 shows the relation between the thermal diffusivity of the batch derived from the 10 kg test result, and plots it with the conductometry signal.

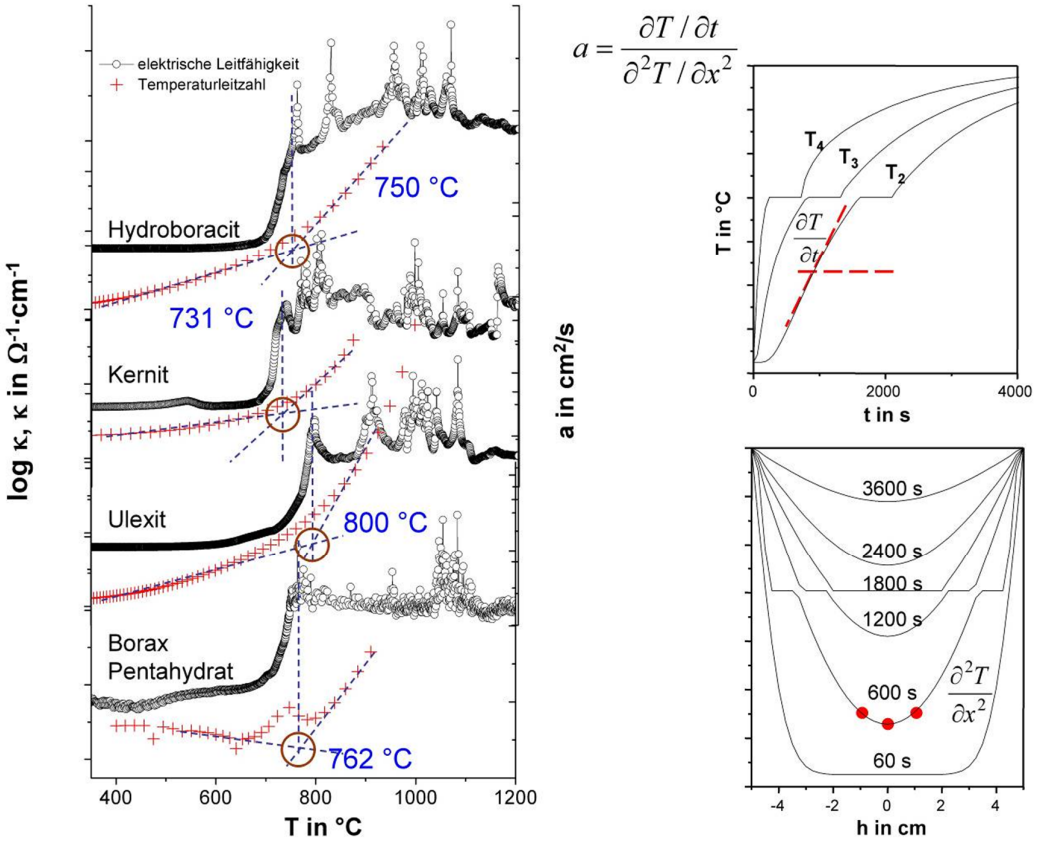

Fig. 67 Conductometry and thermal diffusivity of wool glass batch as a function of temperature (left-hand side); Derivation of thermal diffussivity, ***a***, from temperature profiles (Temperature vs. time and position) of the 10 kg result (right-hand side) [CON 1994]

Based on the conductometry signal of wool glass batches in the previous sub-chapter, the batch melting behaviour in terms of the primary melt formation of ulexite batch is shifted at higher temperatures, while no significant differences were observed among the sodium borate bearing and hydroboracite batches. As the primary melt is formed, the ***a*** value of each batch increases sharply, which indicates higher turnover of the batch-to-melt reactions within the batch. The slope change of ***a*** value at the primary melt formation temperature of reference, kernite, and hydroboracite batches is similar, whereas the ulexite batch has steeper slope, although the temperature of the primary melt formation is shifted 40 K higher than the reference. The sudden change of ***a*** value in the ulexite batch leads to the high melting progress; thus the next melting process, such as foaming phase and dissolution, can be reached at lower temperatures. Furthermore, application of

ulexite in the batch reduces the CO_2-generated raw materials, such as Na_2CO_3 and $CaCO_3$, which contribute to bubbles and foams formation.

4.3.7 Thermochemical calculations

The theoretical heat capacity of the batch-to-melt turnover of a batch complex system can be derived by utilizing thermodynamic concepts, as it is not only a function of the glass tank construction and its operational condition, but also the internal characteristics of the batch. The thermochemical calculation details have been described in Chapter 2.

The results of the thermochemical calculation of heat quantities of laboratory glassware, lamp glass, E-glass, and wool glass batches with various boron oxide carriers will be presented in Table 16, 17, and 18 below.

Table 16 Results of the thermochemical calculation of the industrial batches of laboratory ware glass and lamp glass, with varied boron oxide carriers

	laboratory glassware			lamp glass		
H in kWh/t	**reference**	**Kernite**	**tincal**	**reference**	**kernite**	**tincal**
$H°_{batch}$	4658.10	4649.96	5063.01	4085.07	4070.40	4207.36
$H°_{glass}$	4174.37	4171.88	4171.32	3669.70	3669.05	3669.47
$H°_{gas}$	356.46	349.00	623.67	363.94	352.81	446.50
$H°_{chem}$	127.28	129.08	268.02	51.42	48.55	91.39
T_{off}	650	650	650	650	650	650
T_{ex}	1300	1300	1300	1300	1300	1300
y_C [wt.-%]	39.98	39.98	39.43	22.69	22.69	24.357
H_{TGas} (T_{off})	419.26	419.84	419.90	28.70	28.48	37.71
H_{TGlass} (T_{ex})	33.80	72.54	129.58	407.89	408.33	408.41
H_{ex}	495.66	497.32	582.25	447.65	445.86	477.55

Table 17 Results of the thermochemical calculation of the industrial batches of E-glass, with varied boron oxide carriers

	E-glass			
H in kWh/t	**reference**	**ulexite**	**kernite**	**tincal**
$H°_{batch}$	4837.18	4842.93	4829.53	4859.37
$H°_{glass}$	4050.87	4053.19	4051.64	4051.56
$H°_{gas}$	531.58	532.79	525.51	546.03
$H°_{chem}$	254.73	256.95	252.38	261.78
T_{off} [°C]	650	650	650	650
T_{ex} [°C]	1300	1300	1300	1300
y_C [wt.-%]	0.00	0.00	0.00	0.00
H_{TGas} (T_{off})	46.38	46.54	47.40	49.42
H_{TGlass} (T_{ex})	458.27	458.60	458.49	458.46
H_{ex}	713.00	715.55	710.86	720.24

Table 18 Results of thermochemical calculation of the industrial batches of wool glass, with varied boron oxide carriers

	wool glass				
H in kWh/t	**reference**	**ulexite**	**kernite**	**tincal**	**hydrobor.**
$H°_{batch}$	4365.16	4351.38	4316.15	4520.09	4286.09
$H°_{glass}$	3952.72	3949.01	3952.63	3952.22	3951.57
$H°_{gas}$	330.10	314.87	290.58	429.54	305.17
$H°_{chem}$	82.35	87.51	72.94	138.34	29.35
T_{off} [°C]	650	650	650	650	650
T_{ex} [°C]	1300	1300	1300	1300	1300
y_C [wt.-%]	0.00	0.00	0.00	0.00	0.00
H_{TGas} (T_{off})	39.62	38.48	35.82	49.14	26.04
H_{TGlass} (T_{ex})	453.18	450.78	453.18	453.11	452.92
H_{ex}	535.53	538.29	526.12	591.45	482.27

It is assumed that the off-gas and pull temperatures are set to 650 °C and 1300 °C, respectively, for all batches and individual raw materials involved in the calculation are in the pure phase; hence, only the value of its pure substance (neglecting the impurity factor) is considered. The highest heat demands ($\Delta H°_{chem}$ and ΔH_{ex}) are found in the tincal-containing batch, independent of the glass types. The heat demand of a typical raw material depends on the chemical bonds within the structure as well as the amount of water (H_2O) or hydroxyl (OH) attached to the structure. Stronger bond requires higher energy demand of formation, and additional energy is needed to release either hydrate or hydroxyl within the structure.

Tincal has higher molecule water content, nine water molecules ($9H_2O$), among other borate minerals, thus a higher standard enthaply of formation (4.807 kWh/t). The alternative sodium borate minerals, tincal and kernite, have nearly the same oxide structure with that of borax ($Na_2O{\cdot}2B_2O_3{\cdot}XH_2O$). The difference among those minerals is their water molecule content. The higher water molecule content within the structure leads to higher standard enthaply of formation, thus higher energy demand, in which tincal has the highest content ($9H_2O$) followed by borax pentahydrate ($5H_2O$) and kernite ($4H_2O$). However, borax pentahydrate and kernite have standard enthalpy of formation, i.e. 4.568 kWh/t and 4.564 kWh/t for borax pentahydrate and kernite, respectively. In the E-glass and wool glass batch, the application of alternative borate minerals give no significant impact in terms of heat demand, compared to that of the conventional one. Few parts of non-boron oxide carriers, mostly alkaline and alkaline-earth carbonate, might be replaced by the alternative borate minerals. Gas decomposition of carbonate is a strong endothermal process, thus replacing a few weight percent of carbonate containing raw material by borate minerals lower the total $\Delta H°_{chem}$ of the batch, and consequently, the overall heat demand is decreased.

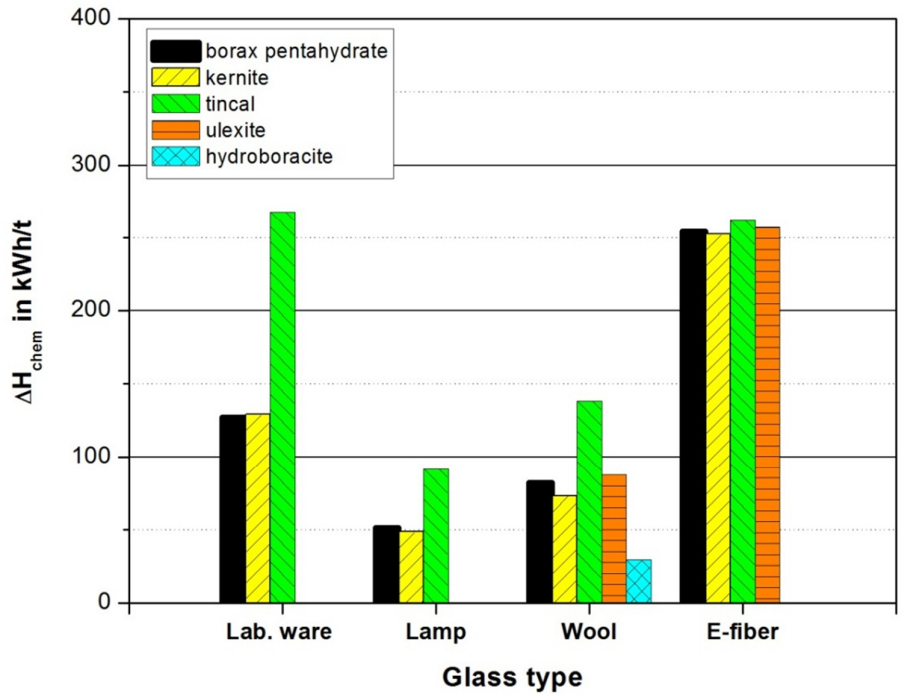

Fig. 68 Chemical heat demand, ΔH°_{chem}, of various batch glass systems with different types of borate minerals as boron oxide carrier

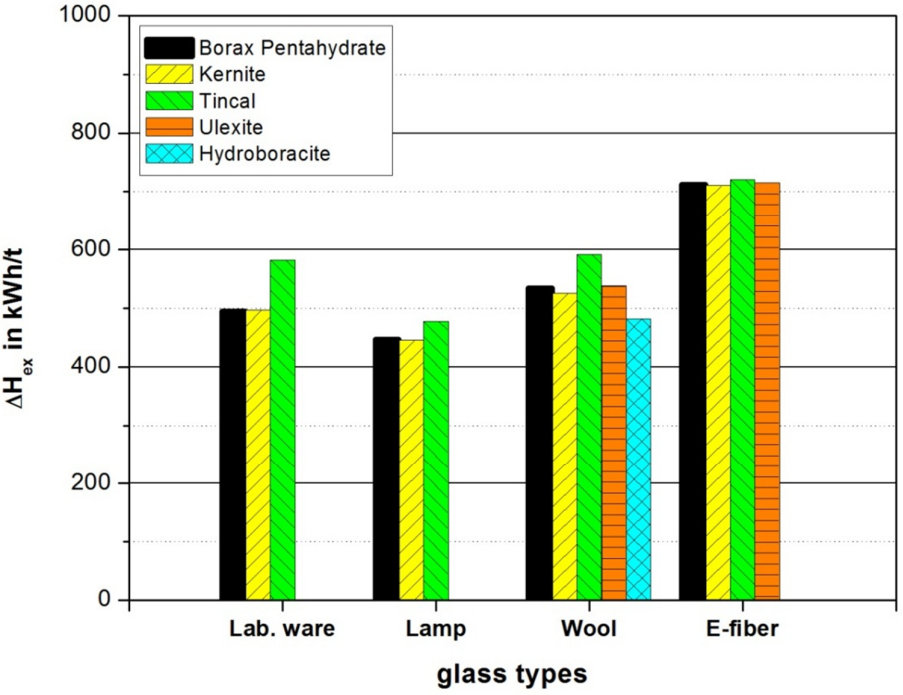

Fig. 69 Calculated exploited heat demand, ΔH_{ex}, of various boron oxide-containing glass types with different borate minerals as boron oxide carrier

5. Application of alternative batch in the industrial melting tank

5.1 Effect of alternative boron oxide carriers on furnace performance

Comprehensive analyses and evaluations of batch melting behaviour have been performed to determine the possible alternative batch/raw material that can be applied for further investigation, i.e. the effect of alternative batch to furnace performance in an industrial glass tank. Daily production data, such as temperatures (crown, bottom, stack, throat, and riser), charge input (composition of glass, batch, and cullet ratio), fuel consumptions (gas, oxygen, and air), and pull/production capacity are utilized to calculate and complete the energy balance, as previously described in Chapter 2.

In the present study, the industrial campaign was performed under an AiF project, 'Alternative boron oxide raw material in glass industry'. Selection of raw materials for the industrial campaign does not only depend on the laboratory results which require large amounts of raw material to obtain a good statistical data, but also on the availability of raw materials. Not all industrial partners were able to perform the trial due to several reasons; mainly because they had difficulties in making the alternative boron oxide carriers in the required volume since only a few were available commercially. Moreover, high risks of quality deviation of the product and complexity in providing additional silos were also the obstacles to the industrial experiment.

Colemanite and ulexite are the alternative borate minerals that are available commercially for the production of B_2O_3-containing glasses. Most of the borate minerals are processed for the production of boric acid and sodium tetraborate pentahydrate, whose applications are not only for glass industries but also for the manufactures of detergent. Colemanite is already renowned as a substitute of boric acid in the E-glass production, but cannot be used for borosilicate glasses due to high content of CaO. The laboratory results of wool glass melts show that colemanite is less favourable than the other alternative boron oxide, as previously discussed in Chapter 4. For that reason, ulexite was the chosen raw material for

the boron oxide carrier to be applied in the glass melting furnace during the campaign.

5.2 Furnace design and process parameter

The methodology of the furnace performance evaluation is a comparison of process parameters, in terms of energy demand, production/pull rate, temperature data between the reference (borax pentahydrate), and the ulexite-containing batch [CON 2012]. Additionally, carryover and boron-compound vapours in off-gas are analysed and compared. Figure 70 shows a schematic view of a typical glass wool melter in longitudinal projection.

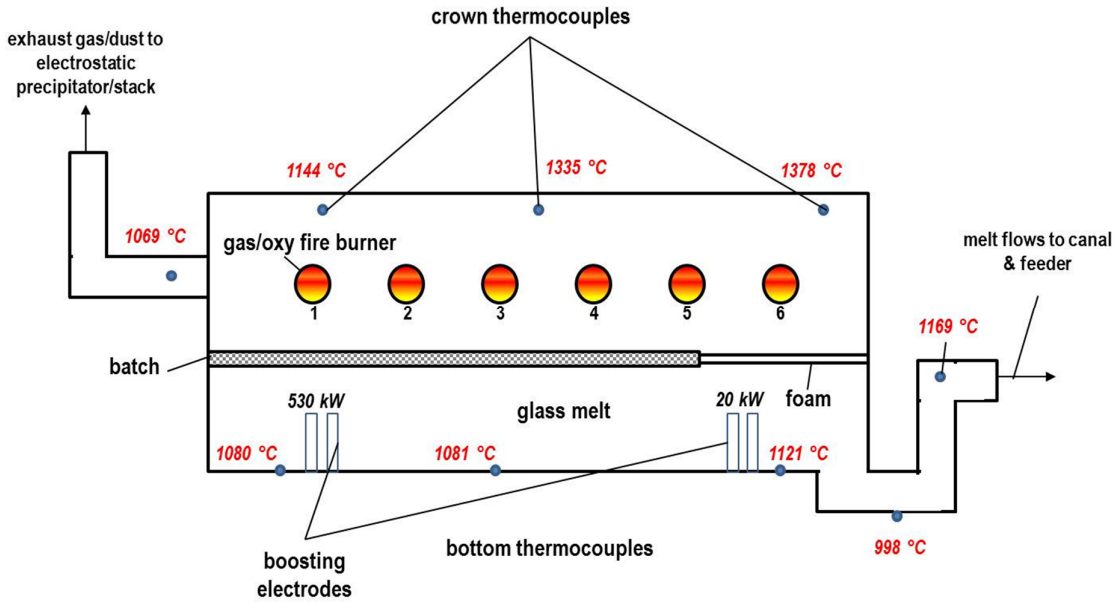

Fig. 70 Schematic view of a wool glass melter in longitudinal projection. The melter is a cross-firing oxy-fuel furnace in which natural gas and high-purity oxygen are used for the combustion process

Based on the melter crown and bottom temperature distribution, unlike flat and container glass production, foam is extended up to the front wall of the melter. Batch and recycled glass cullet are introduced through dog houses by screw chargers installed at the right and left side walls of the melter. The batch heap are exposed by radiation and convective heat from the combustion space and hot molten glass respectively. Electric boosting systems are installed in the rear and front of the melter not only to provide additional heat/energy but also play

important role in controlling the convective current of the glass melt. One electrode system is positioned under the batch blanket for high powerage and the other system is installed in the front part of he furnace with much lower power. The energy from boosting system is provided by Joulean heat due to the passage of electrical current between the electrodes in the glass melt. The campaign that uses ulexite as a B_2O_3 carrier lasted 30 days, and was compared to the current reference data in which borax was used as a B_2O_3 carrier.

Table 19 Furnace set-up and process parameter

Parameter	unit/rate	setting value
cullet percentage	%	49
designed pull rate	t/d	84.00
temperatures	°C	
crown rear	°C	1144
crown center	°C	1335
crown front	°C	1378
bottom rear	°C	1080
bottom middle	°C	1081
bottom front	°C	1121
Throat	°C	998
Riser	°C	1169
Offgas	°C	1069
Stack	°C	350
number of burner		6
gas consumption	Nm^3/h	305
oxygen consumption	Nm^3/h	620
average H_{NCV}	kWh/m^3	9.89
800 kVA transformer (rear)	kW	530
60 kVA transformer (front)	kW	20

The glass composition between reference and ulexite batch was adjusted to keep the properties constant, specifically its viscosity level (η) equivalent to log η = 3.0 dPa·s.

Energy input from the gas-oxy firing depends on the volumetric flow V'_H and the net calorific heat value H_{NCHV} of fuel used for the combustion process.

$$P_{in}\ [kW] = V'_H\ [m^3/h] \cdot H_{NCHV}\ [kWh/m^3] \qquad (28)$$

The chemical heat demand $\Delta H°_{chem}$ calculation presented in Chapter 4 shows that the ulexite batch has a slightly higher heat demand than that of the borax pentahydrate batch. However, small variations in the ulexite batch lead to slight changes in the heat capacity of the glass melt.

The composition of the glass wool insulation is similar to the composition that has been specified in Table 7. Table 19 shows the actual batch composition to produce 1000 kg of glass melt.

Table 20 Comparison of batch compositions to produce 1000 kg of glass between borax pentahydrate and ulexite, during the industrial experiment

	reference [kg]	**ulexite [kg]**
sand [kg]	197.34	190.30
nepheline [kg]	77.51	76.98
dolomite [kg]	70.86	19.03
soda ash [kg]	110.43	131.50
external cullet 1 [kg]	36.95	37.31
external cullet 2 [kg]	471.06	475.52
internal cullet [kg]	55.42	55.97
borax pentahydrate [kg]	99.50	
ulexite [kg]		118.65
sum [kg]	**1115.06**	**1105.47**

Additional to the calculation results shown in Table 18 in Chapter 4, Table 21 shows comparisons of oxide composition and its normative phase standard heat formation of the respective oxide between reference and ulexite batch. The batch composition is adjusted in such a way that the final glass oxide compositions are similar, and the usage of limestone as the CaO carrier is avoided. The change of raw materials was made under the boundary condition that $Na_2O + K_2O$ and CaO + MgO are constant. In fact, the concentration of individual alkali oxide could also be kept constant under the replacement. However, the reference batch yields a glass with 3.63 MgO + 6.87 CaO while the ulexite batch yields a glass with 2.75 MgO and 7.64 CaO. Thus, there is a slight shift not only in $\Delta H°_{chem}$ but also in ΔH_T.

Table 21 Comparisons of oxide composition and its normative standard heat formation between reference and ulexite containing batch using a calculation method proposed by Conradt [CON 2007]

oxide composition j	**reference**	**ulexite**	**difference**
SiO_2	64.53	64.60	-0.07
Al_2O_3	2.52	2.51	0.01
B_2O_3	5.09	5.10	-0.01
MgO	3.62	2.75	0.87
CaO	6.87	7.64	-0.77
Na_2O	16.58	16.60	-0.02
K_2O	0.80	0.80	0.00
sum	**100.00**	**100.00**	
Na_2O+K_2O	17.38	17.40	-0.02
CaO+MgO	10.49	10.39	0.10
standard heat formation of the glass [kWh/t]			
normative phase k	**reference**	**ulexite**	**difference**
$CaO·2B_2O_3$	332.94	333.88	-0.94
$K_2O·Al_2O3·6SiO_2$	184.34	184.92	-0.58
$Na_2O·Al_2O_3·6SiO_2$	348.51	346.77	1.74
$MgO·SiO_2$	374.88	284.67	90.21
$Na_2O·2SiO_2$	1514.11	1486.19	27.92
$Na_2O·3CaO·6SiO_2$	655.34	759.62	-104.28
SiO_2	542.59	552.95	-10.36
sum	**3952.72**	**3949.01**	**3.71**

Since the range of total alkaline earth content in the glass is very narrow, changing of the cullet ratio cannot be avoided, which leads to a similar exploited heat H_{ex} between reference and the ulexite batch (see Equation 8, 9 and 10 in Chapter 2). The internal cullet has the same composition like that of the target glass, and can be treated as the cullet fraction y_C in Equation 8, while the external cullets (recycled bottle and flat glasses) have to be evaluated as raw materials. By applying the thermodynamic concepts of multicomponent system [CON 2009], the calculated standard heat formations of the external cullet 1 and 2 are 4.126 kWh/kg and 3.942 kWh/kg, respectively.

5.3 Results

Figure 71 and 72 show the results of furnace data analysis of reference and ulexite containing batch respectively. The quantities are given in terms of power, which is derived from the products of specific heat value in kWh/t and the pull rate in t/h, in the unit of kW, are plotted as a function of the pull rate p. All entities P_{in}, P_{ex} and, P_{loss} show linear correlation with the production rate.

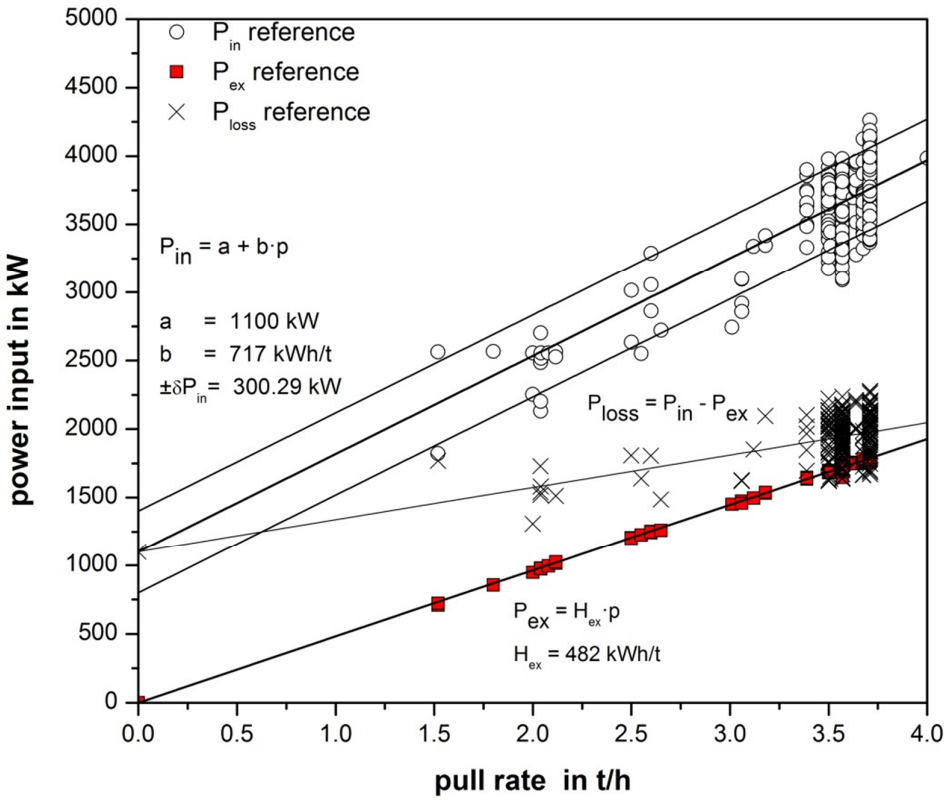

Fig. 71 The input [kW], exploited and loss powers of the reference batch are plotted as a function of pull rate [t/h] [CON 2012]

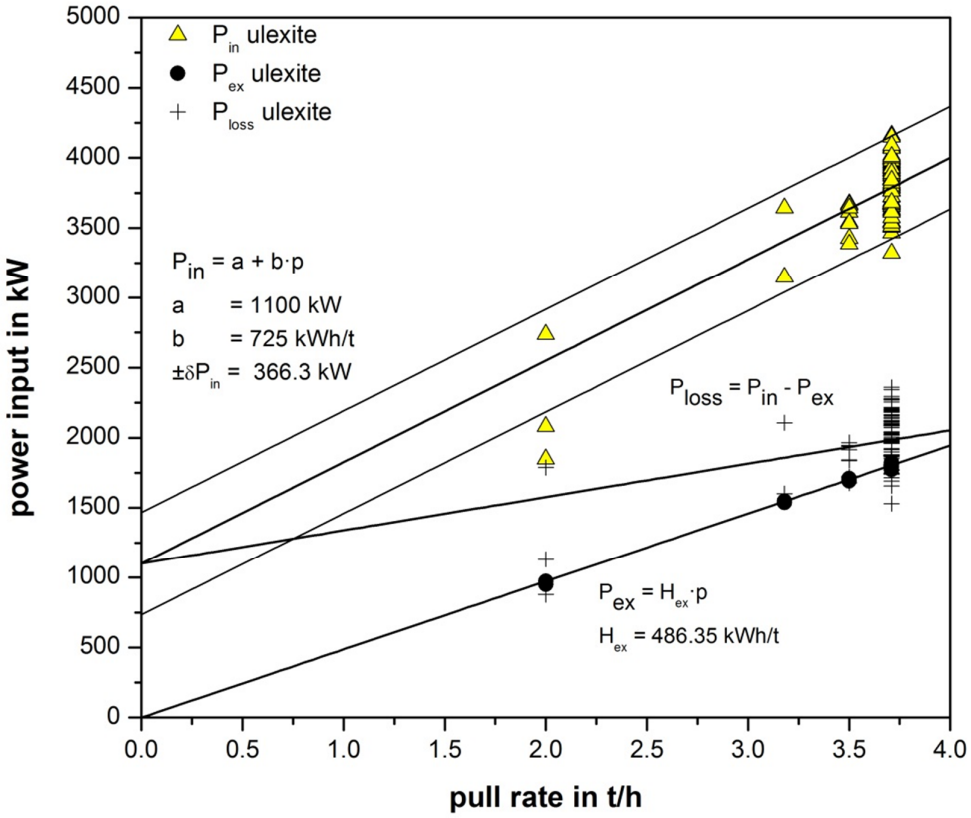

Fig. 72 The input [kW], exploited and loss powers of the ulexite containing batch are plotted as a function of pull rate [t/h] [CON 2012]

According to Conradt [CON 2012], the mathematical linear relationship between power input and pull rate can be derived as:

$$P_{in} = a + b \cdot p \; ; \qquad (30)$$

The exploited power P_{ex} at the drawn temperature

$$P_{ex} = H_{ex} \cdot p \; ; \qquad (31)$$

The energy loss is calculated in a straightforward way, according to the equation;

$$P_{loss} = P_{in} - P_{ex} = a + (b - H_{ex}) \cdot p \qquad (32)$$

All the statistical values described in Figure 71 and 72 (slope, intercept, error range, and exploited heat H_{ex}) are shown in Table 22. The error range ($\pm \delta P_{in}$) is

defined as a standard deviation of power input. Both reference and ulexite batches share the same **b** value since the trial was conducted in the same furnace.

Table 22 Statistical values of linear regressions of the input energy P_{in} curve as shown in Figure 71 and 72

	symbol	**reference**	**ulexite**
number of observation	n	535	97
intercept at zero pull [kW]	a	1100	1100
slope [kWh/t]	b	717	724
error range of P_{in} [kW]	$\pm \delta P_{in}$	300	366
exploited heat [kWh/t]	H_{ex}	482	486

It is a common in glass wool production to keep the pull rate constant over extended periods of time. Several pull rate changes have been observed by using the reference batch, while only four time pull rate adjustments were observed during the trial phase. However, the input power P_{in} fluctuated irrespectively by a constant pull rate. The value of P_{in} in Figure 71 and 72 is an average value, while the vertical error bars represent standard deviation σ of P_{in} in its respective constant pull rate. The exploited power P_{ex} , does not vary much since its value depends on the chemical heat demand $\Delta H°_{chem}$ and the glass exit temperature T_{ex} measured in the melter riser.

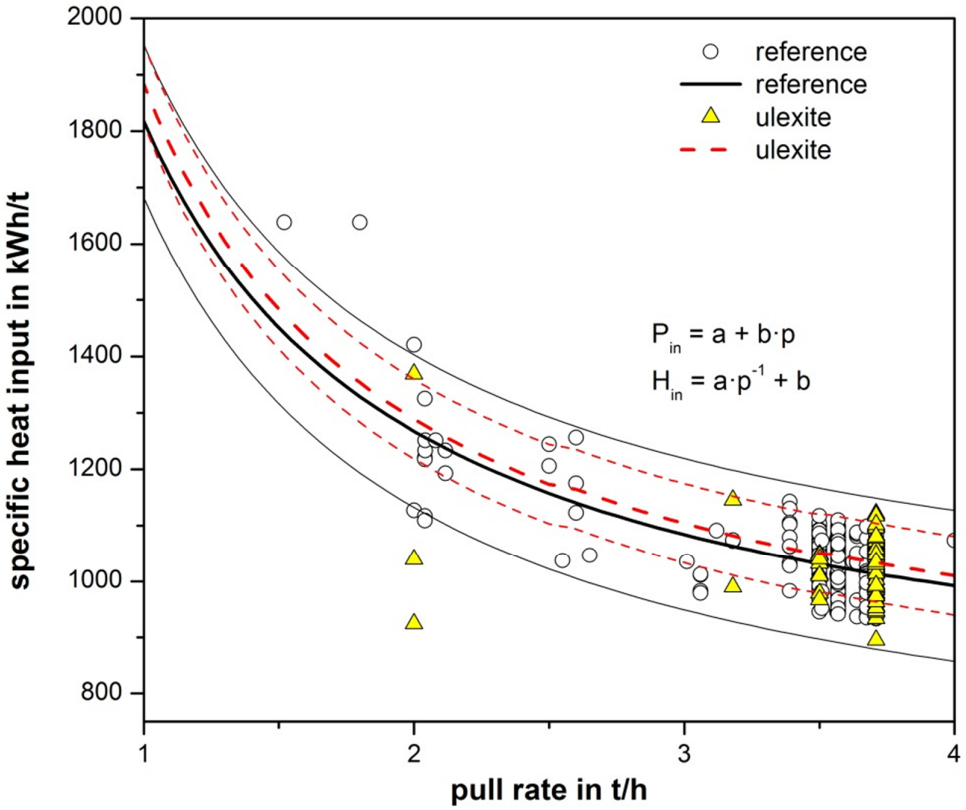

Fig. 73 Specific heat input versus pull rate of reference and ulexite containing batch during the industrial trial. The H_{in} is derived from the input power P_{in} in Figure 71 and 72 divided by the pull rate

Figure 71 and 72 show that the application of ulexite as an alternative raw material does not give significant impact on the input P_{in} and exploited power P_{ex} as compared to that of borax pentahydrate. The large error bars for ulexite batch are due to the small number of observations. Statistically, one can observe in Figure 73, that there is a tendency that less energy is used when the reference batch is applied.

The average pull temperature T_{ex} of the ulexite batch (1163 ± 9 °C) was slightly higher than that of borax pentahydrate (1159 ± 6 °C) as it is shown in Figure 73. According to Equation 8, the physical heat ΔH_T (glass) strongly depends on the glass exit temperature T_{ex} and has a linear correlation with the exploited heat. Therefore, the higher exploited heat is expected for the ulexite batch. In contrast, Figure 74 shows that the average exploited power P_{ex} is slightly lower. The impact, however, is insignificant statistically.

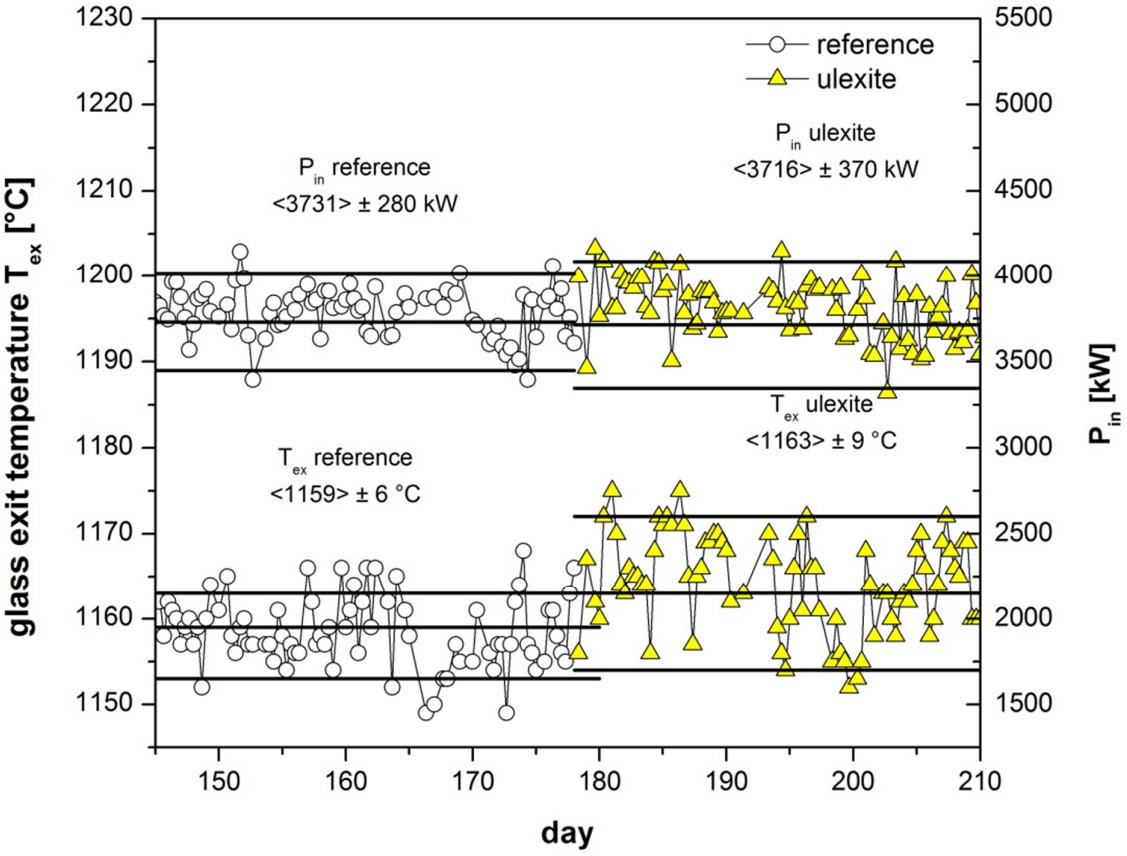

Fig. 74 Glass exit temperatures T_{ex} [°C] and power input P_{in} [kW] on the left and right Y-axis, respectively, as a function of time [day]. The numbers in the bracket "<>" signify the average value and standard deviation σ, respectively

Laboratory results of the 10 kg test in Chapter 4 show that the ulexite batch have melting advantages in terms of foam decay. The effect is reflected by a higher pull temperature T_{ex}. It is likely that the foam is stable up to the melter front wall because the batch composition of glass wool does not contain any fining agents e.g., sodium sulphate and even there is sulphate from the external cullet, the onset of fining temperature in the melt is not sufficient. This can be seen from the crown temperature readings. It is obviously that heat distribution along the furnace longitudinal section is the same, thus hot spot is not likely to form.

However, bubbles in the melt are not considered as defects in the glass wool production. By longer trial times and pull variation one can anticipate that more

energy saving impacts of alternative ulexite against the conventional borax pentahydrate.

Table 23 shows that the average specific heat energy in kWh/t between the batch containing borax pentahydrate or ulexite is similar in terms of the batch melting behaviour. Judging from the results of the batch melting behaviour in the laboratory scale, the application of ulexite in the wool glass batch has a slight advantage in kinetics than that of the borax pentahydrate. However, due to a relatively short trial phase, this effect is difficult to see.

Table 23 Heat balance for the industrial campaign with two different boron oxide carriers relative to the power input

	reference		**Ulexite**	
	kWh/t	***%***	***kWh/t***	***%***
H_{in}	1034.67	100	1029.54	100
H_{re}	1109.69	107.25	1107.75	107.06
H_{sf}	575.07	55.58	576.04	55.67
H_{ex}	125.02	12.08	129.06	12.47
H_{stack}	75.02	7.25	78.21	7.56
H_{off}	34.84	3.37	36.19	3.50
H_{wx}	15.16	1.47	14.66	1.42
H_{wall}	409.61	39.59	402.65	38.92
H_{loss}	424.77	41.05	417.31	40.33
η_{re}	0.60	60.05	0.61	60.60
η_{ex}	0.58	58.14	0.58	58.05
n	535 data		96 data	

5.4 Emission analysis

The Research Association of German Glass Industry, or Hüttentechnische Vereinigung der Deutschen Glasindustrie e. V. (HVG), was responsible to handle the carryover and primary emission in this project since they have experience and equipment in this field. The following substances were determined by taking samples in off-gas location before and after the electro fillter instrument during the industrial campaign of the ulexite batch:

- total dust
- dust composition (B, Ca, K, Mg, Na, S,As, Cd, Co, Cr, Cu, Mn, Ni, Pb, Sb, Se, Sn, V)
- gaseous substances (B, Ca, K, Mg, Na, S,As, Cd, Co, Cr, Cu, Mn, Ni, Pb, Sb, Se, Sn, V)
- nitrogen oxides (NO_x)
- carbon monoxide (CO)
- sulphate oxides (SO_2)
- inorganic gaseous chlorine (HCl)
- inorganic gaseous Flour (HF)

The collection of the emission produced during the melting process is through a steel duct connected to dry electrostatic precipitator, which is 56 m in height and has an entrance area of 2.545 m^2. Four fields type electro filter was used as an instrument that functions to clean the off-gas from carryover and environmentally hazardous gas before their release to the atmosphere through the stack. The off-gas was measured continuously by the paramagnetic analyser for O_2 gas (OXOR 610 Maihak) and infrared spectrometer, the so-called UNOR 610 for analysing CO_2, CO, SO_2, and NOx (UNOR 610). The other gas species, such as SO_2, HCl, HF, and B were measured discontinuously. All the samples were analysed by HCl and HF, independent of vacuum methods and sorption agents used.

Table 24 and 25 show the results of the off-gas emission measurement between the borax pentahydrate and ulexite batches during the industrial trial in raw and clean gas, i.e. before and after filtration.

Table 24 Comparison of the average composition value of off-gas emission between borax pentahydrate and ulexite before they were filtered; the given volume is associated with the dry off-gas in normal condition (NTP)

	borax pentahydrate 28.09.2010		ulexite 10.02.2011	
emission dust particle species	concentration [mg/m^3]	emission [kg/t$_{glass}$]	concentration [mg/m^3]	emission [kg/t$_{glass}$]
As	$192 \cdot 10^{-3}$	$0.347 \cdot 10^{-3}$	$421 \cdot 10^{-3}$	$0.853 \cdot 10^{-3}$
Cd	$336 \cdot 10^{-3}$	$0.609 \cdot 10^{-3}$	$88 \cdot 10^{-3}$	$0.178 \cdot 10^{-3}$
Co	$4 \cdot 10^{-3}$	$0.008 \cdot 10^{-3}$	$< 1 \cdot 10^{-3}$	$< 0.002 \cdot 10^{-3}$
Cr	$3381 \cdot 10^{-3}$	$6.12 \cdot 10^{-3}$	$2788 \cdot 10^{-3}$	$5.65 \cdot 10^{-3}$
Cu	$87 \cdot 10^{-3}$	$0.158 \cdot 10^{-3}$	$115 \cdot 10^{-3}$	$0.233 \cdot 10^{-3}$
Mn	$10 \cdot 10^{-3}$	$0.018 \cdot 10^{-3}$	$15 \cdot 10^{-3}$	$0.03 \cdot 10^{-3}$
Ni	$53 \cdot 10^{-3}$	$0.097 \cdot 10^{-3}$	$39 \cdot 10^{-3}$	$0.079 \cdot 10^{-3}$
Pb	$555 \cdot 10^{-3}$	$1.005 \cdot 10^{-3}$	$110 \cdot 10^{-3}$	$0.223 \cdot 10^{-3}$
Sb	$57 \cdot 10^{-3}$	$0.103 \cdot 10^{-3}$	$77 \cdot 10^{-3}$	$0.156 \cdot 10^{-3}$
Se	$82 \cdot 10^{-3}$	$0.148 \cdot 10^{-3}$	$137 \cdot 10^{-3}$	$0.278 \cdot 10^{-3}$
Sn	$6 \cdot 10^{-3}$	$0.010 \cdot 10^{-3}$	$18 \cdot 10^{-3}$	$0.036 \cdot 10^{-3}$
V	$< 1 \cdot 10^{-3}$	$< 0.002 \cdot 10^{-3}$	$< 1 \cdot 10^{-3}$	$< 0.002 \cdot 10^{-3}$
B	**183.20**	**0.332**	**211.00**	**0.427**
S	32.90	0.060	43.00	0.087
Na	178.00	0.322	49.30	0.100
Ca	23.00	0.040	28.30	0.057
K	59.80	0.108	36.60	0.074
Mg	0.60	0.001	2.50	0.005
total dust	1173.00	2.120	1413.00	2.860
gas species				
B	**4.00**	**0.007**	**4.10**	**0.008**
NO_x as (NO_2)	454.00	0.820	230.00	0.470
SO_2	4.00	0.008	13.00	0.026
HCl	< 0.7	< 0.002	< 0.7	< 0.002
HF	1.12	0.002	1.80	0.004

Table 25 Comparison of average composition value of the off-gas emission between borax pentahydrate and ulexite after cleaned/filtered; the given volume is associated to the dry off-gas in normal condition (NTP)

	borax pentahydrate 29.09.2010		ulexite 10.02.2011	
emission dust particle species	concentration [mg/m^3]	emission [kg/t$_{glass}$]	concentration [mg/m^3]	emission [kg/t$_{glass}$]
As	$5.0 \cdot 10^{-3}$	$0.011 \cdot 10^{-3}$	$15.6 \cdot 10^{-3}$	$0.034 \cdot 10^{-3}$
Cd	$15.6 \cdot 10^{-3}$	$0.033 \cdot 10^{-3}$	$6.4 \cdot 10^{-3}$	$0.014 \cdot 10^{-3}$
Co	$< 0.2 \cdot 10^{-3}$	$< 0.001 \cdot 10^{-3}$	$< 0.2 \cdot 10^{-3}$	$< 0.001 \cdot 10^{-3}$
Cr	$124.4 \cdot 10^{-3}$	$0.263 \cdot 10^{-3}$	$164.8 \cdot 10^{-3}$	$0.360 \cdot 10^{-3}$
Cu	$96.1 \cdot 10^{-3}$	$0.203 \cdot 10^{-3}$	$278.6 \cdot 10^{-3}$	$0.608 \cdot 10^{-3}$
Mn	$< 0.2 \cdot 10^{-3}$	$< 0.001 \cdot 10^{-3}$	$< 0.2 \cdot 10^{-3}$	$< 0.001 \cdot 10^{-3}$
Ni	$< 0.3 \cdot 10^{-3}$	$< 0.001 \cdot 10^{-3}$	$<0.2 \cdot 10^{-3}$	$<0.001 \cdot 10^{-3}$
Pb	$6.1 \cdot 10^{-3}$	$0.013 \cdot 10^{-3}$	$7.7 \cdot 10^{-3}$	$0.0017 \cdot 10^{-3}$
Sb	$1.7 \cdot 10^{-3}$	$0.004 \cdot 10^{-3}$	$3.1 \cdot 10^{-3}$	$0.007 \cdot 10^{-3}$
Se	$1.6 \cdot 10^{-3}$	$0.003 \cdot 10^{-3}$	$5.6 \cdot 10^{-3}$	$0.012 \cdot 10^{-3}$
Sn	$< 0.2 \cdot 10^{-3}$	$< 0.001 \cdot 10^{-3}$	$0.9 \cdot 10^{-3}$	$< 0.001 \cdot 10^{-3}$
V	$< 0.2 \cdot 10^{-3}$	$< 0.001 \cdot 10^{-3}$	$< 0.2 \cdot 10^{-3}$	$< 0.001 \cdot 10^{-3}$
B	**3.80**	**0.008**	**8.60**	**0.019**
S	0.70	0.001	1.70	0.004
Na	6.60	0.014	1.20	0.026
Ca	$127 \cdot 10^{-3}$	$0.27 \cdot 10^{-3}$	$275 \cdot 10^{-3}$	$0.60 \cdot 10^{-3}$
K	1.60	0.003	3.10	0.007
Mg	$25 \cdot 10^{-3}$	$0.05 \cdot 10^{-3}$	$34 \cdot 10^{-3}$	$0.07 \cdot 10^{-3}$
total dust	31.50	0.067	63.30	0.138
gas species				
B	1.60	0.003	1.90	0.004
NO_x as (NO_2)	460.00	0.970	250.00	0.550
SO_2	3.00	0.006	1.60	0.004
HCl	< 0.6	< 0.001	< 0.6	< 0.002
HF	0.60	0.001	0.60	0.001

The average specific dust emission of ulexite as a boron oxide carrier in the unfiltered gas is 35 % higher than the normal condition (borax pentahydrate), i.e. 2.86 kg/t$_{glass}$ (measured concentration is 1.413 mg/m^3). There were two measurement data with high and lower concentration. After the off-gas was filtered, dust emission decreased up to 0.138 kg/t$_{glass}$ (measured concentration is 63.3 mg/m^3), or 95 % lower than the unfiltered one. However, this emission value is still relatively higher, compared to that of borax pentahydrate. The degree of

dust separation in the filter instrument can only be reduced by higher off-gas volume.

The concentration of boron species found in the average total dust in the unfiltered off-gas of the ulexite batch is 211 mg/m^3, or in a specific way, it is accounted as 0.427 kg/t_{glass}. This value is 14.9 % higher than the borax pentahydrate batch. In the filtered off-gas, the average concentration of boron species is lowered up to 8.6 mg/m^3 (0.019 kg/t_{glass}). The gaseous boron formation in off-gas is relatively low for both borax pentahydrate and ulexite batches. In the unfiltered off-gas, the amount of boron-containing gas species is 4.0 mg/m^3 (7.3 g/t_{glass}) and 4.1 mg/m^3 (8.3 g/t_{glass}) for borax pentahydrate and the ulexite batch, respectively; while, in case of the filtered off-gas, it is 1.6 mg/m^3 (3.0 g/t_{glass}) in the borax pentahydrate batch and 1.9 mg/m^3 (4.3 g/t_{glass}) in the ulexite batch. The amount of NOx in the ulexite batch (0.55 – 0.47 kg/t_{glass}) is obviously lower than the borax pentahydrate batch (0.82 – 0.97 kg/t_{glass}). The concentration of the emission of other gas formation species, such as HCl, HF, and SO_2 is very low, and so are the other dust particles.

6. Conclusion

6.1 General conclusion on batch melting characterization

Many efforts have been devoted to reduce the energy required for glass melting by optimization of the batch-to-melt turnover rate. The heat demand of the batch-to-melt conversion can be solely figured by an assessment of the thermodynamic quantities of individual raw materials, the released gas, and the resulting glass. Kinetic influences like the grain size, primary melt formation, gas liberation, and quartz dissolution in the batch melting process is difficult to derive theoretically, and thus, they need to be quantified by laboratory experiments.

The conventional DTA-TG is a powerful tool to examine both physical and chemical reactions in one-compound, binary, and ternary batch systems. However, due to the very small amount of sample size involved in the experiment (less than 150 mg), the boundary conditions and mechanisms of heat transfer are very different from the industrial glass tank. Therefore, the results cannot directly be transferred to the industrial scale. Scaling up the experiments from the milligram to the kilogram range is one of the approaches to close the gap between the laboratory and industrial scale, and to give a comprehensive overview of batch melting occurrences, such as primary melt formation, bubble generation followed by foaming formation, quartz dissolution, among others. The suitable methods are thermal-optical observation (30 g sample), conductometry (200 g sample), modified batch-free time (50 g sample, 250 g cullet), and melting test in the kilogram range experiment (10 kg test). The latter simulates the vertical temperature field in the batch heap similar to the real glass tank situation.

The mechanism of batch-to-melt turnover is mainly driven by the atomic mobility within the batch. In the soda-lime silica glass, the sodium ion Na^+ is the species with the highest atomic mobility. The concept of conductometry is based on the respectivephenomena. It was the question whether this method could also be applied for the poor alkali glass batch like E-glass.

6.2 Batch melting behaviour of alkali-deficient glass systems

Similar to the conventional soda-lime silica glass, CAS and CMAS-based E-glass with additional B_2O_3, a conductivity jump of three to four orders of magnitude denotes the primary melt formation. A comprehensive analysis of the experimental results of DTA-TG, conductometry, observation furnace and calculation of the thermodynamic equilibrium showed a clear correlation among the melting peaks in the DTA signal, the conductivity jump and the thermodynamically calculated liquidus temperature.

In contrast to the soda-lime silica glass, however, the conductivity jump in the E-glass batches is not associated with the melting of batch constituent (soda ash-Na_2CO_3), but it corresponded to the eutectic melting of the entire oxide system. The presence of liquid phase in the batch enhances diffusion, and hence, increases the ionic mobility.

6.3 Batch melting behaviour at varied B_2O_3 content in CMAS-based E-glass

The batch melting of the CMAS-based E-glass, at varying B_2O_3 content was investigated from the milligram (DTA-TG) to the kilogram scale. The DTA-TG results showed water release identified by an endothermal peak followed by a mass loss at temperatures lower than 200 °C for only the B_2O_3-containing batches. The water molecule is mainly associated with the boron oxide carrier. Another endothermal peak is followed by the a mass reduction that indicated the release of CO_2 from the batch. All samples have a similar temperature at 850 °C for this phenomena. The endothermal melting peaks, however, differ considerably. The higher the B_2O_3 content in the batch, the lower is the melting peak temperature.

However, between the conductivity jump and the calculated liquidus temperature were not in agreement, but rather coincided with the change of conductivity prior to final jump. This can be explained by the fact that the applied E-glass batch had various grain sizes. The conductivity jump takes place as the quantity of the melt formed is sufficiently high. The same tendency can also be observed in the BFT and 10 kg tests. The time required for the batch to complete the quartz dissolution and endothermal reactions is shorter at higher B_2O_3 content. Boron oxide acts as a solvent which enhances the diffusion process in the solid-liquid state, thus

accelerates the batch-to-melt turnover. In general, the primary melt formation in B_2O_3-containinig E-glass batches is related to the liquidus temperature in the oxide system.

6.4 Alternative boron oxide carriers in glass industry

The European Union (EU) has issued a new environmental regulation by the name of REACH (Registration, Evaluation, Authorization, of Chemical Substances)—specifically, chemical substances derived from chemical treatments/processing. Some chemical substances strictly limited by this regulation are boric oxide (B_2O_3), boric acid (H_3BO_3), and borax pentahydrate ($Na_2O{\cdot}2B_2O_3{\cdot}5H_2O$) which are mainly used in the borosilicates, insulation wool, and E-fibre glass industries. Economic and feasible way is by replacing the conventional boron oxide carriers by alternative borate minerals.

Prior to the selection of alternative borate minerals, a literature research has been done. It was found that hundreds of borate minerals have been successfully identified. However, not all borate minerals can be readily applied for the production of glass. This is primarily due to the fact that boron is one of the rare minerals to be found in the earth's crust. The mining of alternative borate minerals in tonnage, without any involvement of the chemical beneficiation processes, is economically not feasible, due to its high impurity level. The alternative boron oxide carriers available on the market for the glass industries are colemanite and ulexite. The availability of other minerals, such as tincal, kernite, and hydroboracite were investigated only for the pilot project in the present study.

Two factors played an important role in selecting the alternative boron oxide carriers. Those factors are the impurity levels and its availability. Natural borate minerals typically contain several molecules of water and found in the forms of sodium, calcium, and magnesium salts. Based on the type of the salt, natural borate minerals can be classified into three major classes: sodium bearing, sodium-calcium, and calcium bearing boron minerals. For particular glasses, such as borosilicate and lamp glass, the amount of alkaline earth is very restricted, thus only sodium-bearing borate minerals can be used. In the E-glass batches, the amount of alkali should not exceed 1.0 wt. %. As previously stated, although many different borate minerals identified, at least only five alternative borate minerals

have been collected from various sources; they are kernite, tincalconite, ulexite, colemanite, and hydroboracite. Colemanite has been used as a replacement of boric acid in the E-glass production.

As a main conclusion, the application of alternative boron oxide carriers does not have a negative affect the melting behaviour and glass quality produced. The strict limitation of alkaline-earth content in some glass compositions is the main reason for no further possibilities to use calcium or magnesium-bearing borate minerals in this case. The application of sodium-bearing borate minerals, such as tincal and kernite for the replacement of borax pentahydrate, resulted in a similarly good batch melting behaviour. Both colemanite and ulexite can be applied in the E-glass batches. The amount of sodium oxide, however, is the main limitation for ulexite in the E-glass batches. This time the limiting factor is MgO. In the insulation glass batches, there is no significant problem in applying all the previously mentioned alternative boron oxide carriers. However, stringent composition adjustment should be performed to maintain suitable fibrization temperature (T log η = 3.0) and to avoid crystallization during fibre drawing.

An industrial campaign was successfully conducted in insulation wool glass batches. The thermodynamic assessment showed that the hydroboracite-containing batch has the lowest chemical heat demand and a slightly better batch melting behaviour. However, due to an insufficient quantity available in the market, ulexite was used in the industrial campaign. If compared to the reference batch containing borax pentahydrate, the batch melting behaviour of the ulexite batch was better in terms of foam decay and effective thermal diffusivity. The analysis of daily furnace and production data between borax pentahydrate and ulexite for a one-month trial test showed no significant difference in terms of the power input P_{in}, and the exploited power P_{ex}. The results of the off-gas and dust analysis showed an increase of boron emission by with the ulexite batch. High amounts of boron- containing dust in the ulexite batch generated relatively enhanced dust emission; however, it is still within the allowed level. No significant impact of the amount of gaseous boron species as well as other critical gases such as HCl, HF, and SO_2 was observed. Due to the relatively short period of the industrial campaign, the batch kinetic advantage of ulexite could not be demonstrated in a statistically relevant way.

References

[ABO 1953] A. Abou-El-Azm, Moore: ‘A study on the reaction rates between silica and other oxides at various temperatures. Pt. 1. Reaction rates in binary mixtures. Pt. 2. Reaction rates in ternary mixtures. Pt. 3. Reaction rates in binary and ternary mixtures additional to those described in parts 1 and 2. Pt. 4. Influence of the form in which the non-silica constituents are introduced upon their rates of reaction with silica. Pt. 5. Theory of reaction rates in binary and ternary mixtures’. J. Soc. Glass. Technol. 37 (1953). pp. 129T–154T; pp. 155T–167T, pp. 168T–181T; pp. 190T–212T.

[AIF 2002] AiF/HVG Forschungsvorhaben Nr. 12414 N: ‘Steigerung von Leistung und Prozesssicherheit bei der Schmelze von Gemengen mit und ohne Scherben’ (2000–2002).

[BAB 1985] V. I. Babushkin, G. M. Matveyev, O. P. Mchedlov-Pterossyan: ‘Thermodynamics of silicates’. Springer Verlag, Berlin, 1985.

[BEE 1992–1] A. J. Faber, R. G. C. Beerkens, H. de Waal: ‘Thermal behavior of glass batch on batch heating’. Glastech. Ber. 65 (1992) no. 7. pp. 177–185.

[BEE 1992–2] A. J. Faber, R. G. C. Beerkens, H. de Waal: ‘The heating process of the glass batch’. In: XVI International Congress on Glass, Madrid, 1992. Vol. 6 pp. 155–160.

[BON 1990] Bonnel, D. W, Hastie, J W: ‘Ideal mixing of complex components’. High Temp. Sci. 26 (1990), pp. 313–334.

[BUN 1969] Bunting, J. A: ‘Batch-Free Time Versus Crucible Volume in Glass Melting’, Ceramic Bulletin, Vol. 48, No. 8, pp. 781–783, (1969).

[CEL 1995] Celik, M. S. et. al.: ‘A thermodynamic analysis of decrepitation process’. Thermochimica Acta, 245 (1995), pp. 167–174.

[CHR 1972] C. L. Christ: ‘Some contribution of crystal chemistry to geochemistry’. J. Geol. Education 20. pp. 235–245.

[COS 1977] P. Costa: ‘Untersuchung des Einschmelzverhaltens von pelletiertem Gemenge zur Glasherstellung’. Glastech. Ber. 50 (1977) no.1. pp. 10–18.

[CON 1990] R. Conradt, P. Pimkhaokham: ‘An easy-to-apply method to estimate the heat demand for melting technical silicate glasses’. Glastech. Ber. 63K (1990), pp. 134–143.

[CON 1994] R. Conradt, P. Suwannathada, P. Pimkhaokham: 'Local temperature distribution and primary melt formation in a melting batch heap'. Glastech. Ber. Glass Sci. Technol. 67 (1994) pp. 103–113.

[CON 1997] R. Conradt, N. S. Kham, C. Eiumnog, P. Pimkhaokham: 'Melting behavior of batches containing ground cullets'. Fundamental of Glass Science and Technology (1997) pp. 290–296.

[CON 1998] R. Conradt: 'Effect of minor batch additions on the rate of batch melting'. Proc. XVIII International Congress on Glass, San Fransisco, 10 (1998), 13, pp. 16–21.

[CON 1999] R. Conradt, F. W. Krämer, H. Müller-Simon, R. Beerkens, G. Buchmayer: 'Grundlagen des industriellen Glasschmelzprozesses (2. Auflage)'. HVG-Fortbildungkurs, Publ. Nr : FBCH 009, 1999.

[CON 2004] Conradt, R: 'Chemical structure, medium range order, and crystalline reference state of multicomponent liquids and glasses'. J. Non-Cryst. Solids 345 & 346 (2004), pp. 16–23.

[CON 2007] Conradt, R: 'Production efficiency, environmental sustainability, and glass qualilty-a thermodynamic optimization of three conflicting objectives'. Glass Technol.: Eur. J. Glass Sci. Technol. A., October 2007, 48 (5), pp. 253–241.

[CON 2008] R. Conradt: 'The industrial glass melting process. In: The SGTE casebook – Thermodynamics at work'. Edited by K. Hack, Woodhead Publishing in Materials, 2nd Edition (2008), chapter II.24, pp. 282–303.

[CON 2009] R. Conradt: 'Thermodynamics of glass melting process. In: Continuous glass fibres'. F. Wallenberger, Ed. Springer Verlag, 2009.

[CON 2012a] R. Conradt, K. Gitzhofer: 'Einsatz alternativer boroxidhaltiger Rohstoffe in der Glasindustrie (IGF-Nr. 16181N)'. HVG-DGG final project report, Publication Nr. GFOR16181, 2012.

[CON 2012b] R. Conradt: 'Thermal versus chemical constraint for efficiency of industrial glass melting furnaces'. Processing, Properties, and Applications of Glass and Optical Materials, Ceramic Trans., Vol 231, Am. Cer. Soc., 2012, pp. 25–36.

[DAN 1973] M. Daniels: 'Melting behavior of glass batches'. Glastech. Ber. 46 (1973) no. 3, pp. 40–46.

[DEM 2000] Demirci, Sahinde, et. al.: 'Changes in the structure of ulexite on heating'. Thermochimica Acta 362 (2000), pp. 107–112.

[DFG 2002] DFG-Forschungsvorhaben CO 249/2-1: ‘Stoff- und Wärmeumsatz in Rohstoffgemengen beim Glasschmelzprozess’. (1998–2002).

[DOL 2004a] M. D. Dolan, S. T. Misture: ‘Analysis of glass batch reactions using in-situ x-ray diffraction. Part 1. Batch components and binary quarzt mixture’. Glass Technol., 2004, 45 [3], pp. 410–417.

[DOL 2004b] M. D. Dolan, S. T. Misture: ‘Analysis of glass batch reactions using in-situ x-ray diffraction. Part 2. Soda-lime-silica glass batches’. 2004, 45 (4), pp. 167–174.

[DOL 2004c] M. D. Dolan, S. T. Misture: ‘Analysis of glass batch reactions using in-situ x-ray diffraction. Part 3. Borosilicate glass batches’. 2004, 45 (5), pp. 212–19.

[DUB 2004] O. Dubois, R. Conradt: ‘Experimental study on the effect of cullet and batch water content on the melting behavior of flint and amber container glass batches’. Glass. Sci. Technol. 77 (2004), pp. 137–148.

[ERI 1990] Eriksson, G., Hack, K: ‘ChemSage – A computer program for the calculation of complex chemical equilibria’. Met. Trans. B, 21 B (1990) 1013.

[FLI 1995] C. Flick, G. Noelle: ‘Redox conditions during the melting of batch’. Glastech. Ber. Glass Sci. Techol. 68 (1995), pp. 81–83.

[FRI 1986] E. Gehrmann, G. H. Frischat: ‘Influence of batch moisture on melting behavior of glass’. J. Am. Ceram. Soc. 6 (1986), no. 4, pp. C84–C85.

[FRI 1990] E. De. Kever, G. H. Frischat: ‘Influence of batch moisture and atmosphere on melting behavior of lead oxide containing glass’. J. Am. Ceram. Soc. 73 (1990), no. 2, pp. 2165–2166.

[FRI 1992] E. De. Kever, G. H. Frischat: ‘Influence of batch moisture and atmosphere on melting behavior of As_2O_3- and Sb_2O_3-containing glass’. Glastech. Ber. 65 (1992) no. 2, pp. 64–66.

[FUH 1973] H. Fuhrmann: ‘Beitrag zur näherungsweisen Berechnung des Abschmelzens von Glasgemengeschichten. Pt. 1. Theoretische Ableitungen. Pt. 2. Numerische Ergebnisse’. Glastech. Ber. 46 (1973) no. 10. p. 201–208; no. 11. pp. 209–218.

[GAY 1984] Gaye, H. in: Gay, H., Colombet, D., eds., Donneés thermochimiques et cinétiques relatives à certains matériaux sidérurgiques. Commission de la Communautés Européennes Convention CEEC No. 7210-CF/301 TCM-RE 1064, Bruxelles 1984.

[GTT 2004] GTT Technologies: 'FactSage™ Software Version 5.2'. Thermfact Montreal adn GTT- Technologies Aachen, 2004.

[HIL 1986] G. Hilbig, H. Kirmße: 'Das Temperaturfeld im Gemengekeil brennstoffbeheizter Glasschmelzwannen'. Glastech. Ber. 59 (186). No. 6. pp. 169–173.

[HRM 1982] P. Hrma: 'Thermodynamics of batch melting'. Glastech. Ber. 55 (1982) no. 7, pp. 138–150.

[HRM 1985] P. Hrma: "Reaction between sodium carbonate and silica sand at 874 °C <T< 1022 °C'. J. Am. Ceram. Soc. 68 (1985), no. 6, pp. 337–341.

[HRM 1999] P. Hrma: "Batch melting reactions". In: Paul, A.: Chemistry of Glasses. Chapman and Hall, London, 1999, pp. 157–177.

[IZA 2001a] P. Izak, P. Hrma: 'Charter 19 – Kinetics of conversion of high-level waste of glass', ACS Symposium Series, 2001, 778, pp. 314–328.

[IZA 2001b] P. Izak, P. Hrma, B. W. Arey, T. J. Plaisted: 'Effect of feed melting, temperature history and minor componenet addition on spinel crystallization in high-level waste glass', J. Non. Cryst. Solids, 2001, 289, pp. 17–29.

[KAW 1999] S. Kawachi, M. Kato, Y. Kawase: 'Evaluation of reaction rate of refining agents'. Glastech. Ber. Glass Sci. Technol., 1999, 72 [6], pp. 182–187.

[KAU 1969] K. Kautz: 'Bildung von Reaktionsprodukten beim Aufheizen von Glasgemengen. Untersuchungen in den Systemen SiO_2-Na_2O-CO_2, SiO_2-CaO-CO_2 und SiO_2-Na_2O-CaO-CO_2 (mit Anwesenheit von MgO) –eine Literaturzusammenstellung'. Glastech. Ber. 42 (1969) no. 6, pp. 244–250.

[KIM 1990] D. S. Kim, P. Hrma: 'Volume change during batch to glass conversion'. Am. Ceram. Soc. Bull., 1990, 59 [6], pp. 1039–1043.

[KIS 1975] R. B. Kistler, W. C. Smith: 'Boron and borates', in: S. J. Lefond: Industrial rock and minerals (4^{th} ed.), American Institute of Mining, Metallurgical and Petroleum Engineers, p. 172.

[KRÄ 1980] F. Krämer: 'Gas profile measurements as a means of determining gas evolution during glass melting'. Glastech. Ber., 1980, 53 [7], pp. 177–188.

[KRI 1959] I. M Krieger, T. J Dougherty. 'A mechanism of for non-Newtonian flow in suspensions of rigid spheres'. T. Soc. Rheol, 1959, 3, pp. 137–152.

[KRÖ 1948] C. Kröger: 'Die ternären und quarternären Systeme Alkalioxyd-CaO-SiO2-CO2. Gleichgewichte, Reaktionsgeschwindigkeiten und ihre Beziehung zum Glasschmelzprozess', Pt. 2 Glastech. Ber. 22 (1948/1949) no. 15, pp. 331–338.

[KRÖ 1952] C. Kröger: 'Gemengereaktionen und Glasschmelze'. Glastech. Ber. 25 (1952) no. 10 pp. 307–324.

[KRÖ 1953a] C. Kröger, G. Ziegler, F. Marwan et. al.: 'Über die Geschwindigkeiten der zur Glasschmelze führenden Reaktionen'.
II. Die Umsetzung von Natriumsilicat mit Soda und von Quarz mit Kalkstein.
III. Reaktionsgeschwindigkeiten um quarternären System Na_2O-CaO-SiO_2-CO_2
IV. Due Drückabhängigkeit der Umsetzungsgeschwindigkeiten im quarternären System Na_2O-CaO-SiO_2-CO_2.
V. Die Umsetzung von Natriumdisilicat und Disilicat-Quarz Gemischen.
VI. Der Einfluß von Zusätzen auf die Reaktionsgeschwindigkeit eines Soda-Kalkstein-Quarz-Grundgemenges.
VII. Die Tonerdeumsetzung
Glastech. Ber. 26 (1953) no. 11. pp. 346–353; 27 (1954) no. 6. pp. 199–212; 28 (1955) no. 2. pp. 51–57; no.3 pp. 89–08; 29 (1956) no. 7. pp. 275–289; 30 (1957) no. 6. pp. 222–229; 34 (1961 no. 8. pp. 408–412.

[KRÖ 1953b] C. Kröger: 'Theoretischer Wärmebedarf der Glasschmelzprozesse'. Glastech. Ber. 32 (1953) no. 7, pp. 202–214.

[KRÖ 1955] C. Kröger, E. Vogel: 'Über die Grundreaktionen des Sulfatglas-Schmelzprozess'.
I. Die Sulfatreduktion
II. Die Sulfid-Sulfat-Reaktion und die Umsetzung im quinären System Na-S-O-Si-Ca.
Glastech. Ber. 28 (1955) no. 11, pp. 426–437; 27 (1954) no. 12, pp. 468–474.

[KRÖ 1957] C. Kröger: 'Über die Geschwindigkeit, den Mechanismus und die Phasenbildung bei den unter Schmelzbildung ablaufenden Festkörperreaktionen'. Glastech. Ber. 30 (1957) no. 2, pp. 42–45

[KRÖ 1958] C. Kröger, W. Janetzko, G. Kreilow: 'Der Wärmebedarf der Silicatglasbildung'. Glastech. Ber. 32 (1958) no. 6, pp. 221–229.

[KUB 1993] O. Kubaschewski, C. B. Alcock, O. J. Spencer: 'Materials Chemistry'. Pergamon, Oxford, 1993.

[LAI 1998] P. Laimböck: 'Foaming glass melt'. PhD Thesis, University of Technology Eindhoven, 1998.

[LAI 2000] P. Laimböck: ‘Fining and foaming behaviour of sulphate fined glass melt’, ‘Proceedings of the ICG 2000 Amsterdam, Glass in the Millenium’, Amsterdam, 2000.

[MAD 1996] C. Madiate, F. Müller, W. Wilsmann: ‘Thermochemistry of the glass melting process—energy requirement in melting soda-lime-silica-glasses from cullet containing batches’. Glastech. Ber. Glass Sci. Technol. 69 (1996) no. 6, pp. 167–178.

[MAS 1980] H. Mase, K. Oda: ‘Mathematical model of glass tank furnace with batch melting process’. J. Non-Cryst. Solids 38 & 39 (1980) pp. 807–812.

[MUK 1980] J. Mukerji, A. K. Nandi and K. D. Sharma: ‘Reaction in container glass batch’. Am. Ceram. Soc. Bull., 59 [8], pp. 790–793, 1980.

[PEL 1986] Pelton, A.D., Blander, M.: ‘Thermodynamic analysis of ordered liquid solutions by a modified quasi-chemical approach—application to silicate slags’. Met. Trans. B, 17 B (1986), pp. 805–815.

[PIM 1993] P. Pimkhaokham, R. Conradt: ‘Study on the processes controlling the rate of glass batch melting’. Rep. Asahi Glass Found., 1993, pp. 281–284.

[PIM 1995] P. Pimkhaokham, C. Eiumnoh, N. Sam Kham, R. Conradt: ‘Study on the local and temporal distribution of temperature, oxygen activity and liquid phase formation in a melting batch blanket’. Rep. Asahi Glass Found., (1995) pp. 743–747.

[PHA 1998] Phase equilibra diagrams. CD ROM Database Ver 2.1. The American Ceramic Society, Westerville, Ohio, 1998

[SCH 1983] H. Scholze, G. Tünker, R. Conradt: ‘Verdampfung von Fluor aus Glasschmelze und beim Einschmelzprozeß’. Glastech. Ber. 56 (1983), pp. 131–137.

[SHA 1994] Shakhmatkin, B.A., Vedishcheva, N.M., Schultz, M.M. and Wright, A.C: ‘The thermodynamic properties of oxide glasses and glass forming liquids and their chemical structure’. J. Non-Cryst. Solids 177 (1994), pp. 249–256.

[SHE 1990] C. A. Sheckler, D. R. Dinger: ‘Effect of particle size distribution on the melting of soda-lime-silicate glass’. J. Am. Ceram. Soc. 73 (1990) no. 1. pp. 24–30.

[SIM 2000] J. M Simon, R. A. Smith: ‘Borate raw materials’. Glass Tech., 2000, 41 (6), pp. 169–173.

[SPY 1993a] K.S Hong, R. F. Speyer: ‘Thermal analysis of reactions in soda-lime- silicate glass batches containing melting accelerants. I. One- and two-component system’. J. Am. Ceram. Soc. 76 (1993), pp. 598–604.

[SPY 1993b] K.S Hong, R. F. Speyer: ‘Thermal analysis of reactions in soda-lime- silicate glass batches containing melting accelerants. II. Multicomponent system’. J. Am. Ceram. Soc. 76 (1993), pp. 605–608.

[SPY 1993–3] M. E. Savard, R. F Speyer: ‘Effect of particle size on the fusion in soda-lime-silicate glass containing NaCl’. J. Am. Ceram. Soc. 76 (1993), pp. 671–677.

[TAM 1930] G Tamman: Die Reaktionen beim Zusammenschmelzen von Glassätzen. Z. anorg. Allg. Chem. 193 (1930) pp. 245–269

[UNG 1986] A. Ungan, R. Viskanta: ‘Melting behavior of continuously charged loose batch blankets in glass melting furnaces’. Glastech. Ber. 59 (1986) no. 10, pp. 279–291.

[WAL 2001] F. T. Wallenberger, J. C. Watson, H. Li: ‘Glass fibres’. ASM International, ASM Hanbook, Vol. 21: Composites, 2001, pp. 27–34.

[WAL 2006] F. T Wallenberger, R. J. Hicks, A. T. Bielhals: ‘Effect of oxides on decreasing melt viscosity and energy demand of E-Glass’. Am. Ceram. Soc. Bull. 85 (2006), pp. 38–43.

[WAL 2009] F. T Wallenberger: ‘Design of Energy-Friendly Glass Fibres. In: Continuous glass fibres’. F. Wallenberger, ed. Springer Verlag, 2009.

[WIL 1961] F. W. Wilburn, C. V. Thomasson. ibid. Pt. 3. The calcium carbonate-silica system. Phys. Chem. Glasses 2 (1961), pp. 126–131.

[WIL 1963] R. S. Warburton, F. W. Wilburn. ibid Pt. 4. The calcium carbonate-silica-alumina system Phys. Chem. Glasses 4 (1963), pp. 91–98.

[WIL 1965] F. W. Wilburn, S. A. Metcafe, R. S Warburton: ‘Differential thermal analysis, differential thermogravimetric analysis, and high temperature microscopy of reactions between the major components of a sheet glass batch’. Glass Technol. 6 (1965) no. 4, pp. 107–114.